NOAA-17 SBUV/2 (FM#6)
Activation and Evaluation Phase (A&E) Report

Matthew T. DeLand, Liang-Kang Huang, C. Albert McKay

Science Systems and Applications, Inc. (SSAI)
10210 Greenbelt Rd., Suite 400
Lanham, MD 20706

24 December 2002

Document # SSAI-2015-180-MD-2002-02

Table of Contents

Figure List

Table List

1. Introduction

The SBUV/2 Flight Model #6 (FM#6) instrument is the latest in a series of remote-sensing instruments flown by NOAA to monitor stratospheric profile ozone and total column ozone abundances. SSAI is responsible for providing calibration parameters to NOAA for use in the operational ozone processing system (OOPS). Prelaunch calibration values were developed using data from the Specification Compliance and Calibration Data Book (hereafter Data Book) delivered by Ball Aerospace [*Ball Aerospace*, 2001]. SSAI used these data to derive initial V6 processing parameters, which were delivered to NOAA on May 24, 2002 [*DeLand et al.*, 2002]. The FM#6 instrument was launched on the NOAA-17 satellite on June 24, 2002.

The SBUV/2 FM#6 instrument first collected radiance data on July 8, 2002. FM#6 is the first SBUV/2 instrument that has the capability of collecting Range 3 data from either the cathode or anode. Range 3 anode (R3A) data are expected to have lower noise than R3C data. With the exception of 3 orbits of door-closed R3C data on July 8 and a 1-day test on August 29-30, all NOAA-17 Range 3 data have been collected in anode mode. Initial solar irradiance measurements showed significant wavelength-dependent changes in the radiometric calibration, ranging from –4% at 340 nm to –13% at 252 nm. Additional data gathered during on-orbit Activation and Evaluation (A&E) phase operations evaluated the prelaunch wavelength calibration, inter-range ratio, electronic offset, and goniometric correction results. A memo presenting recommended calibration changes was delivered to NOAA on September 19, 2002. Following the implementation of these changes, regular operations including solar and other calibration measurements began October 1, 2002. NOAA/NESDIS officially began operational ozone processing on September 23, 2002.

This report is intended to summarize the SBUV/2 FM#6 instrument status as of the beginning of operational processing. NOAA-17 inflight data evaluated here end on October 31, 2002 unless otherwise noted. In general, the NOAA-17 SBUV/2 calibration presented in this report is not intended to be completely representative of the instrument status for an indefinite period of time. SSAI will track instrument performance on a regular basis. We expect to update the NOAA-17 instrument characterization within approximately 1 year after the start of normal operations.

2. Executive Summary

The body of this report discusses the detailed procedures used in characterizing the NOAA-17 SBUV/2 instrument and the results obtained. Brief summaries of each major section are provided below.

Operations. Activation and Evaluation phase tests were completed ahead of schedule in late July 2002. Additional special tests were conducted in late August and early September. The instrument began its normal schedule of measurements in October 2002.

Housekeeping Data. Temperature, voltage, and current data are well-behaved. No grating drive problems have been observed.

Electronic Offsets. Range 1 data are fairly noisy, consistent with predictions based on prelaunch tests. Range 2 offset data are well-behaved. Range 3 anode data are also very clean, comparable to Range 2. Range 3 cathode noise is comparable to NOAA-16. There is no evidence of periodic behavior in Range 3 cathode mode data.

Wavelength Calibration. Prelaunch data taken after thermal vacuum testing showed an absolute offset from the reference wavelength calibration. This offset was adopted for initial on-orbit processing. Inflight calibration data are consistent with the revised wavelength calibration, so no changes were made.

Goniometric Calibration. Prelaunch goniometric correction data were taken prior to instrument modification implementing a different diffuser deployment angle. The initial goniometric correction was therefore an approximation, that showed errors when it was applied to on-orbit solar data. An empirical elevation angle-dependent correction was derived. A wavelength dependence correction was derived from inflight position mode data.

Thermal Response. A correction for radiometric sensitivity changes based on PMT temperature variations was derived for all anode data. A separate correction was derived for Range 3 cathode data.

Interrange (Gain) Ratios. IRR_{12} values show a small wavelength dependence ($< 0.5\%$) as with NOAA-11 and NOAA-16. A constant IRR_{12} value is recommended for operational processing. Inflight IRR_{23} values using Range 3 anode data showed small wavelength-dependent variations ($\pm 0.3\%$), and a slight offset relative to the prelaunch value ($< 0.5\%$). A revised constant $IRR_{23}A$ value is recommended for operational processing. Hysteresis effects of up to 1% were observed at high solar zenith angles ($\chi > 80°$) in the Northern Hemisphere. The Range 3 cathode IRR_{23} values measured on August 29-30 are approximately 2.7% lower than the best prelaunch estimate, consistent with the likelihood of time-dependent changes during the first two months of operation.

Non-linearity Correction. The prelaunch non-linearity corrections all have magnitudes < 1%. There is no evidence of error at the 0.3% level.

Diffuser Reflectivity. Initial on-orbit reflectivity values show fluctuations of ±2% relative to the prelaunch baseline data, but no apparent overall shift. The magnitude of reflectivity changes caused by mercury lamp polarity switching is smaller than the polarity term observed for NOAA-14. Discrete and sweep mode data are in good agreement. No correction for diffuser reflectivity changes has been made in the analysis of radiometric calibration changes.

Radiometric Calibration. Sweep mode and discrete mode calibration values agree to within 0.5% after adjusting for nominal integration time differences. Air and vacuum calibration data differ by ±3% at ozone wavelengths, which is larger than the NOAA-16 result. “Day 1” discrete mode solar irradiances at ozone wavelengths are lower than predicted by SSBUV-2 data, with an approximate 10% spectral dependence. The CCR solar irradiance value is consistent with NOAA-16. Sweep and discrete calibration data agree to within ±1%.

Solar Irradiance. Sweep mode irradiance comparisons with UARS data show spectrally dependent differences over a broad region, with a minimum difference of –1% at 360 nm and a maximum difference of –18% at 180 nm. Range 3 cathode solar data are consistent with Range 3 anode data. This suggests that the low values are not caused by PMT anode-only changes. Outgassing of water vapor from MgF_2-coated surfaces is believed to be responsible. Sensitivity decreases have continued to occur during on-orbit operation, but the rate of change appears to be diminishing.

Ozone Validation. Initial ozone processing showed large total ozone pair differences (25-30 DU) using the prelaunch radiometric calibration. When solar flux values with spectrally-dependent calibration changes determined from on-orbit measurements were adopted, the pair differences were reduced to less than 5 DU. Profile ozone comparisons with NOAA-16 show significant altitude-dependent differences, which are influenced by time-dependent calibration errors in both NOAA-16 and NOAA-17 data.

3. Operations

The NOAA-17 satellite was launched on June 24, 2002 (day 175). The SBUV/2 FM#6 instrument high voltage power supply (HVPS) was turned on July 8, and radiance data were first collected on July 9. Initial solar irradiance data were not collected until July 24 (day 205) to allow sufficient time for outgassing. The nominal A&E phase tests were scheduled to last approximately 25 days following HVPS turn-on. The last A&E tests were finished on July 30, 2002, and revised calibration parameters for ozone processing were delivered on September 19, 2002. Following testing by NOAA/NESDIS, operational ozone processing began on September 23, 2002.

Table 3.1 gives the normal operating schedule for NOAA-17 SBUV/2. The SBUV/2 instrument normally makes continuous discrete mode Earth view measurements at the 12 ozone wavelengths over the daytime portion of the Earth. Solar irradiance measurements can only be initiated at the day-night terminator. For NOAA-17, this occurs at the Southern Hemisphere terminator because of the morning orbit. Daily solar observations are made in sweep mode over the wavelength range 160-406 nm, and in discrete mode across the Mg II absorption line at 280 nm. Weekly solar observations are made in discrete mode at the ozone wavelengths, and monthly position mode solar observations are made for tracking the goniometric calibration. Diffuser reflectivity measurements using the on-board mercury lamp calibration system are made every week on the night side of a selected orbit. Supplemental electronic offset data are also collected once per week by closing the calibration lamp door on the night side. Earth view measurements are made in sweep mode for four consecutive orbits once per week.

Three test data sets were collected using special sets of discrete mode wavelengths prior to the start of normal operations. One set of wavelengths used three closely spaced monochromator (FWHM = 1.1 nm) wavelengths to replicate the CCR bandpass, repeating the wavelength sequence 4 times within each discrete scan. A second test set used the EP/TOMS wavelengths (308.5-360.4 nm) in channels 1-6, a 380 nm sample at channel 7, and the standard SBUV/2 wavelengths (308.5-339.9 nm) in channels 8-12. This choice of wavelengths allows comparison of nearly simultaneous total ozone measurements obtained using the TOMS and SBUV/2 wavelength sets. A third wavelength set was constructed to look for the presence of sulfur dioxide (SO_2), using 7 wavelengths between 309-350 nm and repeating 5 of these wavelengths. The exact wavelengths used for all three tests are listed in Table 6.9. These special tests were run for approximately 1 full day each on September 4, 5, 6 respectively. Discrete solar irradiance measurements were made during each test. Further operations using these wavelength sets will be determined at a later date.

The NOAA-17 SBUV/2 instrument can collect Range 3 data in either anode mode or cathode mode. Range 3 anode mode will be used for normal ozone observations because the data have much less noise. However, continuous Range 3 anode operations do not provide independent tracking of PMT gain changes (see Section 9). A schedule of periodic Range 3 cathode operations will be implemented in 2003 to provide data for monitoring the interrange ratio ($IRR_{23}C$). The OOPS will be modified to permit continuous ozone processing during these periods.

The NOAA-16 SBUV/2 instrument is also operating nominally, and is in a reasonably stable orbit (equator-crossing time drift rate = +0.6 minutes/month). This provides an opportunity to revise the operating schedule of one SBUV/2 instrument for specific scientific objectives, without affecting production of the standard ozone product. One option under consideration is to collect additional sweep Earth data (minimum 1 full day/week) to permit testing of differential optical absorption spectroscopy (DOAS) algorithms on SBUV/2 data. Another option is to increase the frequency of Mg II solar measurements to improve the predictive capability of Air Force space weather models, which use the Mg II index as a proxy for solar EUV variations. Any changes to either NOAA-16 or NOAA-17 operations will not take place until at least January 2003, after the end of the 2002 Antarctic ozone hole season.

TABLE 3.1
NOAA-17 SBUV/2 Standard Operational Schedule

Frequency	Mode	View	Wavelengths
Continuous	Discrete	Earth	Ozone [252-340 nm]
Daily	Discrete	Solar	Mg II [276-284 nm]; *9 scans*
Daily	Sweep	Solar	160-406 nm; *2 consecutive scans*
Weekly	Discrete	Solar	Ozone [252-340 nm]; *9 scans*
Weekly	Sweep	Hg lamp	Diffuser reflectivity; *10 scans*
Weekly	Discrete	Lamp (closed)	Ozone [electronic offset]; *30 minutes*
Weekly	Sweep	Earth	160-406 nm; *4 consecutive orbits*
Monthly	Position	Solar	400, 200 nm [goniometry]; *15 minutes each*

4. Housekeeping Data

The most fundamental information about the operational status of the SBUV/2 instrument comes from the digital and analog telemetry data, collectively referred to here as "housekeeping" data. These data consist of voltages, currents, absolute temperatures, and differential temperatures measured at various locations on the instrument. Samples are taken every 16 seconds, so that daily average values each represent the mean of approximately 5000 measurements. Figures 4.1*a*-4.1*m* show time series of daily average data from the Digital "A" telemetry channels taken between July 1, 2002 and October 31, 2002. Values are recorded at 8-bit resolution and converted to engineering units. Nominal telemetry values typically vary over only a small portion of the overall range, leading to visible steps in numerous voltage and current channels which are in reality extremely stable (*e.g.* ECAL reference voltage, Figure 4.1*f*). Figures 4.2*a*-4.2*l* show corresponding time series for the Digital "B" telemetry channels, and Figures 4.3*a*–4.3*p* show time series of analog telemetry data. A complete description of parameters monitored by each telemetry channel can be found in the SBUV/2 User's Guide [*SASC Technologies,* 1986].

In general, the NOAA-17 SBUV/2 instrument has enjoyed good health. All component temperatures, such as the CCR diode (Figure 4.2*f*), PMT cathode (Figure 4.2*k*) and chopper motor (Figure 4.3*f*), were between 19-24^{o}C except the calibration lamp temperature. The calibration lamp temperature values of ~57-59^{o}C (Figure 4.1*e*) appear unreasonably high in comparison with other component temperatures. There is no heater in use to maintain such a large temperature differential. However, variations in this temperature are well-correlated with the calibration lamp current (Figure 4.1*l*). We therefore conclude that the temperature sensor is working correctly, but that there is a problem with the conversion from counts to engineering units. The same problem was observed with previous SBUV/2 instruments. The PMT high voltage power supply (HVPS, Figure 4.1*c*) was stable at 990.90(±0.2) volts. Most low voltage power supplies fluctuated by only ~0.1% of their averages, respectively (Figures 4.1*d-f*).

An additional indicator of good instrumental health is that the NOAA-17 SBUV/2 grating drive behaved very well. The grating drive positions were decoded and monitored for every spectral scan. No grating drive errors were found. The grating drive was firmly locked in the designated grating positions in both the discrete mode and sweep mode. Since no grating drive errors existed, the statistical charts for the grating drive position errors are not included in this report.

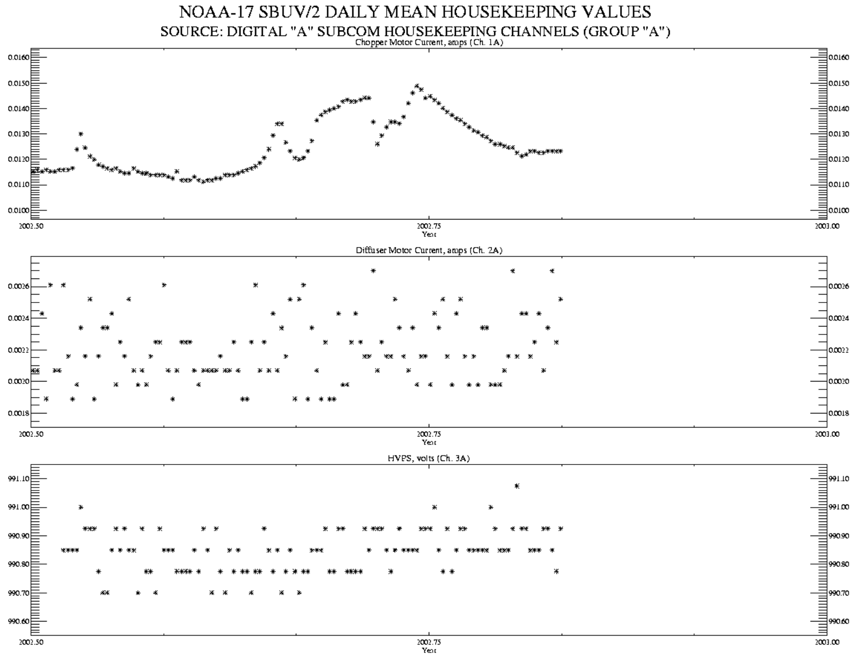

Figure 4.1: Digital A housekeeping values: (*a*) Chopper motor current; (*b*) Diffuser motor current; (*c*) High voltage power supply.

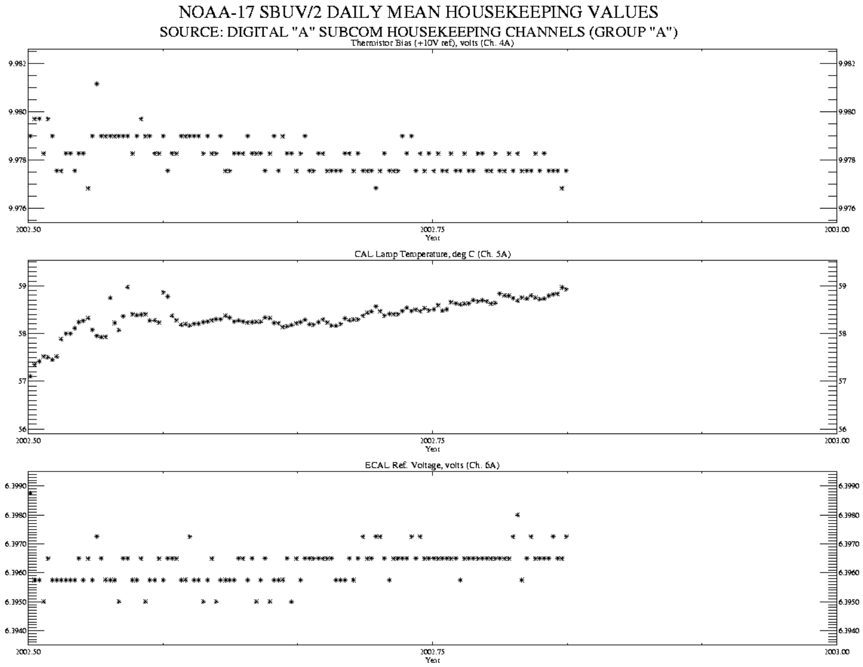

Figure 4.1: Digital A housekeeping values: (*d*) Thermistor bias; (*e*) Calibration lamp temperature; (*f*) ECAL reference voltage.

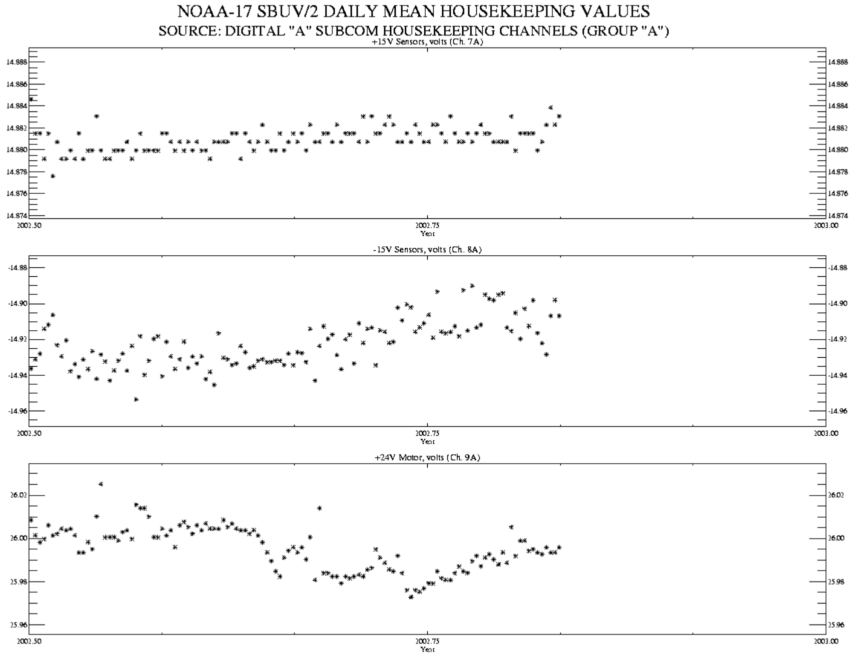

Figure 4.1: Digital A housekeeping values: (*g*) +15 V sensor; (*h*) –15 V sensor; (*i*) +24 V motor.

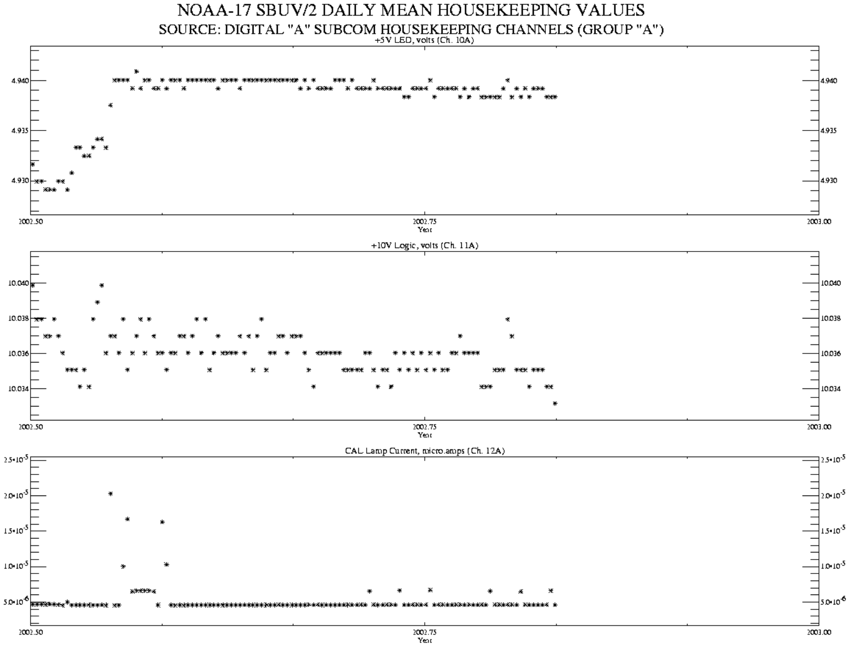

Figure 4.1: Digital A housekeeping values: (*j*) +5 V LED; (*k*) +10 V logic; (*l*) Calibration lamp current.

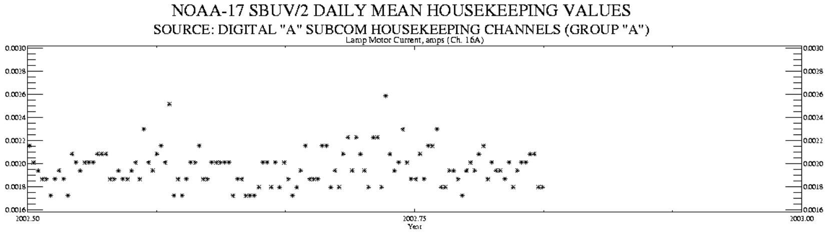

Figure 4.1: Digital A housekeeping values: (*m*) Lamp motor current.

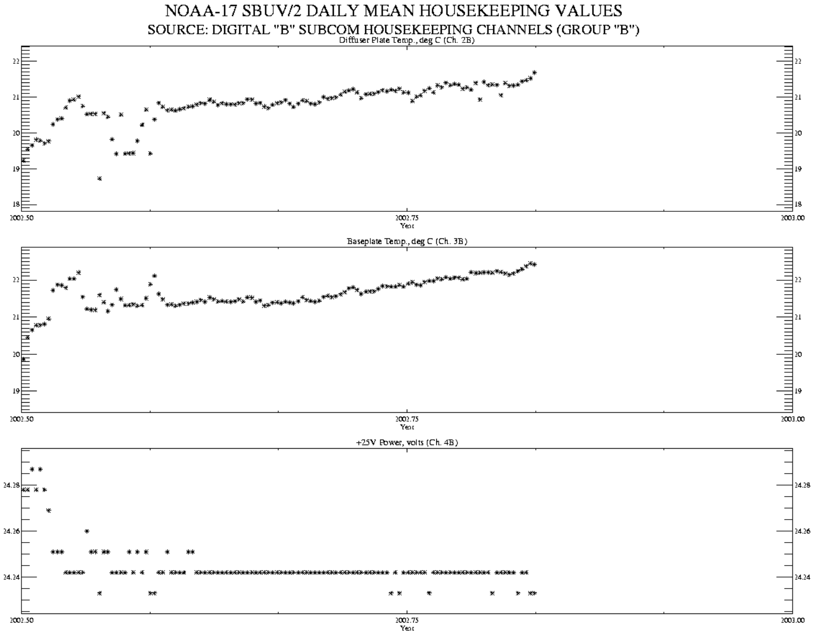

Figure 4.2: Digital B housekeeping values: (*a*) Diffuser plate temperature; (*b*) Baseplate temperature; (*c*) +25 V power.

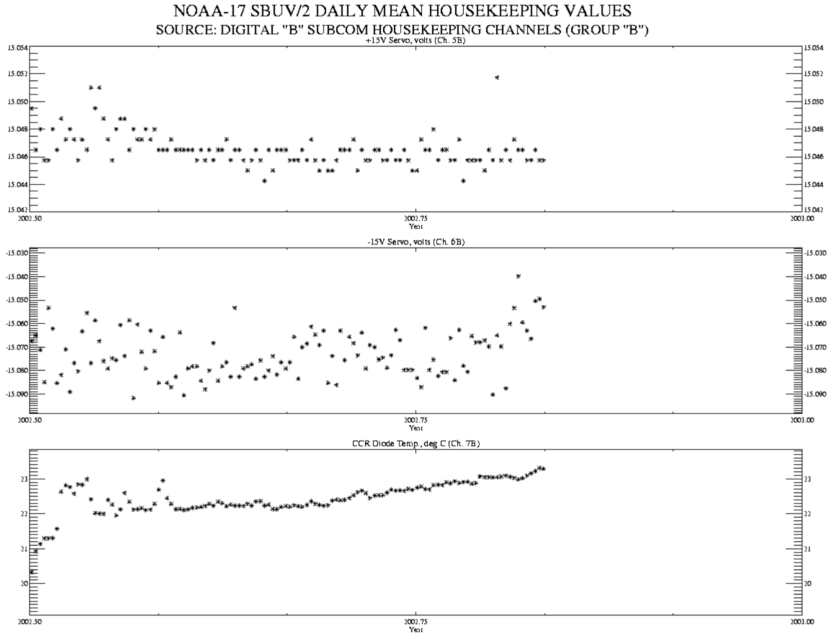

Figure 4.2: Digital B housekeeping values: (*d*) +15 V servo; (*e*) –15 V servo; (*f*) CCR diode temperature.

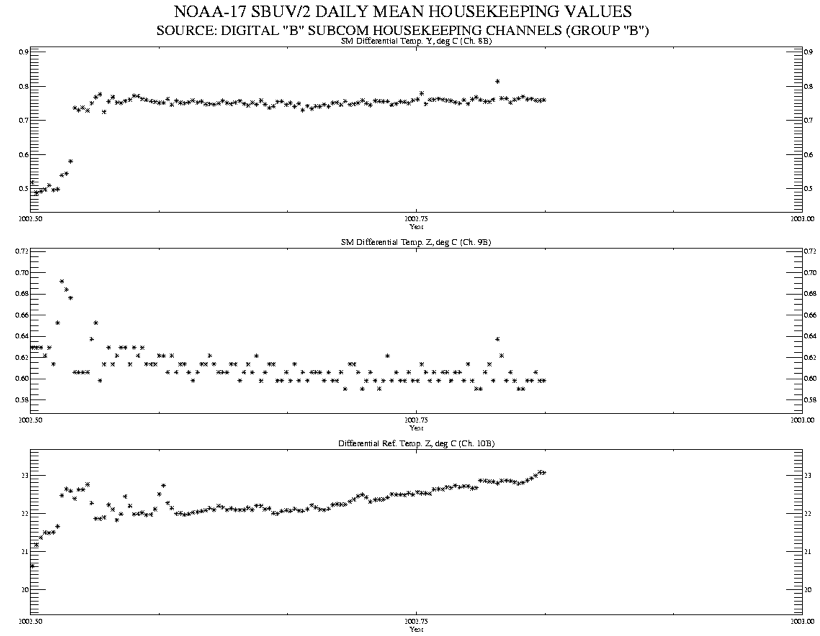

Figure 4.2: Digital B housekeeping values: (*g*) SM differential temperature Y; (*h*) SM differential temperature Z; (*i*) Differential reference temperature Z.

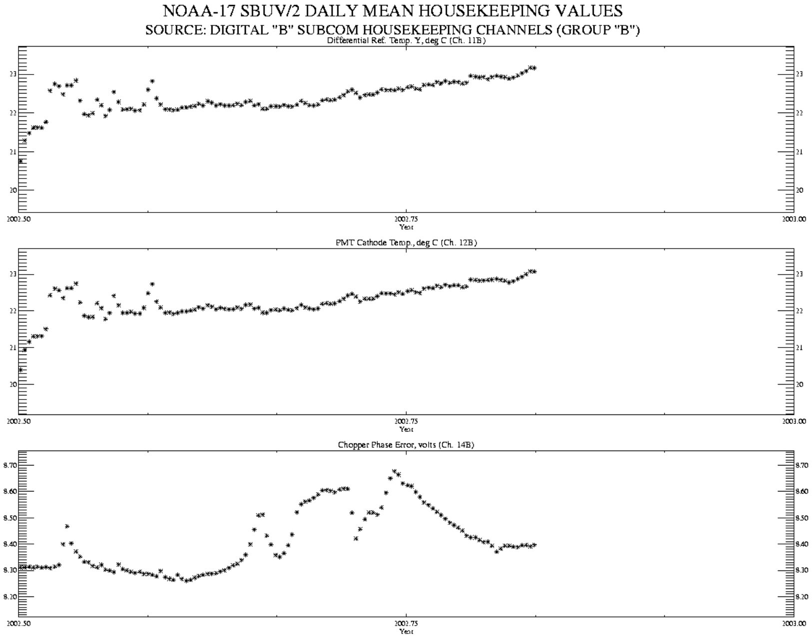

Figure 4.2: Digital B housekeeping values: (*j*) Differential reference temperature Y; (*k*) PMT cathode temperature; (*l*) Chopper phase error.

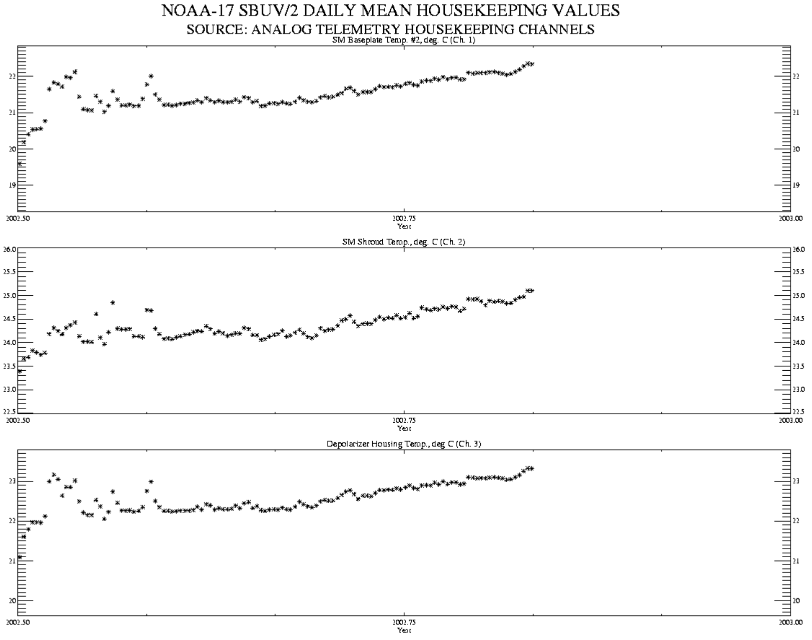

Figure 4.3: Analog housekeeping values: (*a*) SM baseplate temperature #2; (*b*) SM shroud temperature; (*c*) Depolarizer housing temperature.

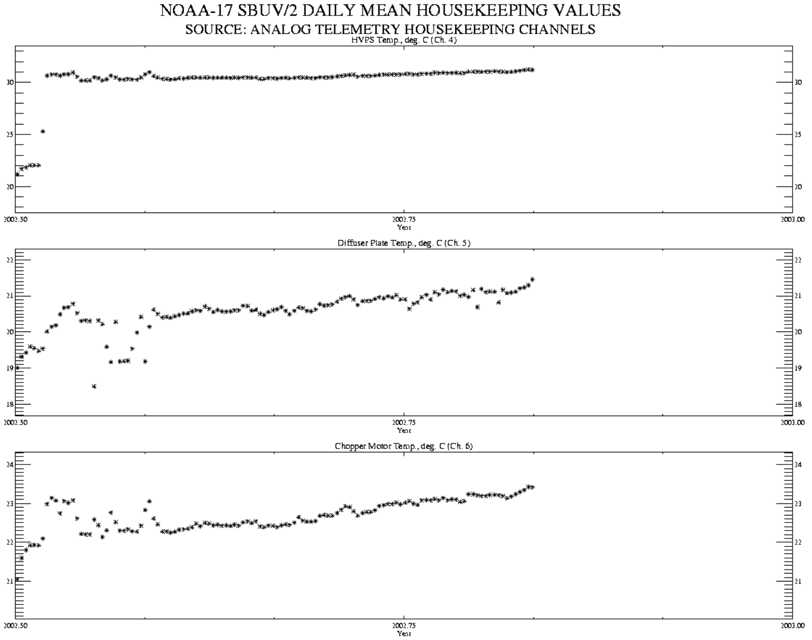

Figure 4.3: Analog housekeeping values: (*d*) High voltage power supply temperature; (*e*) Diffuser plate temperature; (*f*) Chopper motor temperature.

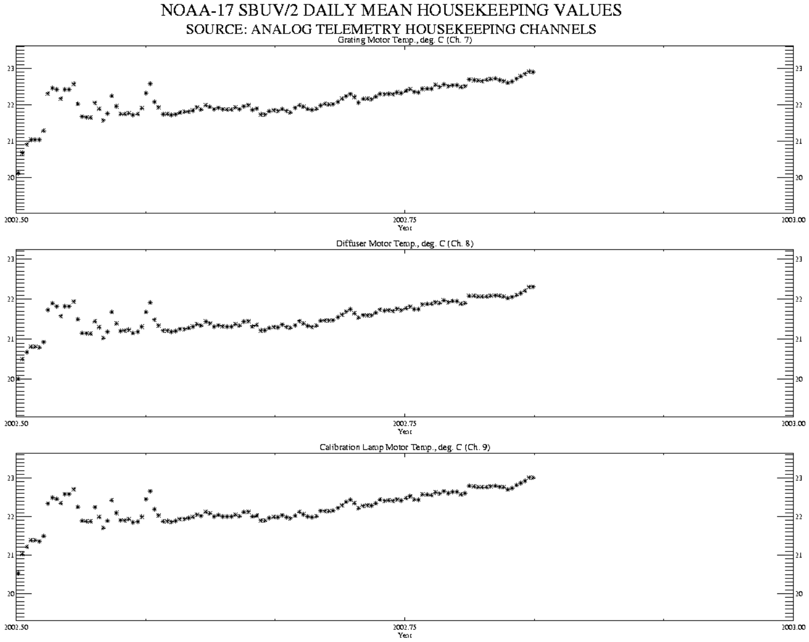

Figure 4.3: Analog housekeeping values: (*g*) Grating motor temperature; (*h*) Diffuser motor temperature; (*i*) Calibration lamp motor temperature.

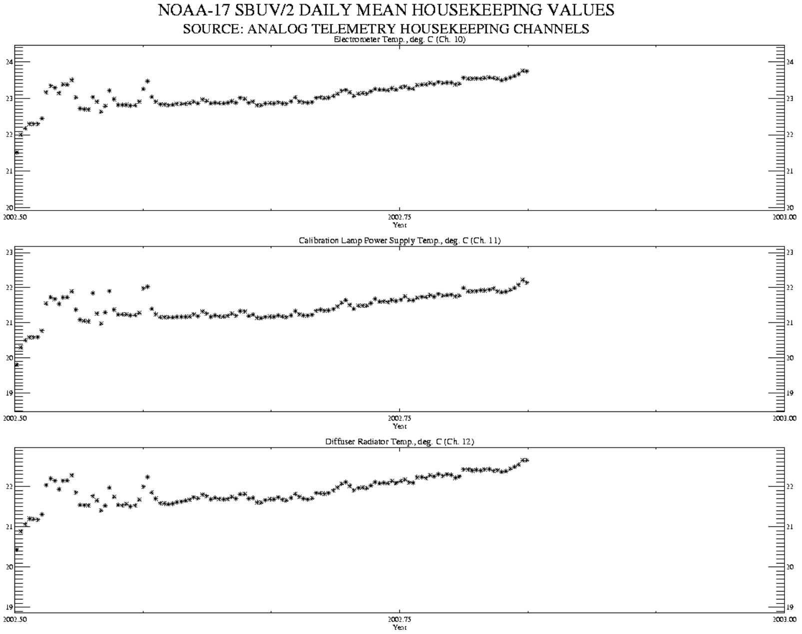

Figure 4.3: Analog housekeeping values: (*j*) Electrometer temperature; (*k*) Calibration lamp power supply temperature; (*l*) Diffuser radiator temperature.

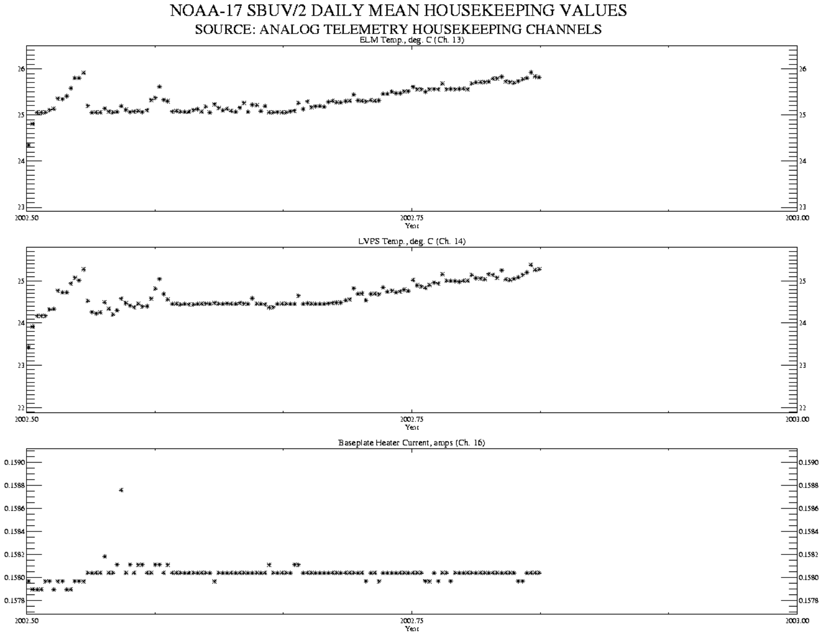

Figure 4.3: Analog housekeeping values: (*m*) ELM temperature; (*n*) Low voltage power supply temperature; (*o*) Baseplate heater current.

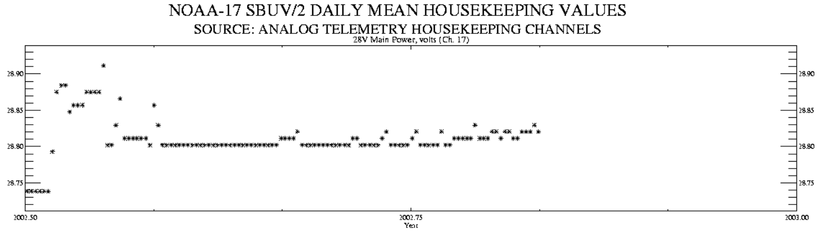

NOAA-17 SBUV/2 DAILY MEAN HOUSEKEEPING VALUES

SOURCE: ANALOG TELEMETRY HOUSEKEEPING CHANNELS

28V Main Power, volts (Ch. 17)

Figure 4.3: Analog housekeeping values: (*p*) 28 V main power.

5. Electronic Offsets

During times when the input signal to the SBUV/2 instrument is very weak (*e.g.* night side of the orbit), normal electronic fluctuations could cause counter underflows that could confuse the ozone processing algorithm. This situation is avoided by setting the digital counters to a nominal value of 64 counts for each PMT gain range and the CCR prior to the start of sample integrations. This value is called the electronic offset. It is monitored during normal operations to track spectral and temporal variations. During the A&E phase, SBUV/2 electronic offset data are examined for contamination from external sources, temporal variations, and spectral dependence.

5.1 Measurement Criteria and South Atlantic Anomaly

Selection of appropriate discrete Earth view measurements for electronic offset calculations requires consideration of weak radiance sources such as near-terminator airglow and reflected moonlight, particularly for Range 1 data. For this analysis, only data with solar zenith angles $\chi > 120^o$ are accepted, and the measurement date is required to be within ±6 days of a new moon. These criteria reject data potentially contaminated by backscattered solar and lunar signals, respectively.

The SBUV/2 instrument has a light chopper and phase lock amplifier to minimize the electronic noise and bias. The chopper wheel is designed to remove biases from charged particles in the South Atlantic Anomaly (SAA) region, roughly defined by 30°N to 60°S latitude and 60°E to 180°W longitude. Figure 5.1*a* shows Range 1 offset data for each channel measured in 5 day periods around new moon from August to October 2002, plotted as a function of latitude in 2 degree bins. The increased offset values for Channel 6 at latitudes larger than 50°N and less than 50°S are believed to represent auroral emissions from the O I line at 297.23 nm. The smallest standard deviations are seen between 0°-50°N. The increased standard deviation values centered at about 20°S are due to noise associated with the SAA. When the SAA region is excluded from the analysis, the standard deviations at 20°S become comparable to the values in the Northern Hemisphere (Figure 5.1*b*). Meanwhile, the average offset around 20°S remains at the same level as expected, indicating the chopper is functioning properly.

Significant signal increases are observed at Channel 6 (297 nm) in a narrow latitude band around 55°S within selected longitude 70°E to 160°E (Figure 5.1*b*), possibly due to crossing a bright segment of the auroral oval ring. Similar behavior with progressively weaker amplitude is observed at Channels 9, 7, 2, and 3. The auroral ring signature at 297.5 nm is greatly reduced in the full data set (Figure 5.1*a*) due to the increased number of samples. For the NOAA-9, NOAA-11, and NOAA-14 SBUV/2 instruments, the average of 11 channels, excluding Channel 6 due to potential contamination, was used for the Range 1 offset calibrations. Since the identification of significant Range 1 offset drift in NOAA-16 SBUV/2 operation, night side earth view measurements at 252 nm (Channel 1) have been used for the Range 1 offset correction. This wavelength is not affected by either auroral emission or lunar contamination, and thus average offset values can be calculated every day. Including the SAA region in the Channel 1 offset calculations increases the average value by only 0.01 count. Night side offset data are also collected with the Hg lamp door closed for one orbit/week to provide measurements where no source is present. The top panel in Figure 5.2 shows the daily average of the Range 1 offset measurements at 252 nm, where diamonds represent measurements with the instrument door closed and long ticks on the date axis indicate new moon days. The measurements at 252 nm are not affected by lunar light and are in good agreement with the door-closed measurements. The daily average standard deviation is approximately 32 counts. While prelaunch tests suggested that FM#6 might be particularly noisy in Range 1, these results are consistent with the FM#3 instrument noise level on NOAA-16.

5.2 Time Dependence

Time series plots of the daily average offset values around new moon days for Range 1, Range 2, Range 3 anode, and CCR data are shown in Figures 5.3*a-d*. Only data for Channel 12 (339.9 nm) are presented as examples. No time dependent trend of the Range 1 daily averages is observed. Day-to-day variations are statistical fluctuations since they were no more than the 2-sigma values in the daily average. Therefore, a constant Range 1 offset is recommended. An average of all Channel 1 daily averages is 68.85 counts with a standard error of 0.10 counts. Noise levels for Range 2, Range 3 anode, and CCR data were very low, with standard deviations of 0.8 counts for the daily averages. The corresponding statistical standard errors were 0.03 counts. The standard deviations for the day-to-day variations are about 0.05 counts. Therefore, all offsets are time independent.

5.3 Spectral Dependence

Figures 5.4-5.7 show the spectral dependence of temporally averaged electronic offset values around new moon days for each gain range and the CCR. As discussed in Section 5.1, many long wavelength channels in Range 1 are susceptible to resonant or fluorescent scattered light from atmosphere constituents such as O, O_2 and N_2. Therefore, only Channel 1 data were used for the Range 1 offset. The spectral variations of Range 2, Range 3 and CCR offset values are less than 0.2 counts, and are negligible. Data from all 12 channels are averaged to derive offset values for Range 2, Range 3 and the CCR.

5.4 Sweep Mode

Sweep mode electronic offsets are typically calculated from discrete values, using the relationship

$$X_{\mathrm{sweep}} = (X_{\mathrm{discrete}} - 64)/12.5 + 64.0$$

We examined the sweep mode offset with door-closed data taken on July 9, 2002. These measurements included both dayside and nightside data. Because the SBUV/2 instrument automatically selects the gain range for sweep mode data, only Range 1 offsets can be examined. The discrete mode offset daily average on the same day, which was 69.76 counts, was used in the above equation to derive a nominal sweep mode offset correction. The average residual signal after applying the sweep mode offset was effectively zero for samples taken at 392-406 nm and

SZA > 110°, as shown in Figure 5.8*a*. A slight increase is observed for dayside data, reaching 8-12 counts at SZA < 40°. Typical Earth view signals are greater than 2000 counts Range 3 at these wavelengths and solar zenith angles, so that the magnitude of the contamination is less than 10^{-6}. This result verifies the assumption that the "door closed" night side measurements eliminate all radiance sources. Sweep mode door closed net count values averaged over 160-175 nm, where the terrestrial radiance is very low, are approximately zero at all SZA (Figure 5.8*b*). The average net value of –0.07(±0.14) counts is not statistically significant.

5.4 Range 3 Cathode Data

The first three orbits of NOAA-17 following the SBUV/2 high voltage turn-on were in the Range 3 cathode output mode. Because the instrument door was closed, about 550 scans of useful data were taken for offset analysis. Figure 5.9 shows the statistical averages and standard errors at 12 channels. All channels have approximately the same noise level (3.9 counts standard deviation). There is no evidence of patterns in timing or location, such as the regular 8-second variation observed in NOAA-16 Range 3 data. Since channel-to-channel fluctuations are within the statistical uncertainty, an average of all 12 channels to create the R3C offset value is recommended. This value is also listed in Table 5.1.

TABLE 5.1
Electronic Offset Values

Range	***Inflight (A&E)***	***Prelaunch***
1	**68.85**(±0.10)	67.07
2	**64.01**(±0.01)	64.00
3 (*anode*)	**63.91**(±0.01)	63.92
3 (*cathode)*	**63.76**(±0.03)	64.23
CCR	**63.90**(±0.00)	63.88

* *All values are in counts*.

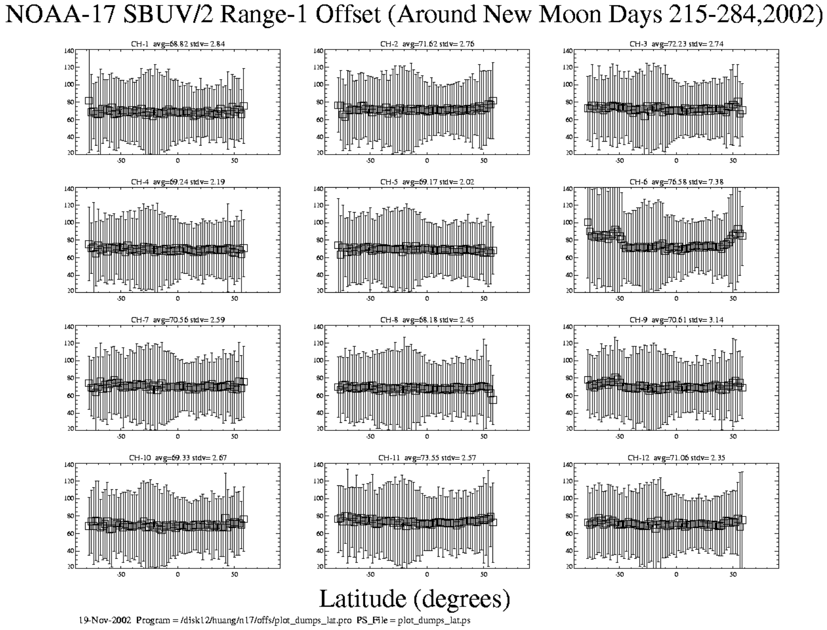

Figure 5.1: (*a*) Range 1 offset: Latitude dependence.

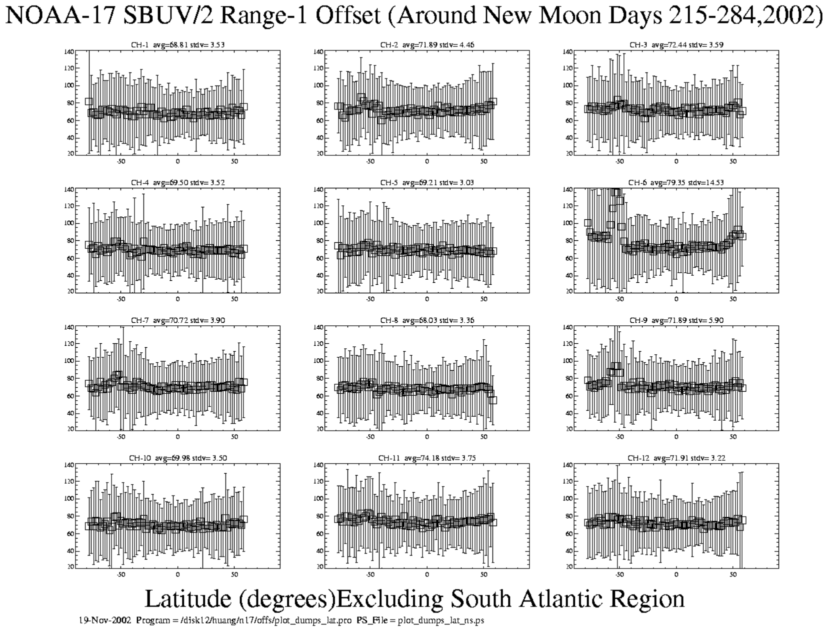

Figure 5.1: (*b*) Range 1 offset: Latitude dependence (excluding South Atlantic Anomaly).

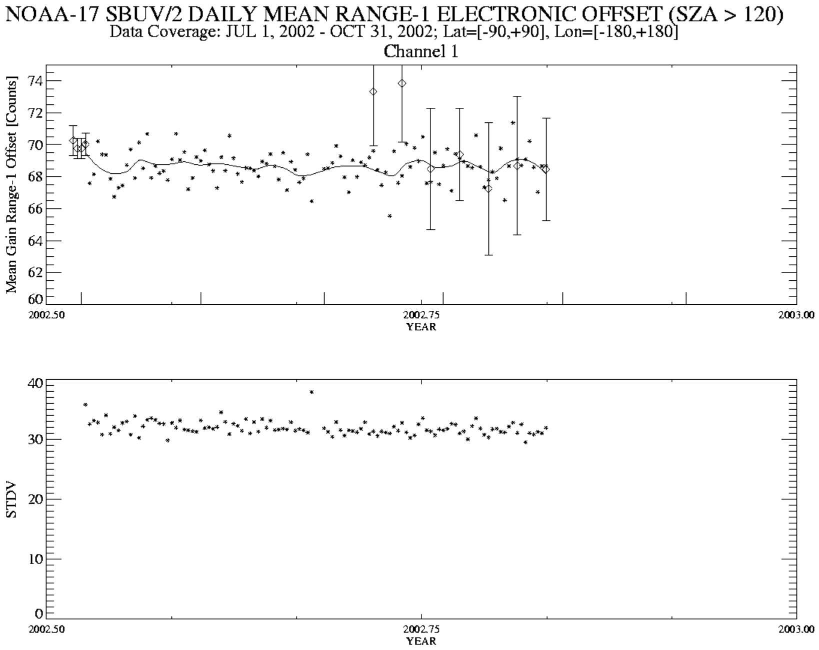

Figure 5.2: Range 1 offset data at 252 nm: (*a*) Daily average; (*b*) Standard deviation.

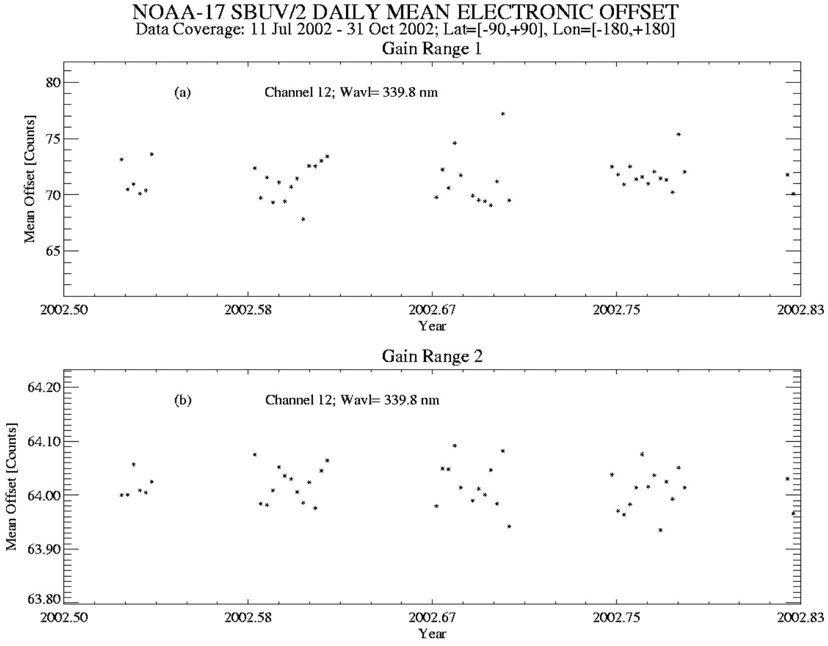

Figure 5.3: (*a*) Daily average Range 1 offset data (new moon dates); (*b*) Daily average Range 2 offset data (new moon dates).

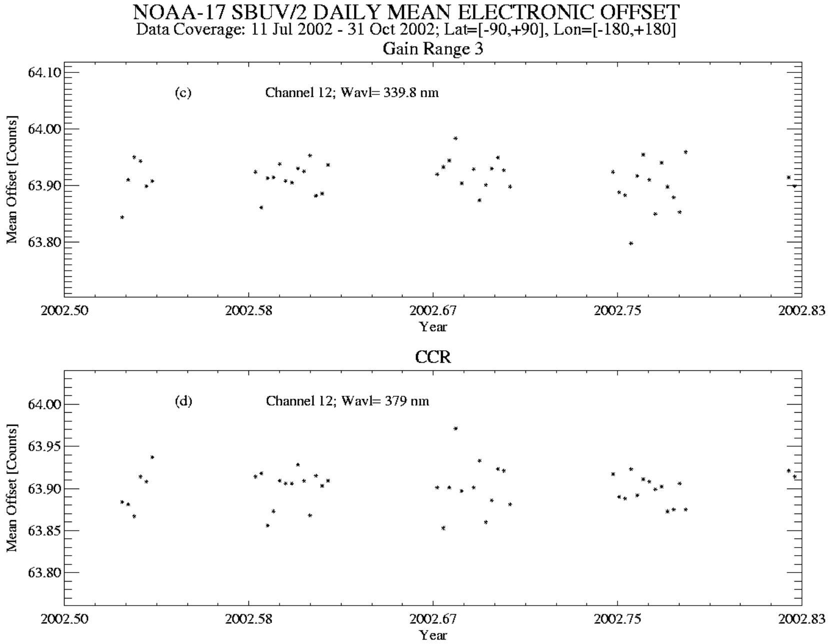

Figure 5.3: (*c*) Daily average Range 3 anode offset data (new moon dates); (*d*) Daily average CCR offset data (new moon dates).

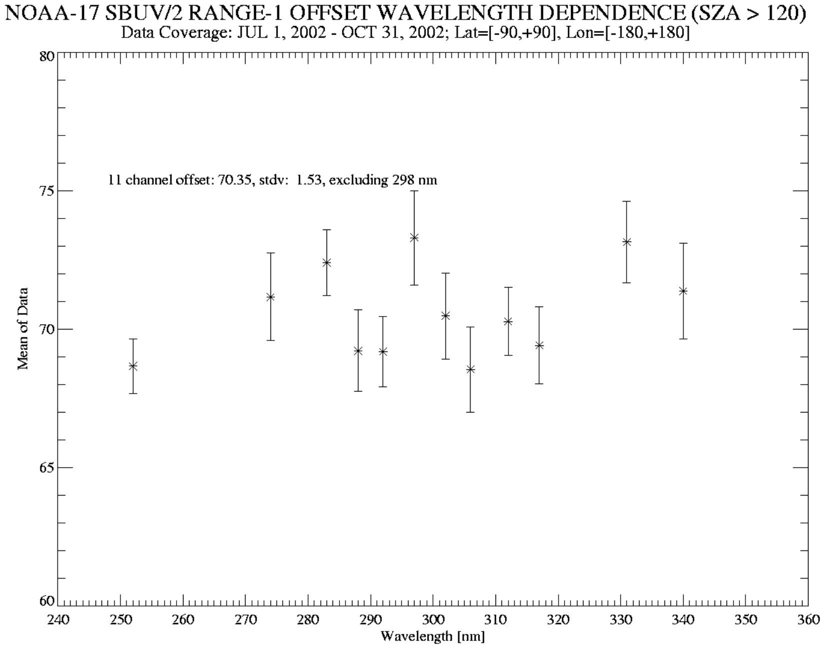

Figure 5.4: Spectral dependence of Range 1 offset, July-October 2002.

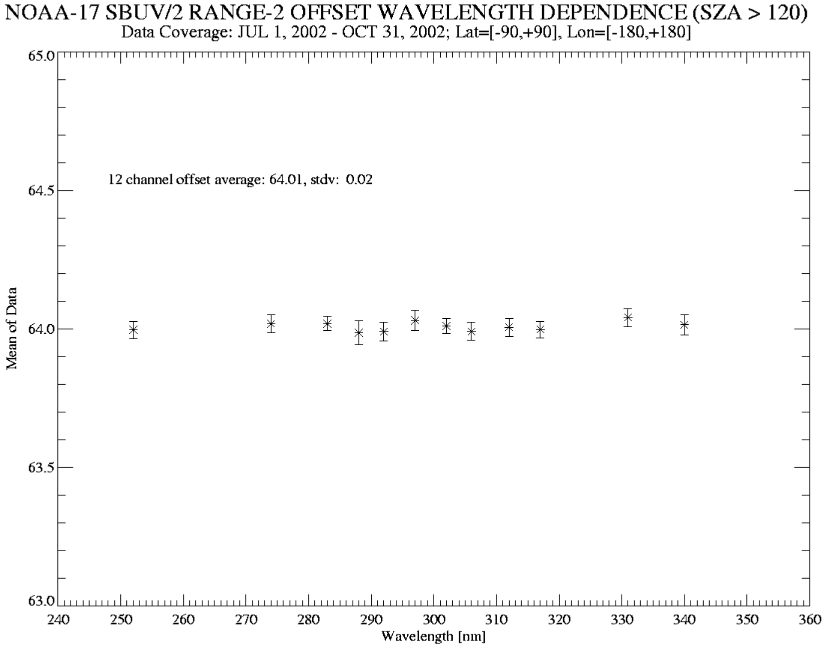

Figure 5.5: Spectral dependence of Range 2 offset, July-October 2002.

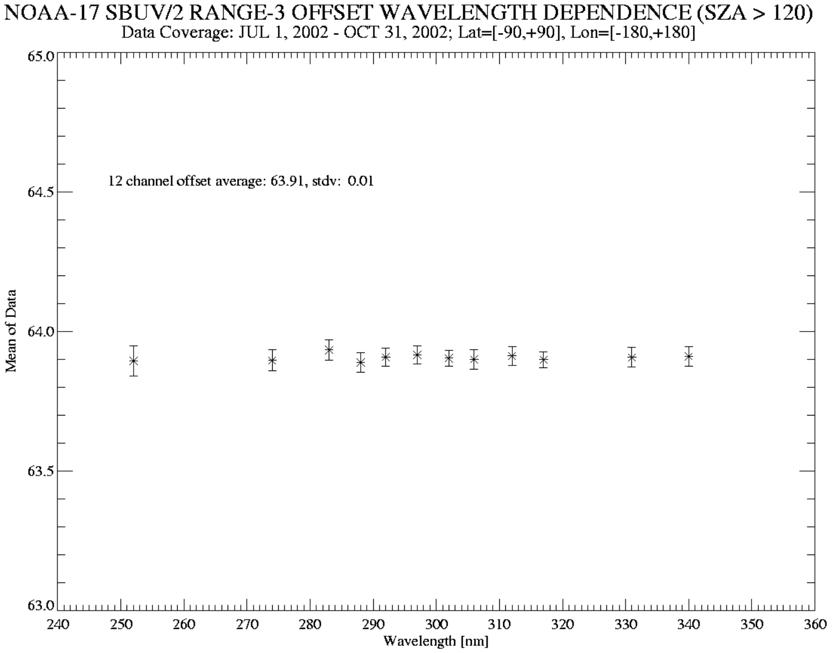

Figure 5.6: Spectral dependence of Range 3 anode offset, July-October 2002.

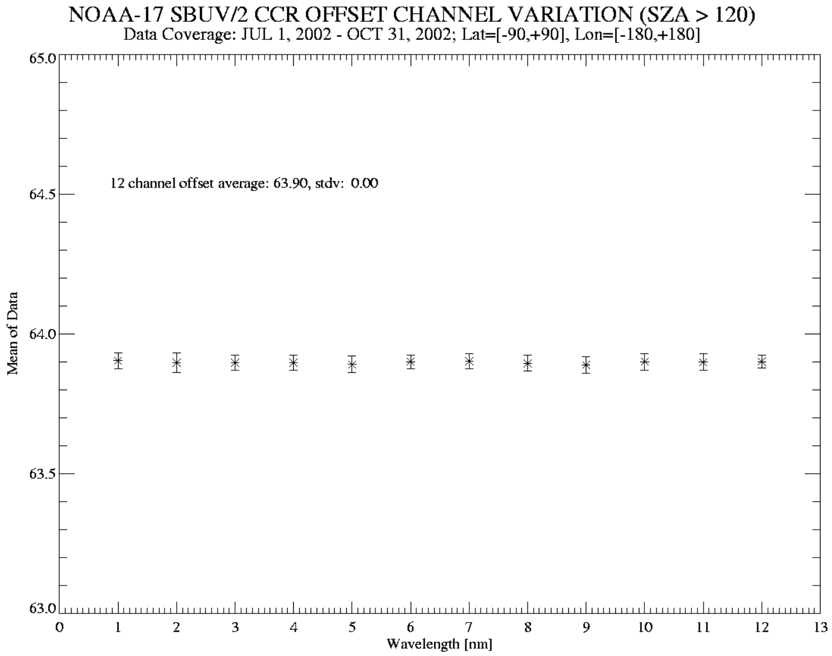
NOAA-17 SBUV/2 CCR OFFSET CHANNEL VARIATION (SZA > 120)

Data Coverage: JUL 1, 2002 - OCT 31, 2002; Lat=[-90,+90], Lon=[-180,+180]

Figure 5.7: Spectral dependence of CCR offset, July-October 2002.

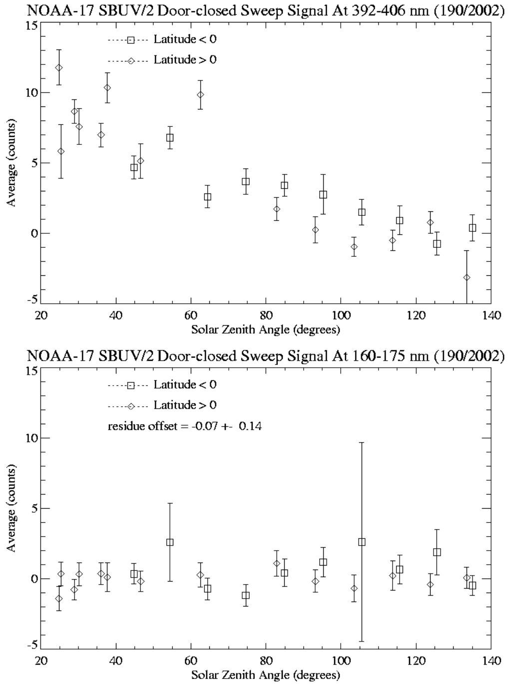
NOAA-17 SBUV/2 Door-closed Sweep Signal At 392-406 nm (190/2002)

NOAA-17 SBUV/2 Door-closed Sweep Signal At 160-175 nm (190/2002)

Figure 5.8: Sweep mode Range 1 offset *vs*. solar zenith angle for 2002 day 190: (*top*) 392-406 nm; (*bottom*) 160-175 nm.

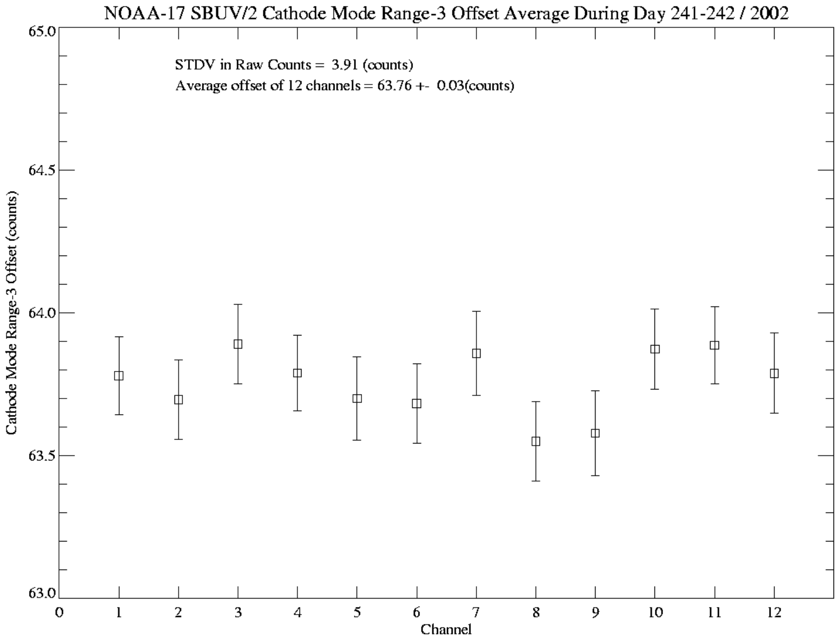

Figure 5.9: Spectral dependence of Range 3 cathode offset, 2002 days 241-242.

6. Wavelength Calibration

The prelaunch wavelength calibrations were performed at Ball Aerospace in July 1991 with four hollow cathode discharge tubes (Pt-Ne, Zn-Ne, Mg-Ne and Cr-Cu-Ne) and a low pressure mercury arc lamp. An integration sphere, illuminated by each lamp, provided a depolarized uniform spectral source. A reliable wavelength calibration must be performed with narrow spectral lines that are well understood and with uniform coverage of the full spectral range. A total of 10 spectral lines, 7 from the hollow cathode discharge tubes and 3 from the mercury lamp, were used to derive the wavelength calibration. The SBUV/2 instrument also has an on-board wavelength calibration system to monitor the wavelength stability. The on-board system has a mercury lamp-door assembly, which is generally considered to provide less usable spectral lines and less uniform illumination than the laboratory system. Because of the variety and stability of the spectral sources in the laboratory, we would expect the prelaunch wavelength calibration to be more reliable than the on-board wavelength calibration. The relationship between instrument grating position and wavelength is defined by Equation 6.1, where A_0, A_1, and A_2 represent the Ebert coefficients.

$$\lambda = A_0 * \mathit{sin}(A_1*(A_2+\mathrm{GPOS})) \qquad [6.1]$$

There were 106 wavelength calibration measurements taken during the 10 years before launch to evaluate the stability of the instrument wavelength scale. Most of these measurements were taken during the course of other calibration tests, and therefore only the major Hg emission lines at 185.0, 253.7, and 404.7 nm were tracked. In September 1991, shortly after the reference prelaunch wavelength calibration, additional tests showed a shift of about 1 grating position step in the spectral line positions. Ebert coefficients derived from the prelaunch wavelength calibrations were modified to follow this 1-step change. The adjusted Hg line positions derived from the September 1991 calibration are called the baseline positions for later analysis of wavelength scale stability. The modified Ebert coefficients recommended for NOAA-17 SBUV/2 on-orbit operation are listed in Table 6.1.

6.1. Sweep Mode

Extensive on-board wavelength calibrations in sweep mode were performed during the first 4 months in orbit. The sweep mode wavelength calibration sequence performs 10 scans over the wavelength range 160-406 nm. The first 4 scans are in diffuser view, followed by 2 scans in lamp view, 2 scans in diffuser view and 2 scans in lamp view (see Figure 11.2). Scans 5-9 are typically used for wavelength calibration. The Hg lamp is warming up and stabilizing during scans 1-4, and scan 10 is occasionally contaminated by solar light. In sweep mode, each data sample represents two consecutive steps of the grating drive, so that the average grating position during signal integration is approximately 0.5 GPOS less than the grating position at the end of the signal integration (when discrete mode grating position values are obtained). Thus, we expect the sweep mode wavelength calibration to be shifted by 0.5 GPOS in comparison with discrete mode for the same wavelength. In addition, sweep mode grating position values are recorded only for every tenth sample, requiring interpolation to assign GPOS values to intervening samples. As noted in Section 4, no grating drive errors have been observed for NOAA-17 SBUV/2.

All data were processed with the corrections derived in this report for offset, thermal drift, nonlinearity and converted to Range 3 counts. Figure 6.1 shows an example of the observed sweep mode line profile at 185.0 nm. The centroid of the line profile is defined as the intensity-weighted average grating position over 16 or 17 samples around the peak, depending on how the line is centered with respect to the sampled grating positions. In the prelaunch analysis, the sample with maximum intensity was defined as the center of the line profile and 15 points around the center were taken for the average. When we simulated the prelaunch calculation algorithm using in flight data, the two algorithms agreed to better than 0.05 GPOS. Even though the grating position with the intensity maximum in a spectral scan is often not the center of the line profile, the bias in the centroid calculation can be negligibly small as long as the background is negligible relative to the line peak intensity and the full line profile (32 or more grating steps) is covered for the average. We also determined line center positions using linear regression fits to 4 data points on each side of the profile. Two or three points near the peak are excluded from the fitting since they deviate from an ideal triangle model.

The line center values were very stable in the first 4 months. Figures 6.2*a*-*c* show time history plots of the sweep mode line center positions from lamp view measurements derived using the centroid method (×) and linear regression method (☐). Table 6.2 lists the differences between the centroid and the fitted peak positions. These values are very consistent for most lines except at 404.8 nm. It is not clear why the two methods have this large difference of 0.43 steps for the 404.8 nm. The base line of sweep mode centroids in September 1991, corrected for air-to-vacuum wavelength changes, are also plotted in Figure 6.2 for comparison. Prelaunch and in-flight values agree with each other within 0.12 GPOS at 253.7 nm, 0.25 GPOS at 404.8 nm, but differ by 0.87 GPOS at 185.0 nm. The intensities of the 185 and 405 nm lines are 2 orders of magnitude weaker than the 254 nm line, which could affect the centroid calculation algorithms. Sweep mode signal levels from diffuser view measurements are an additional 2 orders of magnitude weaker in intensity. Therefore, quantitative diffuser view results for individual lines are not presented here. A brief qualitative discussion is given in Section 6.5.

6.2. 4-step Discrete Mode

At the end of each sweep mode wavelength calibration sequence, a series of lamp view discrete mode scans over the 253.7 nm line are executed, with the grating drive moving 4 steps between samples. Figure 6.3 shows an example of the spectral line profiles measured on October 30, 2002. The centroid was calculated as the intensity-weighted average grating position average over 11 samples around the peak from GPOS = 656 to GPOS = 696. Inclusion of the sample at GPOS = 652 would shift the calculated centroid by ΔGPOS = –0.04. The peak position also can be characterized by fitting two straight lines to 3 data points on each side of the peak, respectively. The peak grating position derived using this method is only about 0.02 GPOS smaller than the centroid calculation result.

Figure 6.4 shows the time history of inflight 4-step discrete mode measurements for NOAA-17. The error bar in each measurement is the standard deviation of 9 scans, which is substantially smaller than the day-to-day variations. The first two measurements were about 0.15 GPOS higher than all other measurements because the scan was initially performed at odd numbers of the grating steps, later shifted to the even numbers of the grating steps. Excluding the initial 2 points, the day-to-day variation is less than 0.02 GPOS. Thus, the wavelength scale is very stable during the first four months.

6.3. 2-step Discrete Mode

The wavelengths listed in Table 6.2 were also measured in the 2-step discrete mode for wavelength calibration in August 2002. Each calibration sequence had about 60 scans grouped in both lamp view and diffuser view. Each spectral line profile was scanned with a 2-step grating position increment. About 20 scans were selected from each viewing condition after the lamp warming up. Details of the discrete calibration sequence are illustrated in Figure 11.7.

The spectral coverage of the 2-step discrete scans is not sufficient to use the intensity-weighted method to calculate the line center position. Therefore, the line peak position is estimated using two straight lines fitted respectively to 4 data points on the 2 sides of the line profile. Figures 6.6*a-c* show examples of the measured spectral line profiles. As with the sweep mode analysis, the centermost samples are excluded from the regression fits. Table 6.3 lists the derived centroids that are equal to the fitted peak positions plus the difference between the centroid and the fitted peak position in the sweep mode.

The centroids of the mercury lines in the prelaunch wavelength calibration in position mode, corrected for the air-to-vacuum wavelength differences, are also listed in Table 6.3. They are about 1 step lower than the values derived in orbit. This result is consistent with the Ebert coefficient shift described in the introduction to this section, and represents on-orbit confirmation of the laboratory correction.

6.4. Inflight Ebert Coefficients

The orbital measurements of the on-board Hg lamp spectral lines can also be used to derive the wavelength calibration. The centroids in both sweep and discrete modes are separately fit using the following equation, which is inverted from Equation 6.1:

$$GPOS = \arcsin\left(\lambda / a_0\right) / a_1 - a_2 \qquad [6.2]$$

A nonlinear regression procedure, CURVEFIT in the IDL program library, is used for calculation of the line center grating position. Each centroid or the peak position of the six mercury lines is weighted according to its standard deviation. Derived Ebert coefficients are also listed in Table 6.1 for comparison with the prelaunch calibration.

In order to evaluate the collective effect of the differences between sets of Ebert coefficients, we calculated reference wavelengths for all four sets of coefficients (discrete and sweep, prelaunch and inflight), using the line center positions observed during inflight wavelength calibrations. Figures 6.7 show differences between the calculated and referenced wavelengths. The fitting procedure in the present calibration was weighted according to the measurement error bars. Therefore, the residual wavelength errors for the strong lines are much smaller than those for the weak lines. The largest deviations at 185 nm are due to the discrepancies in the centroids, as mentioned in Section 6.1. Since these results are all within ±0.5 GPOS of the nominal values, we find no reason to revise the prelaunch wavelength calibration.

6.5. Wavelength Scale Comparison Between Earth View and Solar View Data

We examined Hg lamp view and diffuser view data to verify that the wavelength calibration is consistent between Earth view and solar view measurements. The Hg lamp centroids for these operational modes are listed in Table 6.4 and Table 6.5. Most of the results are in excellent agreement, although larger differences are seen at 253.7 nm. We also made comparisons between sweep Earth radiance and solar irradiance spectra. Because the solar spectrum contains many Fraunhofer absorption lines that are also present in backscattered radiance data, any difference in the wavelength scale between irradiance and radiance spectra will appear as small-scale fluctuations in a spectral ratio. Shifting the wavelength scale for the earth radiance data to minimize noise in the ratio then provides a quantitative estimate of wavelength shift. We used an average of 33 Earth view scans between ±20° latitudes in October 2002 for radiance data, and an average of 15 solar scans in the same period for irradiance data. The albedo spectrum was ratioed to a smoothed version of itself to reduce the dynamic range, where the smoothed albedo spectrum was created using 3 applications of a 14-point boxcar average. The top panel in Figure 6.8 shows the results with no wavelength shift. The low frequency features in the 300-340 nm wavelength region are due to the ozone absorption spectrum. Standard deviations of the ratio in the 340-405 nm region were calculated using a cubic spline shift of the radiance spectrum, and the results are plotted in bottom panel in Figure 6.8. The standard deviation was minimized with a wavelength shift of $\Delta\lambda = -0.0038$ nm, which has a negligible effect on the albedo ratio, as shown by the middle panel in Figure 6.8. We conclude that a single wavelength calibration is appropriate for both diffuser and direct view data.

6.6. Instrument Bandpass

In the SBUV/2 forward model calculation for ozone processing, the width of the instrument slit function is required. During the prelaunch wavelength calibration, slit function widths are determined for the same set of spectral lines. The full width of the bandpass at half maximum intensity (FWHM) is derived from linear extrapolation of measurements. Table 6.6 lists the results as reported in Data Book. We derived the slit function width from inflight sweep mode data for the Hg lamp lines, and obtained the results listed in Table 6.7. The wings of the line profile were interpolated and subtracted from the line profile. In the FWHM calculation, the peak intensity is defined as the maximum of the cubic spline interpolated profile, and the half maximum is then determined from linear fitting. The on-orbit bandpass values in Table 6.7 are larger than the prelaunch values at 185.0 and 253.7 nm. Some increase in bandpass is expected in sweep mode due to the 2-step integration process. It is also possible that the optical alignment changed slightly since the reference measurements in 1991. We also calculated the slit function width from discrete mode data. Without the background subtraction, the width in discrete mode is overestimated slightly and not listed here. For NOAA-17 SBUV/2 operational ozone processing, an average of the prelaunch data was used to create a bandpass value of 1.096 nm.

TABLE 6.1
Ebert Coefficients

Coefficient	***Prelaunch***		***Inflight***	
	Discrete	***Sweep***	***Discrete***	***Sweep***
a_0	**820.0**	**820.0**	816.517	815.086
a_1	**-9.58790×10^{-5}**	**-9.58838×10^{-5}**	$-9.62684\text{x}10^{-5}$	$-9.64638\text{x}10^{-5}$
a_2	**–3956.8**	**–3957.0**	–3728.78	–3728.43

TABLE 6.2
Sweep Mode Hg Lamp Line Centers: Inflight

Wavelength [nm]	***Line Position*** **[centroid method]**	***Line Position*** **[regression method]**	***Difference*** **[cent. – reg.]**
184.950	1583.89	1583.89	0.00
253.733	676.33	676.28	0.05
289.449	194.52	194.53	–0.01
296.819	94.16	94.13	0.03
334.249	–421.80	–421.84	0.04
404.776	–1427.30	–1426.87	–0.43

TABLE 6.3
2-step Discrete Mode Hg Lamp Line Centers: Inflight

Wavelength [nm]	***Line Position*** **[prelaunch, centroid]**	***Line Position*** **[inflight, centroid]**	***Difference*** **[inflt. – pre.]**
184.95	1584.56	1583.43	–1.13
253.73	676.79	675.89	–0.90
289.44	—	194.13	—
296.81	—	93.81	—
334.24	—	–422.07	—
404.77	–1426.78	–1427.68	–1.10

TABLE 6.4
Line Centroid Comparison: Discrete Mode

Reference Wavelength [nm]	***Lamp View Centroids***	***Diffuser View Centroids***	***Difference***
184.950	1583.43(±0.01)	1583.43(±0.04)	0.00(±0.04)
253.728	675.89(±0.01)	676.03(±0.02)	0.14(±0.02)
289.444	194.13(±0.06)	194.18(±0.68)	0.05(±0.68)
296.814	93.81(±0.01)	93.87(±0.06)	0.06(±0.06)
334.244	–422.07(±0.04)	–421.99(±0.46)	0.08(±0.46)
404.770	–1427.68(±0.02)	–1427.63(±0.03)	0.05(±0.04)

TABLE 6.5
Line Centroid Comparison: Sweep Mode

Reference Wavelength [nm]	***Lamp View Centroids***	***Diffuser View Centroids***	***Difference***
184.950	1583.87(±0.01)	1583.84(±0.01)	–0.03(±0.02)
253.728	676.32(±0.01)	676.12(±0.01)	–0.20(±0.02)
289.444	194.52(±0.03)	194.60(±1.21)	0.08(±1.21)
296.814	94.15(±0.01)	94.24(±0.04)	0.09(±0.04)
334.244	–421.80(±0.02)	–421.68(±0.46)	0.12(±0.46)
404.770	–1427.29(±0.01)	–1427.21(±0.01)	0.08(±0.02)

TABLE 6.6
Spectral Resolution in Discrete Mode Based on Prelaunch Wavelength Calibration

Wavelength [nm]	***FWHM*** [nm]
184.900	1.0799
253.666	1.0636
285.228	1.0660
299.812	1.1107
306.487	1.1095
307.606	1.1022
324.771	1.0913
327.413	1.1137
404.676	1.1275
average	1.0960(±0.0223)

TABLE 6.7
Spectral Resolution in Sweep Mode Based on A&E Tests

Wavelength [nm]	***Lamp View***		***Diffuser View***	
	Triangle [nm]	***FWHM*** [nm]	***Triangle*** [nm]	***FWHM*** [nm]
184.950	2.1845(±0.0012)	1.1825(±0.0060)	2.1922(±0.0058)	1.1836(±0.0050)
253.733	2.1483(±0.0007)	1.1413(±0.0003)	2.1518(±0.0016)	1.1507(±0.0051}
404.776	2.0532(±0.0047)	1.1065(±0.0037)	2.0603(±0.0048)	1.1098(±0.0022)

TABLE 6.8

Recommended Operational Grating Positions and Wavelengths

Channel	*OZONE Grating Position*	*Calculated Wavelength* [nm]	*Mg II Grating Position*	*Calculated Wavelength* [nm]
1	700	**251.911**	365	276.841
2	410	**273.509**	363	276.989
3	281	**283.049**	347	278.173
4	219	**287.619**	339	278.765
5	157	**292.178**	325	279.799
6	84	**297.534**	323	279.947
7	24	**301.925**	321	280.095
8	–29	**305.795**	311	280.834
9	–121	**312.494**	305	281.277
10	–190	**317.503**	297	281.868
11	–380	**331.222**	281	283.049
12	–500	**339.830**	279	283.196
CCR	—	**378.62**	—	378.62

TABLE 6.9

Special Test Grating Positions and Wavelengths

Channel	*CCR Grating Position*	*Calculated Wavelength* [nm]	SO_2 *Grating Position*	*Calculated Wavelength* [nm]	*EP/TOMS Grating Position*	*Calculated Wavelength* [nm]
1	-1033	**377.507**	-643	**350.03**	-68	**308.64**
2	-1049	**378.623**	-500	**339.83**	-122	**312.57**
3	-1065	**379.739**	-377	**331.01**	-191	**317.58**
4	-1033	**377.507**	-128	**313.00**	-257	**322.35**
5	-1049	**378.623**	-116	**312.13**	-381	**331.29**
6	-1065	**379.739**	-96	**310.68**	-789	**360.38**
7	-1033	**377.507**	-84	**309.08**	-1069	**380.02**
8	-1049	**378.623**	-128	**313.00**	-29	**305.80**
9	-1065	**379.739**	-116	**312.13**	-121	**312.49**
10	-1033	**377.507**	-96	**310.68**	-190	**317.50**
11	-1049	**378.623**	-84	**309.08**	-380	**331.22**
12	-1065	**379.739**	-643	**350.03**	-500	**339.83**

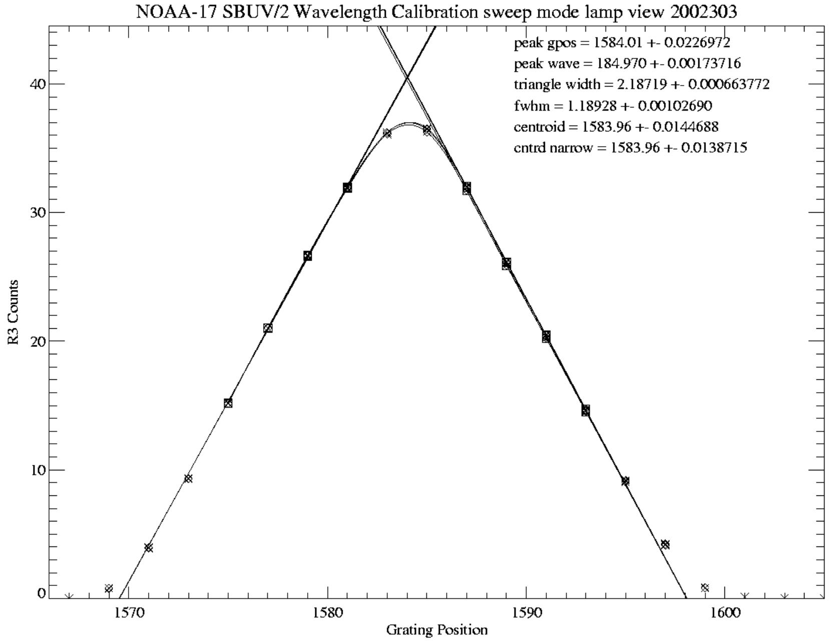

Figure 6.1: Mercury lamp sweep mode line profile at 185.0 nm.

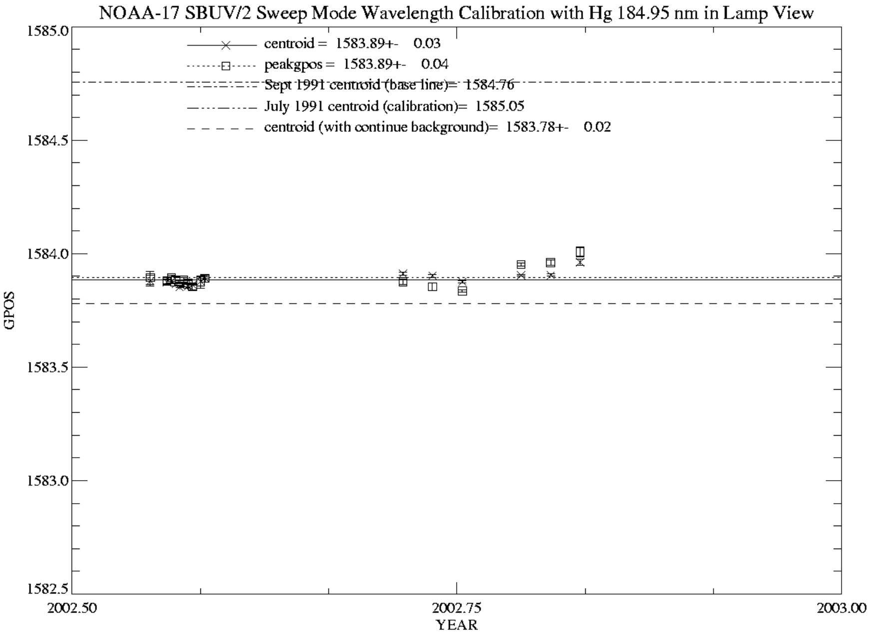

Figure 6.2: (*a*) Sweep mode line center time dependence at 185.0 nm.

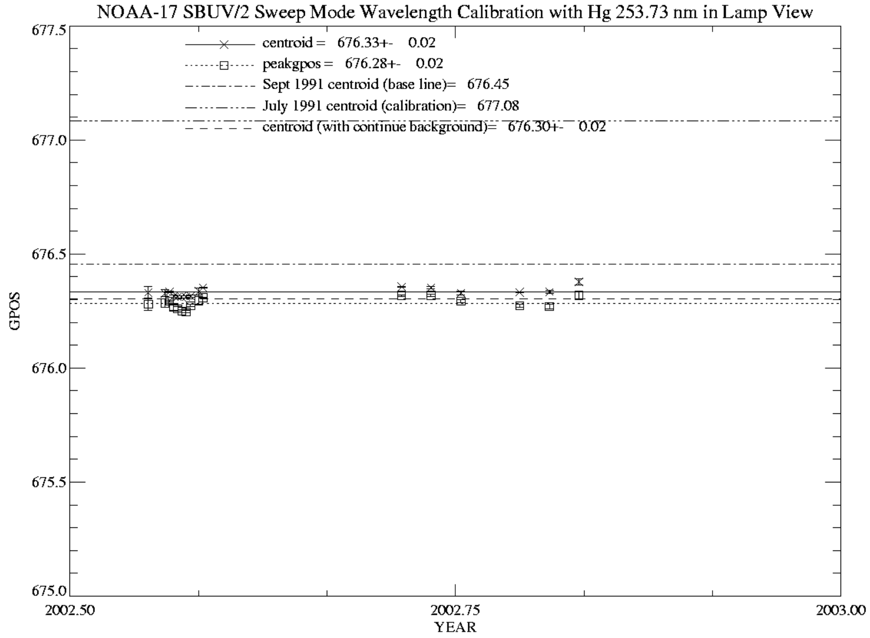

Figure 6.2: (*b*) Sweep mode line center time dependence at 253.7 nm.

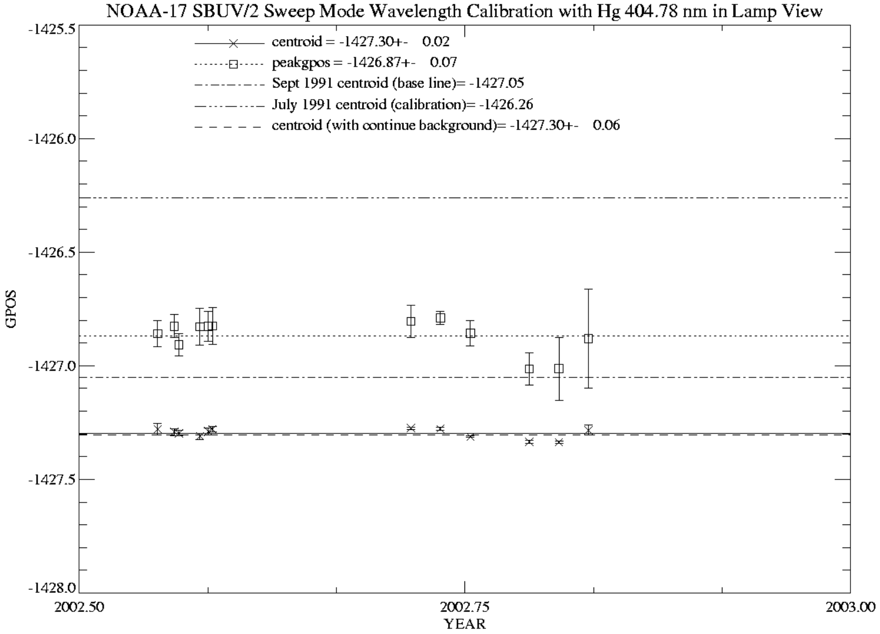

Figure 6.2: (*c*) Sweep mode line center time dependence at 404.8 nm.

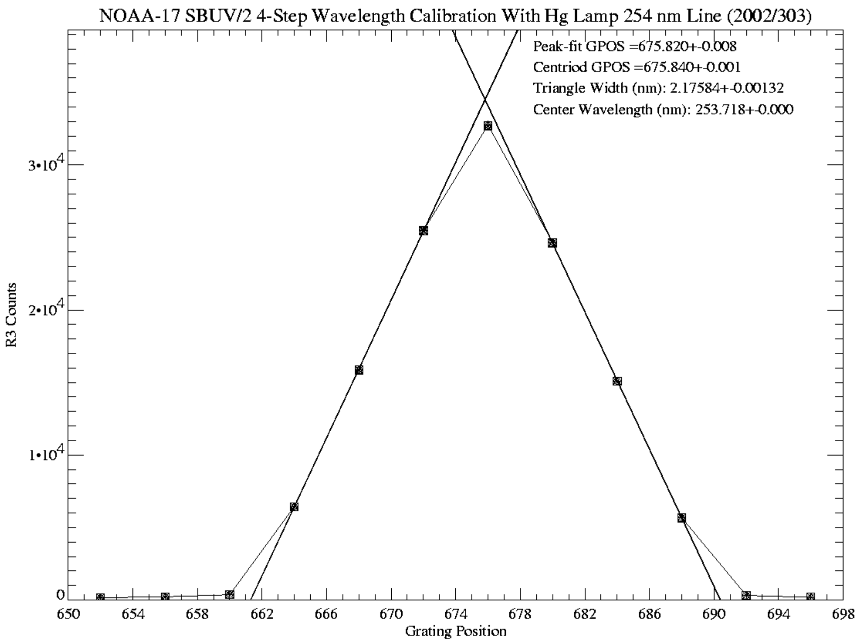

Figure 6.3: Discrete mode line profile at 253.7 nm (4-step sampling).

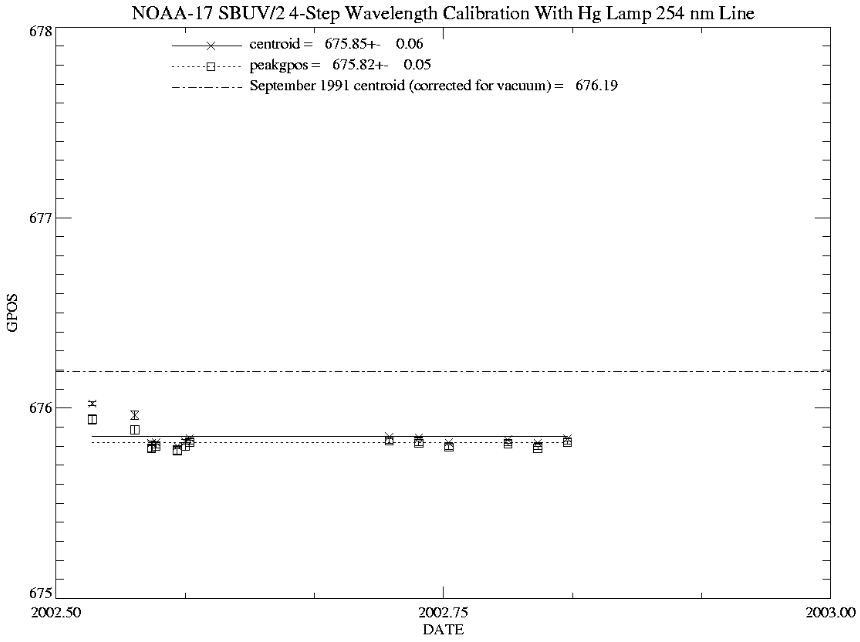

Figure 6.4: Discrete mode (4-step sampling) line center time dependence at 253.7 nm.

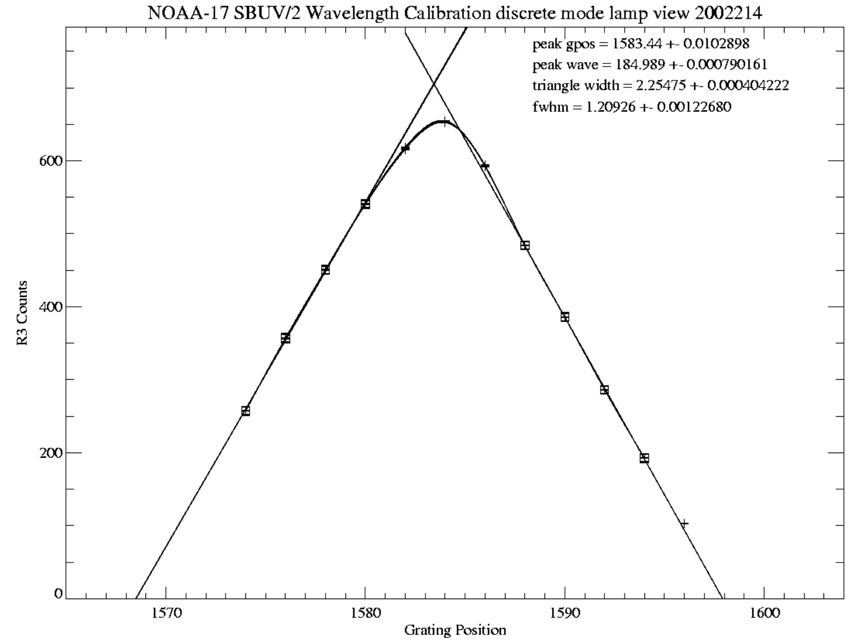

Figure 6.5: Discrete mode line profile at 185.0 nm (2-step sampling).

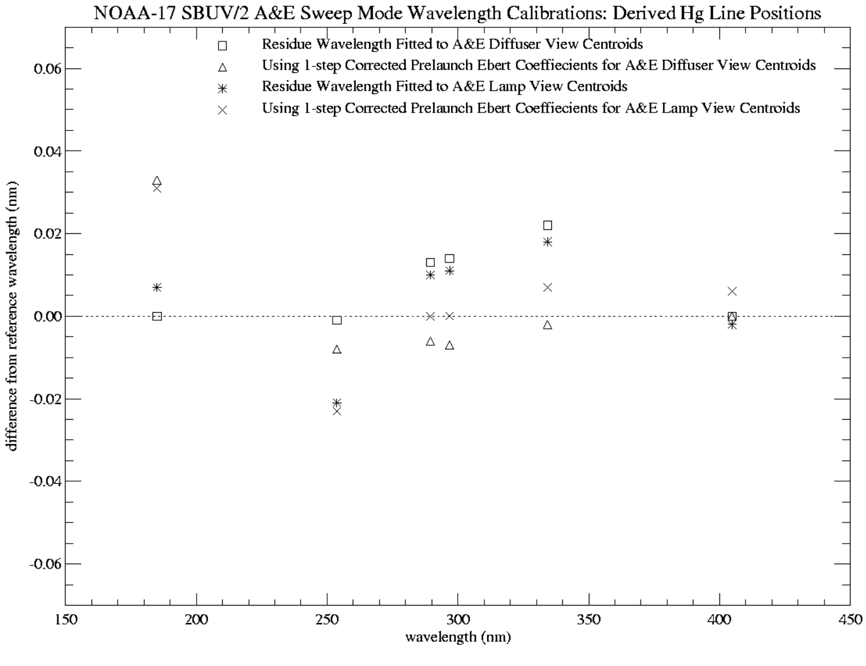

Figure 6.6: (*a*) Wavelength residuals for derived Hg lamp line positions: Sweep mode data.

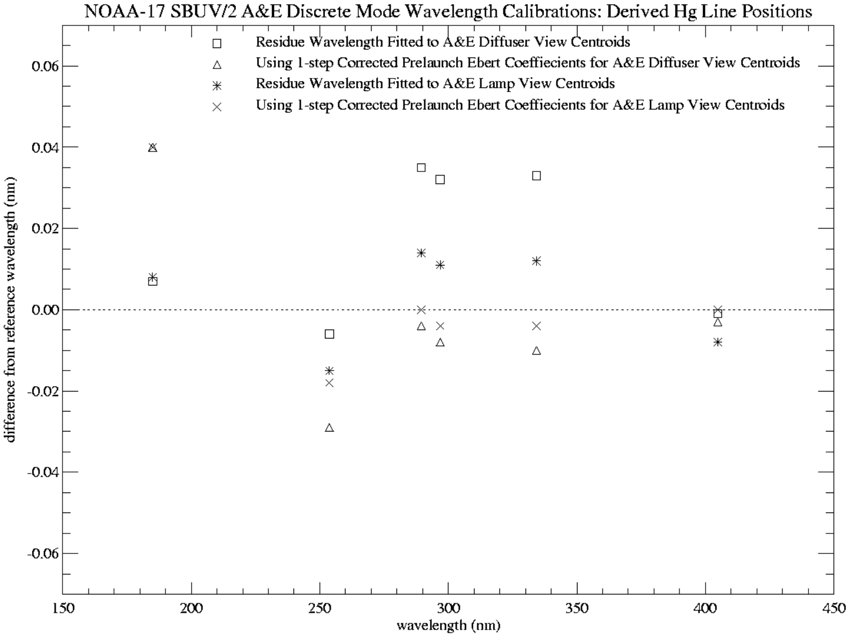

Figure 6.6: (*b*) Wavelength residuals for derived Hg lamp line positions: Discrete mode data.

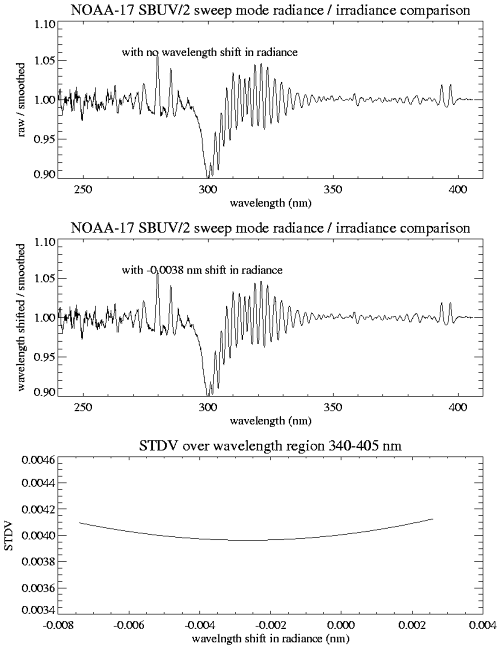

Figure 6.7: Sweep mode wavelength calibration comparison (Earth view *vs.* solar view): (*a*) Normalized albedo; (*b*) Albedo spectrally shifted to minimize residual; (*c*) Variation of 340-405 nm residual with wavelength shift.

7. Goniometric Calibration

7.1. Prelaunch Characterization

The SBUV/2 instrument views the Sun using a reflecting diffuser plate to direct solar illumination into the nadir-viewing aperture and fill the field of view. Solar measurements are made at high incidence angles on the diffuser ($\theta \approx$ 55-80°). The diffuser has an approximately Lambertian (*cos*θ) response, so that the observed signal from a constant source varies by a factor of 2.0-3.0 during a typical inflight measurement sequence. Ball Aerospace performs prelaunch laboratory calibrations to characterize this goniometric response as a function of elevation angle [α] and azimuth angle [β]. Data are taken on a regular grid ($\Delta\alpha = 2°$, $\Delta\beta = 5°$), then normalized to a reference orientation of $\alpha = 0°$, $\beta_{inst} = 34°$. These values are chosen because they are the closest measurement positions to the angles used for radiometric calibration measurements. Goniometric measurements are made at two wavelengths (254, 405 nm) using a mercury lamp, and at four wavelengths (270, 300, 350, 406 nm) using a FEL lamp. An example of the raw FEL data at 406 nm is shown in Figure 7.1, where the data are expressed as the inverse of the measured response to illustrate the correction needed for solar irradiance processing. The measurement angles have been converted to spacecraft-centered coordinates for convenience, where $\beta_{S/C} = \beta_{inst} + \beta_{ref}$, and $\beta_{ref} = 26.01°$.

FM#6 prelaunch goniometric data were taken in December 1993 and January 1994, using a diffuser incidence angle of 62° (diffuser deployed 28° below the spacecraft). In 1996-1997, the FM#6, FM#7, and FM#8 instruments were modified to reduce the incidence angle by increasing the diffuser deployment angle to 37°. No FM#6 laboratory goniometry data were taken in the new configuration. FM#7 and FM#8 laboratory goniometry data are available in the new configuration. The ratio of FM#7 data at the new diffuser angle to FM#5 data at the old diffuser angle data is shown in Figure 7.2. Separate comparisons of FM#7 and FM#8 show that their goniometric responses agree to within ~2%. FM#6 prelaunch goniometry data were multiplied by the FM#7/FM#5 ratio shown in Figure 7.2 to create a baseline FM#6 goniometry data set suitable for creating a smooth function for on-orbit use.

7.2. On-Orbit Validation

It is preferable to have a continuous goniometric correction function in α and β to process on-orbit solar irradiance data. In order to reduce the dynamic range that must be characterized, we first remove from the raw data simple geometric functions denoted by $S_1(\alpha)$ and $S_2(\beta)$, which represent the majority of the variation (Equation 7.4). This step reduces the dynamic range of the revised goniometric correction data to ~10%, as shown in Figure 7.3. Note that the azimuth angle dependence $S_2(\beta)$ has been increased to third order for FM#6, whereas a second order function was sufficient for previous instruments. The scaled data were then fit with a fourth order Taylor series expansion in α and β (Equation 7.2). The fit represents the adjusted data to approximately ±1.5%, as shown in Figure 7.4. This residual is twice as large as the results found for previous instruments. Because the residual in Figure 7.4 shows regular variations over the azimuth angle range expected for on-orbit measurements (β = 50-70°), further corrections are likely to be needed. A minimum of 6-9 months of inflight data will be needed to map out the full range of azimuth angles. A wavelength-dependent goniometric response has been observed with previous SBUV/2 instruments. We adopted the FEL 406 nm fit as the baseline goniometric correction for NOAA-17 solar irradiance measurements to best represent the wavelength region where no wavelength dependence is observed. The coefficients of this fit are given in Table 7.1. The NOAA-17 satellite is expected to have a stable orbit, with less than 30 minutes drift in Equator-crossing time during the first 5 years of operations, similar to other NOAA morning satellites. Thus, we expect to remain within the valid range of the prelaunch goniometric correction for many years.

7.3. Wavelength Dependence

Position mode solar irradiance measurements are taken over a wide range of wavelengths during A&E activities. Figure 7.5 shows the observed data at 400 nm, processed with the prelaunch goniometric correction and normalized at α = 4°. A residual elevation angle dependence is observed in the monochromator data, with a magnitude of ~1.5% at α = 20° [*top panel*]. This error was characterized by fitting the coincident CCR data [*middle panel*] with a third order function. This function is listed as Equation 7.6. After applying the cubic correction to all position mode data, a significant wavelength dependence is observed. Figure 7.6 shows elevation angle-dependent drifts of –0.5% at 400 nm (*triangle*), zero at 301.9 nm (*asterisk*), +1% at 257.9 nm (*diamond*), and +4.6% at 198.9 nm (*cross*).

Because the position mode data are taken during a relatively short period of time, there is very little variation in azimuth angle among the measurements. We therefore derived a correction for goniometric wavelength dependence as a function of λ and incidence angle θ, where the incidence angle is calculated from the spacecraft-centered elevation and azimuth. The coefficients for the third order Taylor series expansion fit (Equation 7.5) are listed in Table 7.2. The variation of this fit is shown in Figure 7.7, and is most important for sweep mode measurements because of the large increase in magnitude at $\lambda < 250$ nm.

TABLE 7.1
Standard Goniometry Fit Coefficients

Coefficient	*Term*	*Value*
C_1	—	**4.25203E-01**
C_2	α	**3.14113E-03**
C_3	β	**5.55845E-02**
C_4	α^2	**–9.53318E-06**
C_5	$\alpha\beta$	**–4.72321E-04**
C_6	β^2	**–1.44482E-03**
C_7	α^3	**1.98374E-05**
C_8	$\alpha^2\beta$	**–4.84052E-06**
C_9	$\alpha\beta^2$	**1.37440E-05**
C_{10}	β^3	**1.33511E-05**
C_{11}	α^4	**–4.24037E-07**
C_{12}	$\alpha^3\beta$	**–1.62547E-07**
C_{13}	$\alpha^2\beta^2$	**6.76082E-08**
C_{14}	$\alpha\beta^3$	**–1.06865E-07**
C_{15}	β^4	**–3.28302E-08**

TABLE 7.2
Wavelength-Dependent Goniometric Fit Coefficients

Coefficient	*Term*	*Value*
D_1	—	**–2.6895E+00**
D_2	θ	**1.3096E-01**
D_3	λ	**7.8785E-03**
D_4	θ^2	**–1.5393E-03**
D_5	$\theta\lambda$	**–1.8829E-04**
D_6	λ^2	**–5.1214E-06**
D_7	θ^3	**7.2999E-06**
D_8	$\theta^2\lambda$	**3.4639E-07**
D_9	$\theta\lambda^2$	**2.1250E-07**
D_{10}	λ^3	**–8.7160E-09**

TABLE 7.3
Goniometric Elevation Correction Coefficients

Coefficient	*Term*	*Value*
F_1	—	**1.0113E+00**
F_2	α	**–4.1771E-03**
F_3	α^2	**3.9673E-04**
F_4	α^3	**–8.8289E-06**

$$G_{corr}(\alpha,\beta,\theta,\lambda) = [G_{fit}(\alpha,\beta) * G_{norm}(\alpha_{ref}, \beta_{ref}) * S_1(\alpha) * S_2(\beta)] / [G_{wav}(\theta,\lambda) * G_{elev}(\alpha)] \quad (7.1)$$

$$G_{fit}(\alpha,\beta) = c_1 + c_2\alpha + c_3\beta + c_4\alpha^2 + c_5\alpha\beta + c_6\beta^2 + c_7\alpha^3 + c_8\alpha^2\beta + c_9\alpha\beta^2 + c_{10}\beta^3 + c_{11}\alpha^4 + c_{12}\alpha^3\beta + c_{13}\alpha^2\beta^2 + c_{14}\alpha\beta^3 + c_{15}\beta^4 \quad (7.2)$$

$$G_{norm}(\alpha_{ref}, \beta_{ref}) = \frac{1}{G_{fit}(\alpha_{ref}, \beta_{ref}) * S_1(\alpha_{ref})} \quad (7.3)$$

$$\alpha_{ref} = 0.849° \qquad \beta_{ref} = 60.211°$$

$$S_1(\alpha) = \cos(53°)/\cos(53°+\alpha) \qquad S_2(\beta) = 1 / \cos^3(\beta-\beta_{ref}) \quad (7.4)$$

$$G_{wav}(\theta,\lambda) = d_1 + d_2\theta + d_3\lambda + d_4\theta^2 + d_5\theta\lambda + d_6\lambda^2 + d_7\theta^3 + d_8\theta^2\lambda + d_9\theta\lambda^2 + d_{10}\lambda^3 \quad (7.5)$$

$$G_{elev}(\alpha) = f_1 + f_2\alpha + f_3\alpha^2 + f_4\alpha^3 \quad (7.6)$$

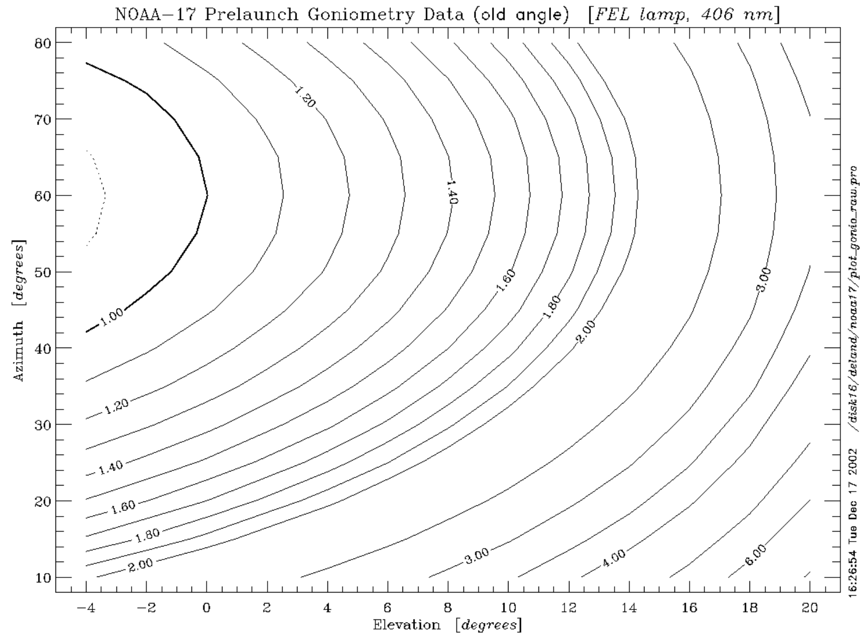

Figure 7.1: FM#6 prelaunch goniometry data at 406 nm using FEL lamp (diffuser deployment angle = 28°).

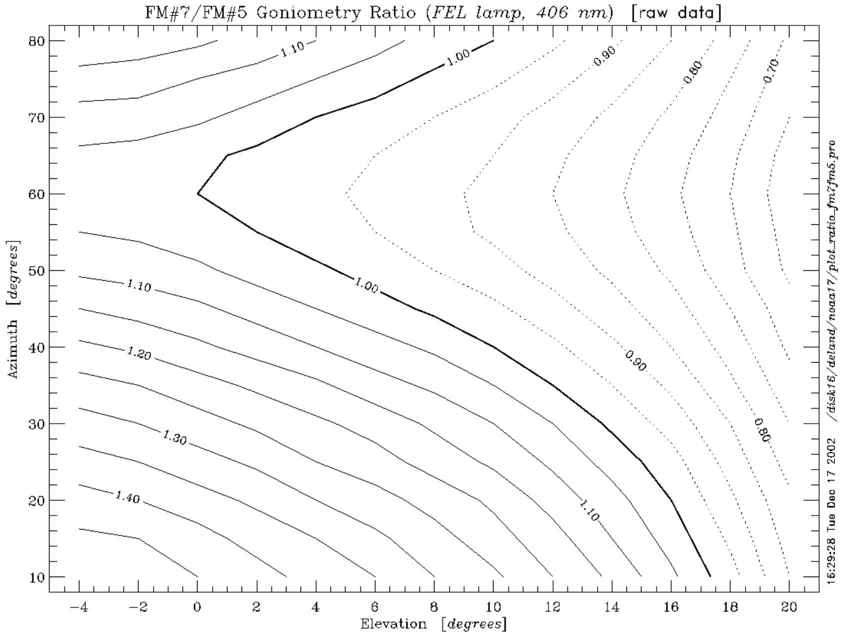

Figure 7.2: Ratio between FM#7 goniometry data taken at $\angle_{\text{deploy}}$ = 37° and FM#5 goniometry data taken at $\angle_{\text{deploy}}$ = 28°.

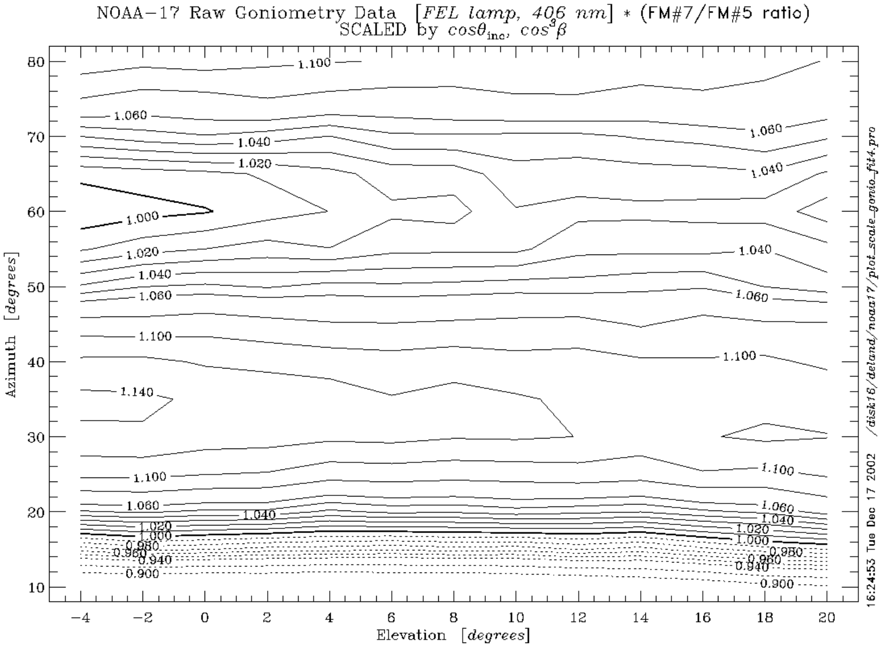

Figure 7.3: FM#6 prelaunch goniometry data scaled by deployment angle change ratio, elevation angle scaling function, azimuth angle scaling function.

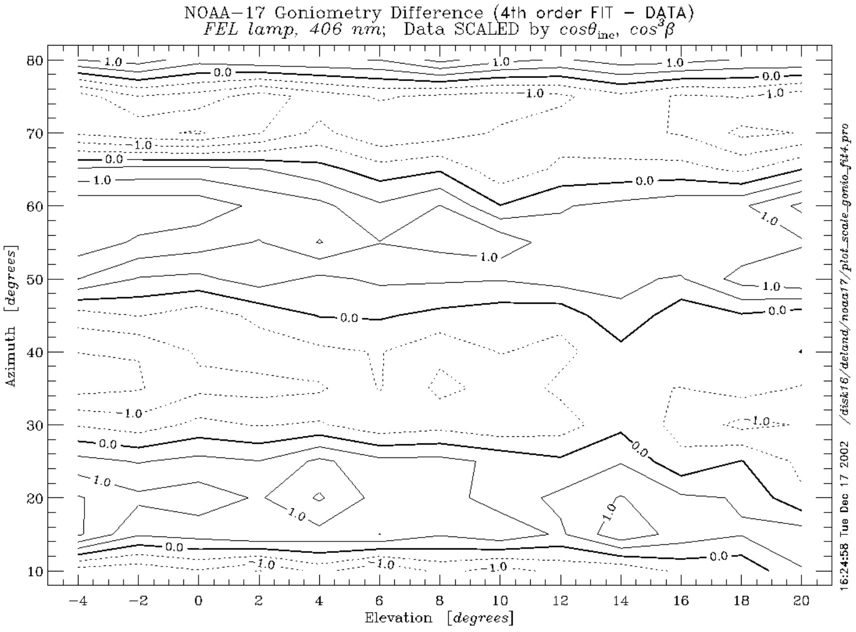

Figure 7.4: Difference in percent between 4th order fit and scaled goniometry data.

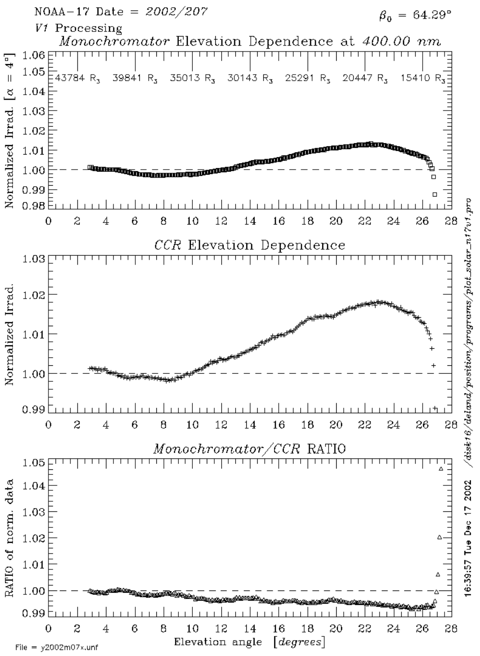

Figure 7.5: Position mode solar data at 400.0 nm processed with prelaunch goniometry: (*top*) Monochromator elevation dependence; (*middle*) CCR elevation dependence; (*bottom*) Monochromator/CCR ratio.

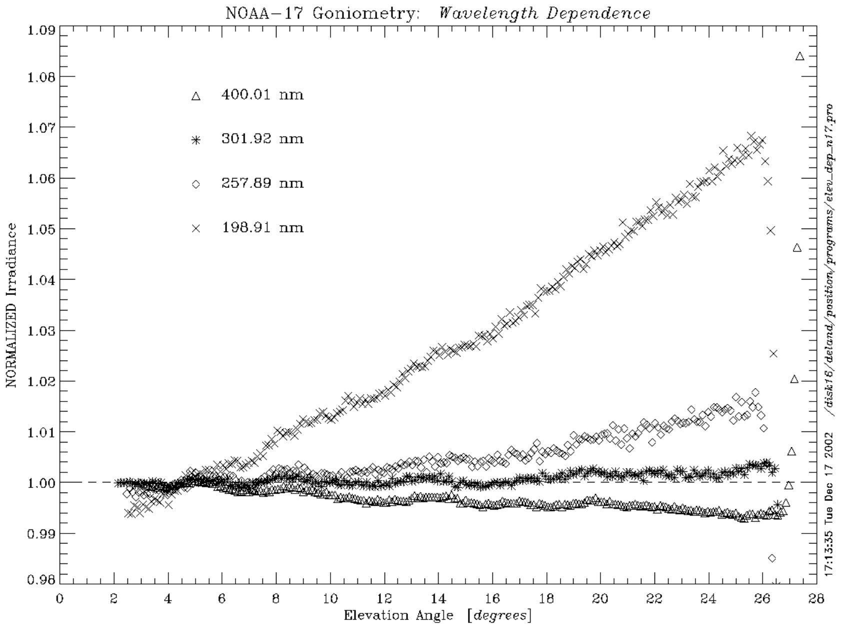

Figure 7.6: Wavelength dependence error of prelaunch goniometry.

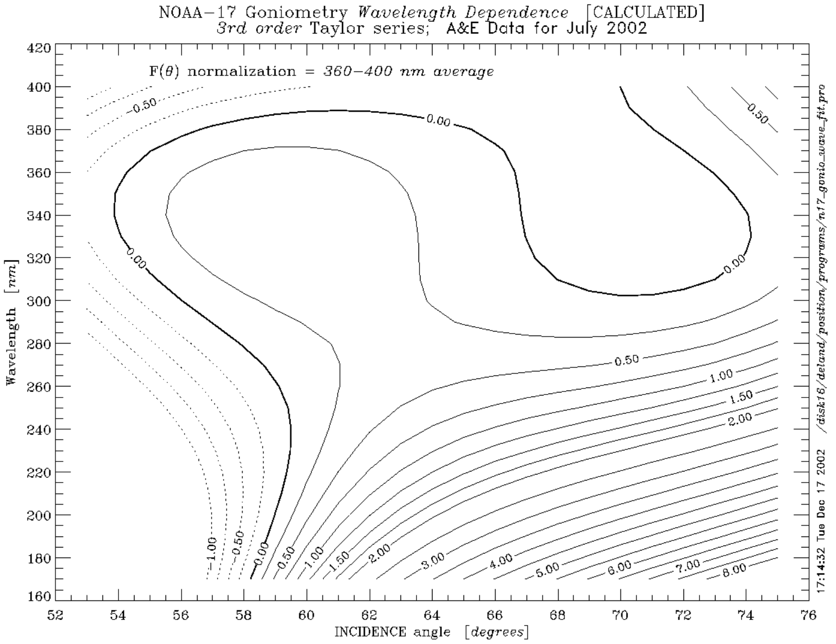

Figure 7.7: Wavelength-dependent goniometry error [*percent*]; 3rd order fit to inflight data.

8. Thermal Response

Prelaunch tests were conducted in November 1997 to characterize the sensitivity of the FM#6 radiometric response to photomultiplier tube (PMT) temperature variations. Laboratory raw data were listed in Tables 6.1 through 6.3, Volume 2A [*Ball Aerospace*, 2001]. Measurements were taken at temperatures 22.0°C, 2.0°C, 12.7°C, 31.7°C and 22.0°C in a sequence. The two measurements at 22.0°C can be used to monitor the source irradiance drift during the entire sequence. However, Ball Aerospace did not correct the lamp source irradiance drift in its derivation of the temperature coefficients in Tables 6.4 through 6.6, Volume 2A [*Ball Aerospace*, 2001]. The observed drift was greater than 2.5%, which is comparable to the sensor's thermal response change over a 30°C temperature range during the tests. We reprocessed the data with corrections for the lamp source drift. This increased the magnitude of the derived PMT temperature sensitivity by more than a factor of 2.

The PMT temperature sensitivity coefficients derived from the reprocessed data are plotted in Figure 8.1. Range 2 measurements were repeated with both Range 3 anode mode and Range 3 cathode mode, and the two sets of data were consistent with each other. Range 3 anode measurements covered a wavelength range from 310 nm to 406 nm, and they agreed very well with the results in Range 2 where the two data sets overlapped. The thermal drift is primarily related to the PMT, while the amplifier thermal effect that would cause differences between Range 2 and Range 3 anode data is often negligible. Therefore, all of the Range 2 measurements and the Range 3 anode mode measurements were fitted together to provide a temperature coefficient function for all anode outputs including Range 1. The spectral dependence uses a cubic fit between 250-360 nm, with constant values at longer and shorter wavelengths, and is shown as the solid curve in Figure 8.1.

The thermal test for Range 3 cathode mode covered only from 340 nm to 406 nm, whereas Earth view data are observed in R3C down to 300 nm. The spectral dependence of the temperature sensitivity (*diamonds*) is consistent with the anode data, since both outputs share the same PMT cathode temperature response. The average Range 3 cathode temperature sensitivity (*dot-dashed line*) is lower because the anode output includes additional thermal response from the PMT dynodes. The recommended thermal correction for Range 3 cathode data therefore uses the same spectral dependence as the anode function, adjusted in absolute value to match the laboratory data at long wavelengths. Measurements for the CCR were too noisy to determine a useful result. Therefore, no thermal correction is recommended for the CCR.

TABLE 8.1
PMT Temperature Dependence [anode data]

Wavelength Range	C_0	C_1	C_2	C_3
$\lambda < 250$ nm	–1.4704E-03	0.0	0.0	0.0
250-360 nm	–4.2078E-02	3.7451E-04	–1.1275E-06	1.1143E-09
$\lambda > 360$ nm	–1.3896E-03	0.0	0.0	0.0

$$X_{PMT} = C_0 + C_1*\lambda + C_2*\lambda^2 + C_3*\lambda^3$$

$$\text{Correction factor} = 1.0 + (X_{PMT}*(20°\text{C} - T_{PMT}))$$

PMT Temperature Dependence [cathode data]

$$X_{PMT} = C_0 + C_1*\lambda + C_2*\lambda^2 + C_3*\lambda^3 + 5.9817\text{E-}04$$

$$\text{Correction factor} = 1.0 + (X_{PMT}*(20°\text{C} - T_{PMT}))$$

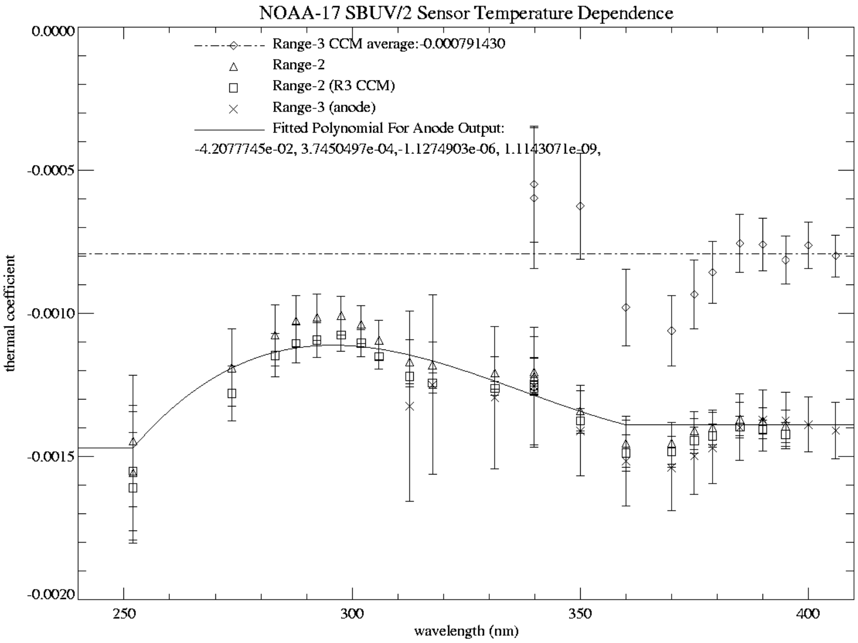

Figure 8.1: FM#6 thermal sensitivity: Radiometric calibration change for 1°C increase in PMT temperature.

9. Interrange Ratios

The SBUV/2 instrument is required to observe signals which span six orders of magnitudes in intensity with better than 1% linearity. This is accomplished, in part, by the use of three gain ranges, each accommodating a range of two orders of magnitude in signal intensity. Range 1 is the most sensitive of the three gain ranges, while Range 3 is the least sensitive. In order to process data with a single radiometric sensitivity calibration, the data are converted to a common gain range using “interrange (gain) ratio” values. When discrete mode samples are observed with low counts in Range 2 (or Range 3), the simultaneous reading in Range 1 (or Range 2) may be also valid. After correcting the raw counts in each sample for calibration, the ratio of the corrected counts gives a direct measure of the interrange ratio between Range 1 and Range 2, denoted by IRR_{12}. A comparable quantity, IRR_{23}, is defined for Range 2 and Range 3 data.

NOAA-17 SBUV/2 is the first instrument in orbit to have the capability of reading the Range 3 signal from the photomultiplier tube (PMT) anode. The Range 3 anode mode is expected to be used in routine ozone monitoring operation because it has less noise than Range 3 cathode data for total ozone wavelengths. This puts all three output ranges common with the PMT gain. Thus, the PMT gain is canceled in gain ratios derived from this operating mode. NOAA-17 SBUV/2 can also read the Range 3 output from the cathode current monitor, like all previous SBUV/2 instruments. The interrange ratio between Ranges 2 and 3 in Range 3 cathode mode ($IRR_{23}C$) characterizes the multiplication of photoelectron current from the cathode to the anode (PMT gain), including a constant factor associated with the electronics. It has a significant wavelength dependence (5-10% over total ozone wavelengths) and time dependence (*e.g.* –10% for NOAA-16 SBUV/2 in the first year). The SBUV/2 ozone retrieval algorithm does not require separate calibration of the monochromator PMT gain throughput. Nevertheless, the PMT gain change will directly affect the NOAA-17 SBUV/2 solar irradiance calibration, and represents the largest single component of the overall throughput change. For previous SBUV/2 instruments, derivation of albedo correction factor (ACF) values was simplified by first removing a smooth characterization of $IRR_{23}(t)$. In the event that the NOAA-17 SBUV/2 solar irradiance measurement is not available, independent information on changes in the PMT gain will be an essential item for accurate ozone retrieval calibration.

In selecting the data for this analysis, we limit the signal in the less sensitive gain range to lie between 350-750 counts after adjustments for the electronic offset, the thermal response and the nonlinearity. The lower limit of 350 counts is chosen to reduce the uncertainty introduced by digitization and increasing non-linearity effects. The upper limit is chosen to avoid saturation in the more sensitive range. Data values exceeding 65,535 counts cause the 16-bit counter to roll over, but can still be used for the analysis if the instrument response is not saturated. Accepting these values increases the number of samples at low SZA.

9.1 IRR_{12}

The data from Range 1 and Range 2 counters both come from the PMT anode and the preamplifier. The difference between Range 1 and Range 2 is due to the different electronic gains after branching into two different assemblies of the secondary amplifier, the voltage-frequency converter and the counter. The interrange ratio of Range 1 to Range 2 (IRR_{12}) is an electronic gain factor only. Thus, we expect little or no spectral or temporal dependence for IRR_{12}. Figure 9.1 shows the normalized time dependence of IRR_{12} measured with Channel 3 (283.1 nm). There was a 0.064% increase in the first four months, which is negligible. Figure 9.2 shows examples of measured IRR_{12} at other wavelengths relative to Channel 3, which are constant to better than ±0.1%. This confirms that IRR_{12} is constant over time, as expected.

NOAA-17 IRR_{12} values measured for all ozone wavelengths on 2002 day 193 are shown in Figure 9.3 (*squares*). Also shown in the same figure are averages for the first four months (*crosses*), which are about 0.04% higher than the first day values. The value at 273 nm is about 0.1% higher than the values at longer wavelengths, which occur later in the scan sequence. Similar wavelength-dependent behavior was seen for NOAA-11 and NOAA-16 SBUV/2, but not for NOAA-14. Valid IRR_{12} samples are obtained over a wide range of solar zenith angles, depending on the wavelength selected. Measurements for the seven longest wavelength channels were taken at SZA between 85°-95°, while the four short wavelength channels were measured at SZA between 27°-80°. There are no physical reasons to believe IRR_{12} is wavelength dependent. We believe that the behavior shown in Figure 9.3 is caused by instrumental effects experienced at high SZA as the signal strength changes rapidly. We therefore calculated IRR_{12} using only samples at SZA < 85°, which effectively limits the analysis to channels 2-5. This restriction is consistent with the current limit of the SBUV/2 ozone retrieval. The average IRR_{12} value calculated from all A&E data for these channels is **99.39**(±0.01). This value is recommended for future processing.

9.2 IRR_{23}: Range 3 Anode Mode

The difference between the Range 2 and Range 3 anode outputs is only in the electronic amplifiers and digitizers, similar to Range 1 and Range 2. Thus, the gain ratio of Range 2 to Range 3 anode mode ($IRR_{23}A$) is expected to also be wavelength independent and very stable. No prelaunch calibration results for $IRR_{23}A$ were reported in the Data Book. At SSAI's request, Ball Aerospace provided radiometric calibration data taken with the integrating sphere and external diffuser plates for further analysis. After correcting the data for non-linearity, derived $IRR_{23}A$ values at all discrete ozone wavelengths agreed within the uncertainty at each wavelength. We therefore recommended a value of $IRR_{23}A = 95.77(\pm 0.12)$ for the prelaunch calibration [*DeLand et al.*, 2002].

Figure 9.4 shows normalized daily averages of IRR_{23} measured on-orbit with Channel 8 (305.8 nm) over the first four months. The day-to-day variation is less than 0.01% (standard deviation), which is no larger than the statistical noise in the daily average. The smoothed daily average (*solid curve*) shows less than 0.05% drift, which is negligible. Figure 9.5 shows that there are no significant temporal changes in the channel-to-channel differences relative to Channel 8, as expected.

Figure 9.6 shows the spectral dependence of $IRR_{23}A$ values at total ozone wavelengths, with squares representing initial values on 2002 day 193 and crosses representing averages over the first four months. The error bars are the standard deviations in the averages. While the statistical noise is small, the maximum channel-to-channel variation is almost 0.6%. To examine any possible periodic oscillation in the sensor electronics, which exists in NOAA-16 SBUV/2 Range 3 cathode output, measurements in earth view position mode for different wavelengths were used to derive $IRR_{23}A$. The results are plotted in Figure 9.7 as a function of sample position with statistical standard errors. Data points without error bars had only a single measurement. The average of standard deviations for all valid measurements is 0.43, which is comparable with the channel-to-channel variation. Thus, no conclusion can be drawn from the position mode measurement due to poor statistics.

Another possible cause for the channel-to-channel variation is hysteresis, which was significant for NOAA-9 SBUV/2. Figure 9.8 shows monthly IRR_{23} values plotted as a function of solar zenith angle, where negative values represent Southern Hemisphere data and Positive values indicate Northern Hemisphere data. As a morning satellite, NOAA-17 emerges from the night in the Northern Hemisphere, where the sensor signal level immediately increases by several orders in magnitude. IRR_{23} values for Channels 10-12 (317.5, 331.2, 339.8 nm) at SZA = 90° are more than 1% below the prelaunch estimate, but increase ~1% by $\chi = 80°$. IRR_{23} values at these wavelengths in the Southern Hemisphere, where NOAA-17 moves from daylight into darkness, show no SZA dependence. This is consistent with the NOAA-9 hysteresis model, where decreased IRR_{23} values are only observed coming out of darkness. Channel 9 (312.5 nm) IRR_{23} data do not begin until $\chi = 83°$ in the Northern Hemisphere, and increase by ~0.3% for $\chi < 70°$. Channel 8 data show no SZA dependence or hemispheric differences. Channel 7 (301.9 nm) IRR_{23} data are available for NOAA-17 SBUV/2 at low SZA because of the increased instrument sensitivity, but show significantly more scatter than other wavelengths. The absolute value of IRR_{23} for these data is ~0.5% lower than Channel 8. Because the mechanism responsible for $IRR_{23}A$ channel-to-channel variations is not fully understood, we have derived a constant value of **95.27**(±0.25) for operational use. The uncertainty value reflects our questions about spectral dependence. The statistical uncertainty is considerably less, as shown in Figure 9.6. This revised $IRR_{23}A$ value is approximately 0.5% lower than the prelaunch calibration estimate.

9.3 IRR_{23}: Range 3 Cathode Mode

$IRR_{23}C$ is expected to be both wavelength and time dependent since it involves the PMT gain. Previous SBUV/2 instruments have shown that the behavior of $IRR_{23}C$ can be decomposed into two factors: wavelength-dependent "Day 1" values $IRR_{23}C(\lambda,t_0)$, and a wavelength-independent drift factor, $D(t)$. Prelaunch $IRR_{23}C$ wavelength dependence tests were performed in June 1991, prior to the addition of the Range 3 anode output in 1997. While the absolute IRR_{23} values were approximately a factor of 2 lower than the current instrument configuration, this represents the only time that the full wavelength range was covered. Additional $IRR_{23}C$ wavelength dependence tests were conducted in August 2000, using the wavelength range 313-405 nm. Data from both tests are shown in Figure 9.9. The 1991 data have been multiplied by a scale factor derived from measurements at common wavelengths during both sets of tests. An initial analysis using only the August 2000 data recommended a wavelength-independent value of $IRR_{23}C$ = 191.57. The solid line in Figure 9.9 shows a fifth-order polynomial fit to the combined data set. As shown by previous SBUV/2 instruments, the wavelength dependence of $IRR_{23}C$ remains unchanged even after the PMT gain degrades substantially (15-20%). If the electronic modification in 1997 did not change the voltage across the cathode and the first dynode, the wavelength dependence of the PMT gain should remain the same. Therefore, we recommend using the 5th order polynomial fit as the prelaunch calibration spectral dependence of $IRR_{23}C$.

The inflight measurements in the Range 3 cathode mode were performed for approximately 24 hours on 2002 days 241-242, which was 49 days after the first earth view radiance measurement. Average $IRR_{23}C$ values derived from these data are shown in Figure 9.10, where the measurements in earth view have 393 samples at 306 nm and 32 samples at 340 nm, and the measurement at 252 nm in solar view has only 8 samples. The $IRR_{23}C$ values derived from the earth view radiance measurements show a similar channel-to-channel variation to the IRR_{23} anode mode measurements in Figure 9.5. The different behavior at 331 nm may be due to statistical fluctuation. Further solar measurements with Range 3 cathode data are needed to determine if the difference at 252 nm is significant. The 5th order polynomial fit has been reduced by 2.7% to fit the orbital data. The weighted average of earth view measurements over 306-340 nm is 186.96, which is 2.6% lower than the wavelength-independent prelaunch $IRR_{23}C$ value. This represents a time-dependent degradation rate of approximately –1.6%/month since the first Earth view measurement on July 8. The rate would be reduced if the initial on-orbit value of $IRR_{23}C$ was lower than the prelaunch value, as appears to be true with $IRR_{23}A$. If the decrease in $IRR_{23}C$ represents a linear rate of change, the magnitude of $D(t)$ is comparable to the NOAA-16 SBUV/2 IRR_{23} behavior during the first six months of operation. Implementation of regular Range 3 cathode mode operations will allow $D(t)$ to be tracked accurately.

Interrange Ratio IRR_{12}

IRR_{12} = **99.39**(±0.01)

Interrange Ratio IRR_{23}: Range 3 anode mode

$IRR_{23}A$ = **95.27**(±0.25)

TABLE 9.1
Wavelength Dependence Fit Coefficients for $IRR_{23}C$ (Range 3 cathode mode)

Coefficient	***Value***
c_0	1.52185E+03
c_1	–2.15858E+01
c_2	1.36628E-01
c_3	–4.23508E-04
c_4	6.45184E-07
c_5	–3.87584E-10

$$IRR_{23}C(\lambda,t_0) = c_0 + c_1*\lambda + c_2*\lambda^2 + c_3*\lambda^3 + c_4*\lambda^4 + c_5*\lambda^5$$

TABLE 9.2
IRR$_{23}$C Values at Ozone Wavelengths

Channel	*Grating Position*	*Wavelength* [nm]	*IRR$_{23}$C Prelaunch*	IRR$_{23}$C 2002/241
1	700	**251.911**	189.22	184.05
2	410	**273.509**	190.82	185.60
3	281	**283.049**	191.39	186.15
4	219	**287.619**	191.61	186.37
5	157	**292.178**	191.81	186.56
6	84	**297.534**	191.99	186.74
7	24	**301.925**	192.11	186.86
8	–29	**305.795**	192.19	186.93
9	–121	**312.494**	192.27	187.02
10	–190	**317.503**	192.30	187.04
11	–380	**331.222**	192.24	186.98
12	–500	**339.830**	192.12	186.87

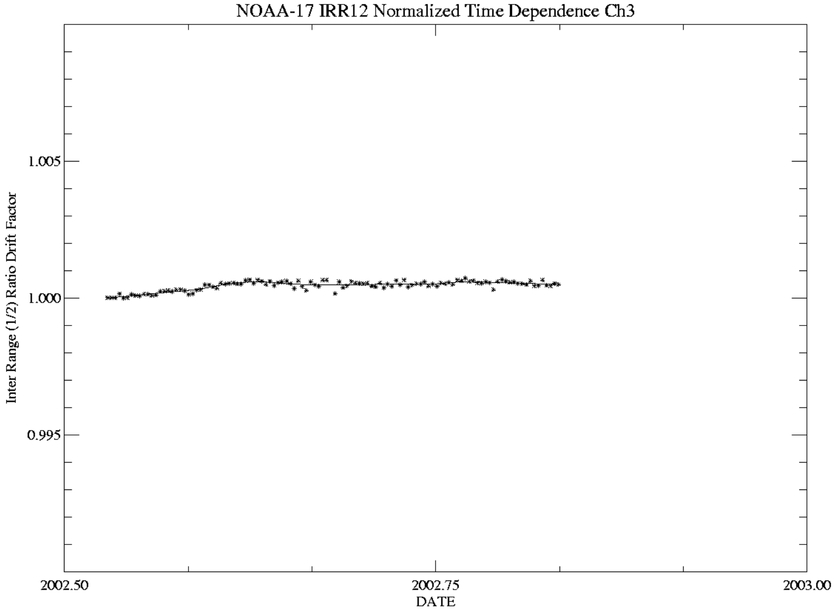

Figure 9.1: Time series of normalized IRR_{12} data at 283.0 nm.

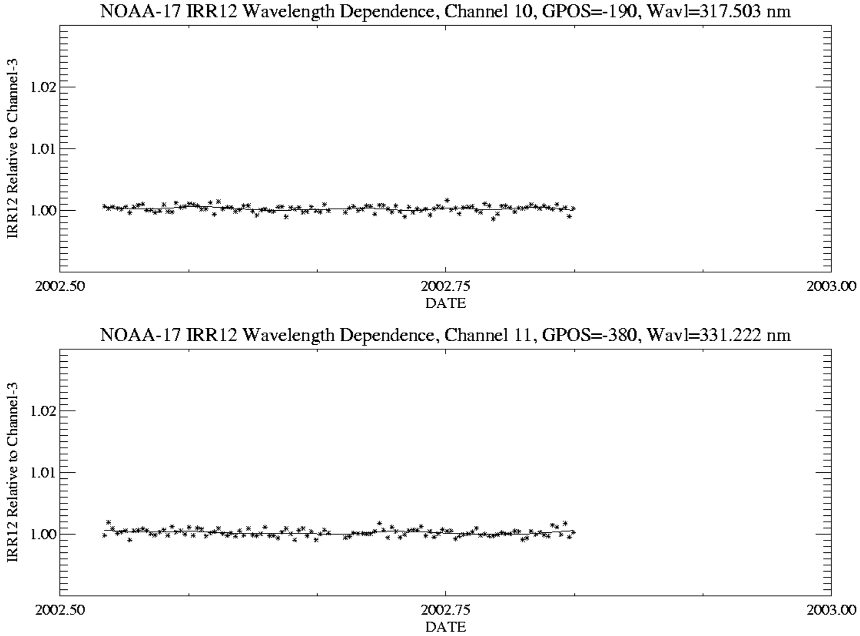

Figure 9.2: IRR_{12} spectral dependence *vs.* time: (*top*) 317.5 nm/283.0 nm; (*bottom*) 331.2 nm/283.0 nm.

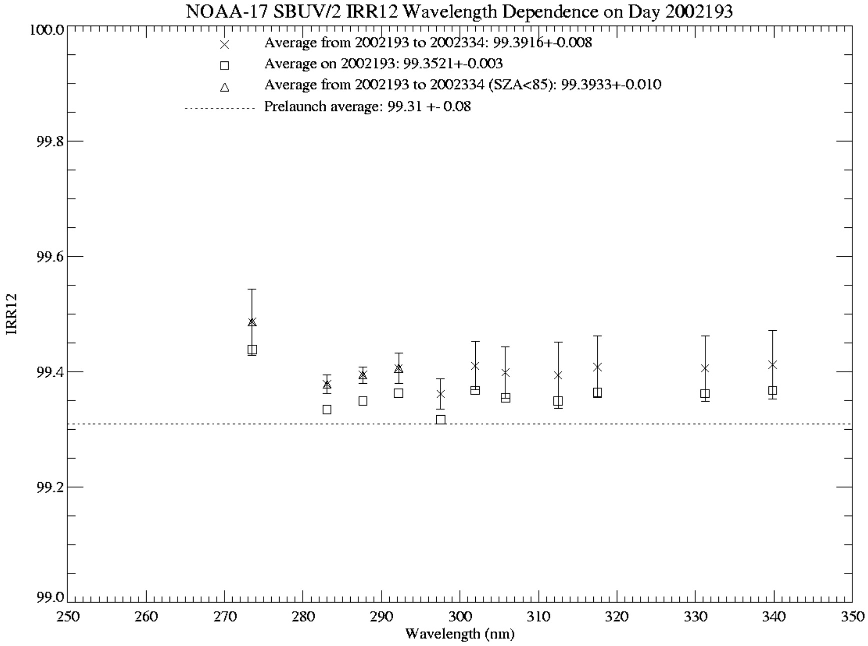

Figure 9.3: IRR$_{12}$ spectral dependence for first day of ozone measurements.

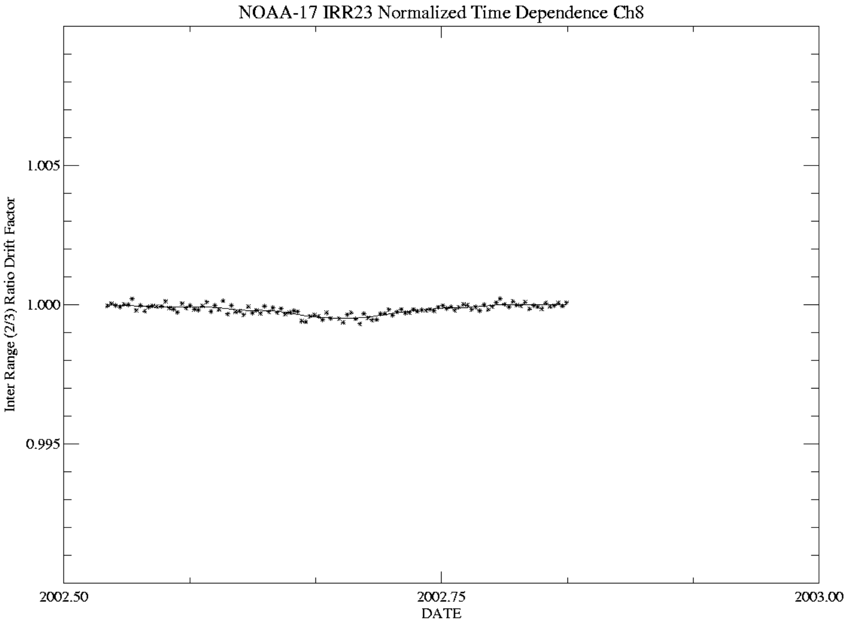

Figure 9.4: Time series of normalized IRR$_{23}$A (Range 3 anode) data at 305.8 nm.

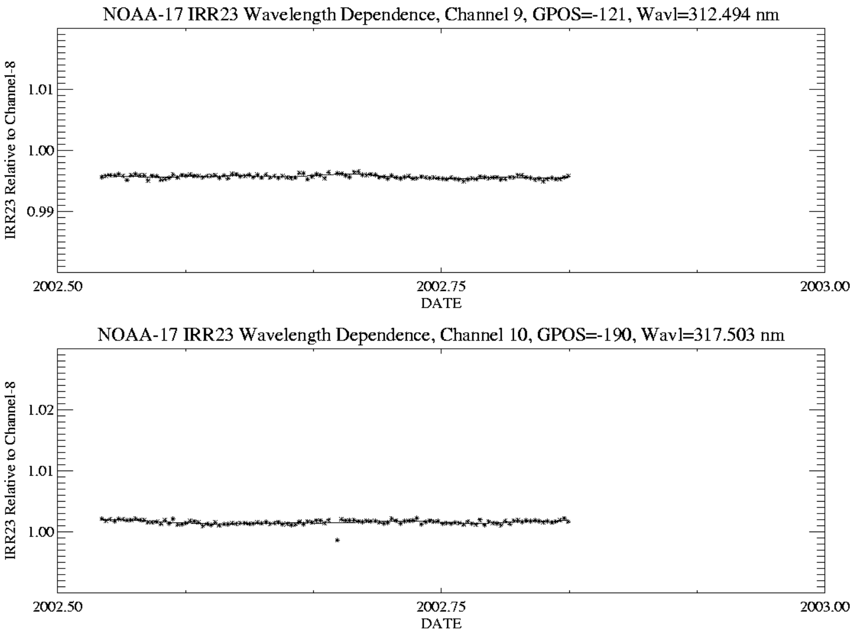

Figure 9.5: $IRR_{23}A$ spectral dependence *vs.* time: (*top*) 312.5 nm/305.8 nm; (*bottom*) 317.5 nm/305.8 nm.

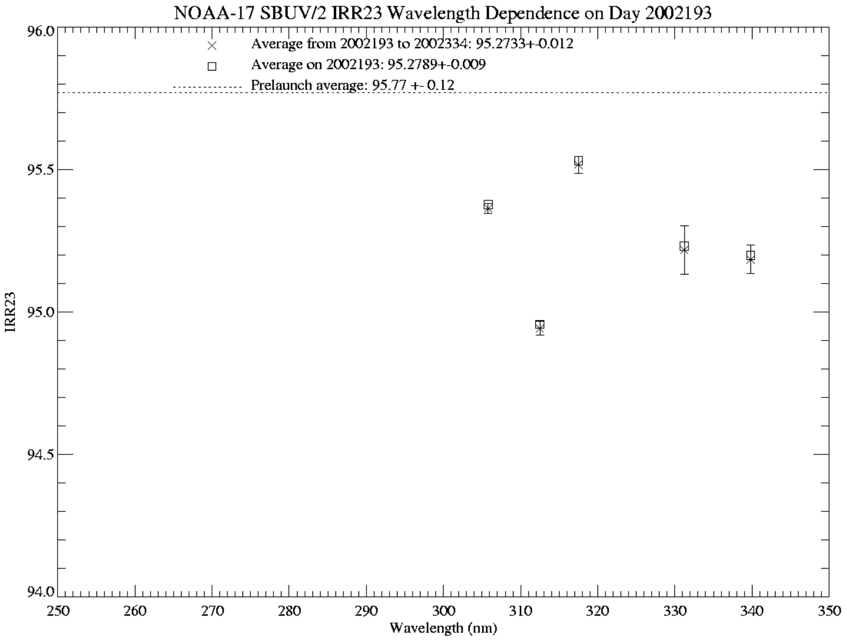

Figure 9.6: $IRR_{23}A$ spectral dependence for first day of ozone measurements.

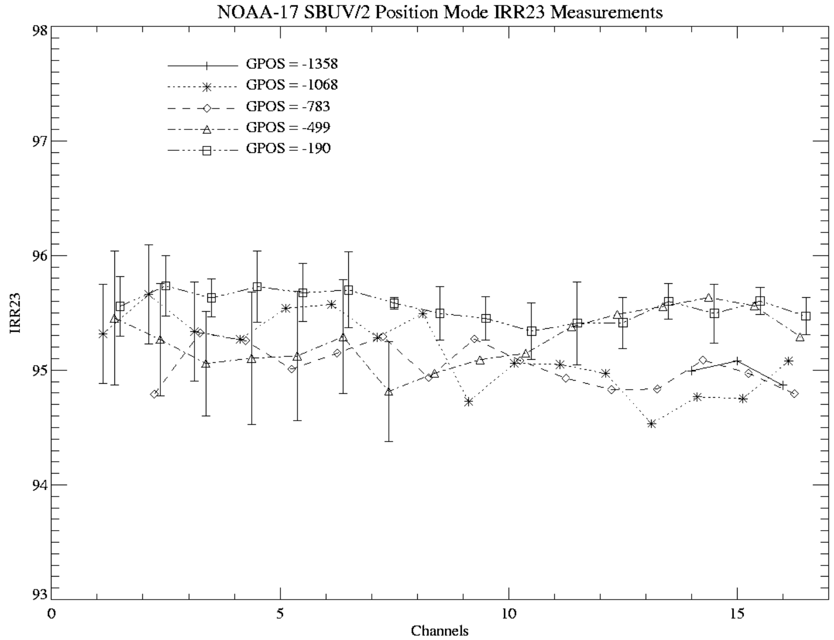

Figure 9.7: Position mode Earth view IRR$_{23}$A data *vs.* scan position: 400.0, 380.0, 360.0, 339.8, 317.5 nm.

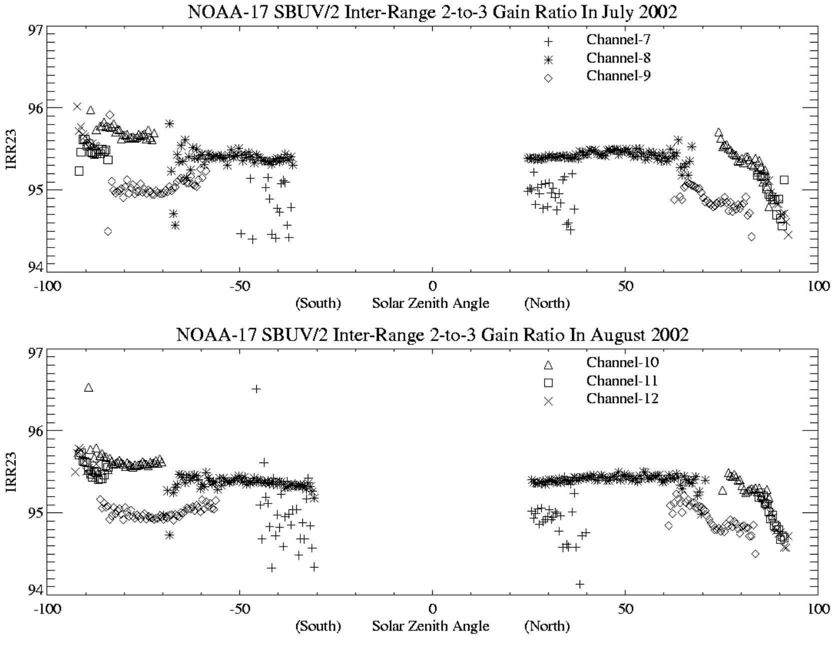

Figure 9.8: Monthly average IRR$_{23}$A values *vs.* solar zenith angle: (*top*) July 2002; (*bottom*) August 2002.

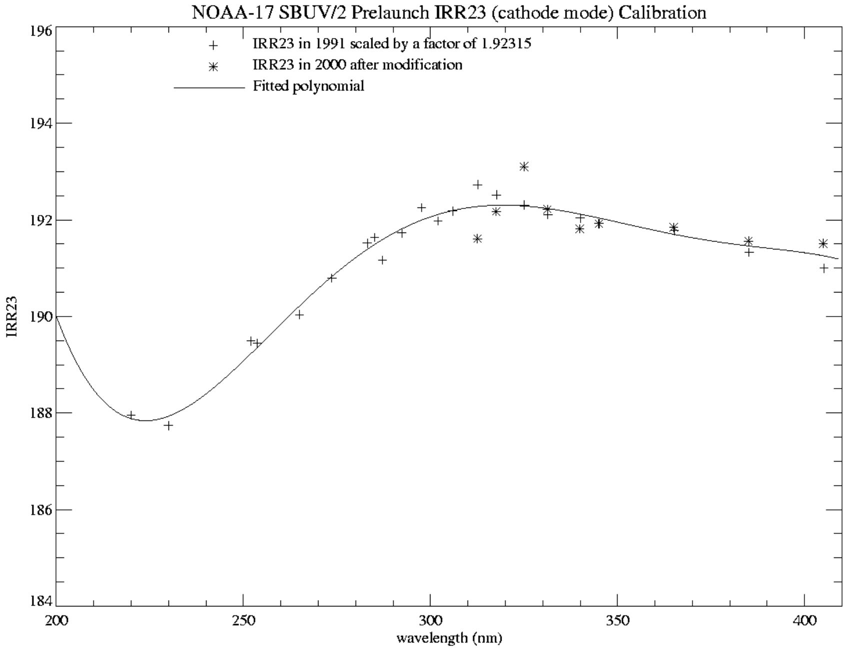

Figure 9.9: Spectral dependence of IRR$_{23}$C (Range 3 cathode) prelaunch data.

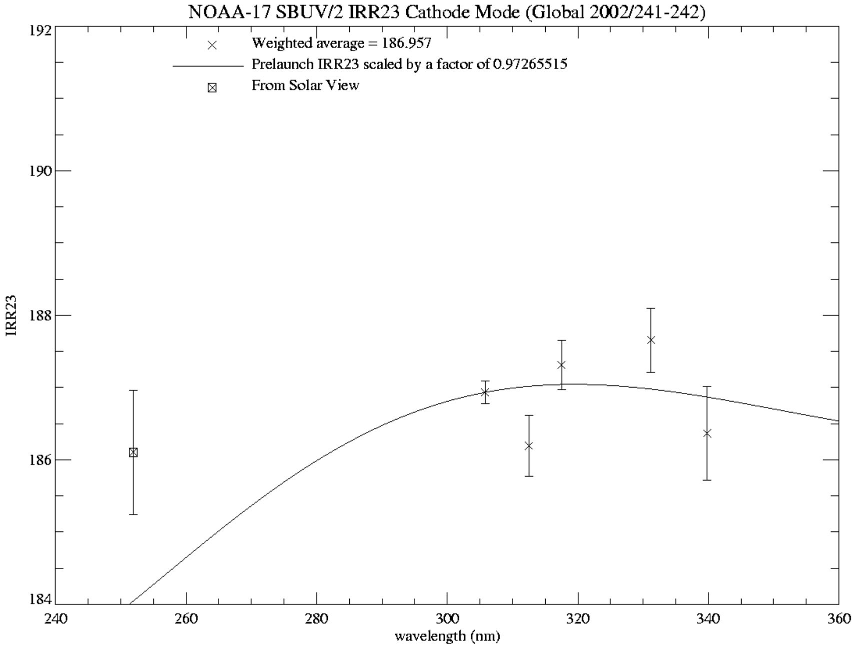

Figure 9.10: IRR$_{23}$C inflight spectral dependence for August 29-30, 2002.

10. Non-linearity Correction

The linearity calibration is based on data from laboratory tests performed in June 1998 by Ball Aerospace. The test procedure uses combinations of different size apertures and neutral density filters (NDF) to approximately double the observed signal in successive steps. Differences in the observed response from the nominal change due to aperture size change are considered to represent non-linear behavior. The results are then normalized to a fiducial value for each range. A paper by *Pitz* [1979] explains this method further. Measurements with the same neutral density filter were first normalized at 15,000 counts, based on a linear interpolation of 3 measurements around 15,000 counts. After the normalization, all measurements were combined together. A detailed discussion on the importance to choose a high count level in the normalization procedure to reduce the calibration uncertainty was presented in the NOAA-16 SBUV/2 A&E report [*DeLand and Huang*, 2001]. Ball Aerospace has adopted this normalization scheme for the FM#6 prelaunch calibration.

We evaluated the prelaunch non-linearity measurements to validate the functional fits. Different from previous SBUV/2 instruments, FM#6 had two runs of the same calibration procedure for the Range-3 anode output and cathode output, respectively. However, only results from the Range 3 anode run were included for the Range 1 and Range 2 non-linearity analysis in the Data Book. Since there is no expected physical difference in the Range 1 and Range 2 output between the two runs, we can combine the two runs for the Range 1 and Range 2 calibrations. As shown in Figure 10.2, the Range 2 non-linearity measurements from both runs fully agree with each other at high signal level (counts > 1000). At count rate less than 1000, the measurement accuracy is limited by the digitizer resolution and the difference between the two runs is consistent with the digitizer uncertainty. Therefore, inclusion of both runs for the Range 1 and Range 2 calibrations will reduce the noise and provide some estimate of the calibration uncertainties.

10.1 Range 1

Figure 10.1 shows that measurements with Range 1 signal levels between 12,000 and 50,000 counts in both runs tracked each other very well. The nonlinearity errors in this range are less than 0.1%. At low counts (< 1000), the noise level increased to 1%, which was consistent with expected uncertainty largely due to the digitizer uncertainty, the Range 1 offset noise and scattered light. Data values below 1000 counts Range 1 are rarely observed in discrete ozone measurements, and should be even less frequent for NOAA-17 SBUV/2 because of the increase in instrument sensitivity. We calculated a 3rd order fit to the combined data from both runs as a function of raw counts to emphasize the instrument behavior in the data region most commonly used on-orbit. This method effectively averages all low count samples together, resulting in a value near zero. At signal level near 60,000 counts, the fitted curve deviates from zero but less than 0.1%. The average of two measurements at 69,000 counts is –0.19% with a 0.2% deviation. The downward trend beyond 60,000 counts of the fitted curve is due to large uncertainty at 69,000 counts and the open end. Operational ozone processing transitions to Range 2 data at Range 1 signal levels of 55,000-60,000 counts, so the deviation in the revised fit has no impact. The finding of a negligible nonlinearity in Range 1 is consistent with the commonly known fact that the PMT and electronic amplifiers working at low signal level usually have good linearity. Since the magnitude of the polynomial fit is less than the scatter in the data over the full dynamic range, we recommend no nonlinearity correction to the Range 1 output.

10.2 Range 2

The Range 2 output has significant nonlinearity at high count levels. It is saturated above 80,000 counts. One data point at 47,319 counts with NDF6 in the cathode run deviates significantly from the average, and was considered to be an error. Measurements with NDF2 in the cathode run from 1000 counts to 2000 counts showed a +0.4% step, which was also about 4 times larger than the noise level. Thus, the measurements at less than 2000 counts in the cathode run were shifted so that the measurement at 1000 counts agreed with the extrapolation of the measurements at 2000 and 4000 counts. In the fitting procedure, the normalized measurements were renormalized such that the fitted polynomial gives zero nonlinearity at 1000 counts. The combined data sets are shown in Figure 10.2. We found that a 3rd order polynomial as a function of net counts fits the measurements very well. It produces no nonlinearity correction for signals less than 5000 counts. Therefore, measurements valid in both Range 1 and Range 2 will have no nonlinearity correction in either range. The correction increases from –0.3% at 40,000 counts to +0.7% at 68,000 counts. The fitted curve traces the nonlinearity measurements very well.

The change from $\log_{10}$(counts) to net counts for the independent variable in the Range 2 nonlinearity correction function was based on our experience with previous SBUV/2 instruments. The NOAA-16 SBUV/2 prelaunch Range 2 non-linearity calibration data showed a similar behavior at high signal levels. The functional fit recommended by Ball Aerospace used $\log_{10}$(counts) as a variable, and had a smaller magnitude than the data above 40,000 counts. Inflight solar irradiance data showed that the laboratory data were in fact accurate, and a linear correction function was derived for high Range 2 count values [*DeLand and Huang*, 2001]. Since the FM#6 prelaunch non-linearity data demonstrated the same behavior, it was logical to use a direct function of counts for the characterization.

10.3 Range 3 in Anode Mode

Significant nonlinearity was observed in the Range 3 anode output. The measurements are very well fitted with a 3rd order polynomial as a function of $\log_{10}$(counts), as shown by the solid curve in Figure 10.3. The measurements were renormalized at 1000 counts. The fitted curve agrees with the curve provided by Ball Aerospace, except for an absolute offset of about 0.2%. The Ball-fitted polynomial passes zero at about 5500 counts, which was not explained in their report. Since there are no prelaunch calibrations using the Range 3 nonlinearity correction, the choice of the normalization at 2000 counts will not affect any prelaunch calibrations. (In fact, the only prelaunch calibration signal in Range 3 occurred in the direct Hg lamp measurements at 254 nm. However, Ball prelaunch calibration analysis for the relative reflectivity never made any nonlinearity correction, which is discussed in the diffuser reflectivity calibration.) Figure 10.4 shows the inflight Range 2 to Range 3 gain ratio (IRR_{23}), using Range 3 anode data, as a function of Range 2 counts. The cross symbols are averages of IRR_{23} measurements in 2000-

counts bins. The variation is approximately ±0.1%, indicating that the nonlinearity corrections in both Range 2 and Range 3 are reasonably accurate.

10.4 Range 3 in Cathode Mode

The Range 3 cathode prelaunch non-linearity calibration data are shown in Figure 10.5. There is no measurable nonlinearity above 3000 counts, where the noise level is less than 0.1%. Deviations of measurements at low counts are generally within estimated uncertainty due to noise. An uncertainty weighted average of all measurements at low counts is –0.04%. If the average is over measurements with counts greater than 1000, the result is 0.005%. A weighted linear fit of the data set as a function of $\log_{10}$(counts) (solid line) provides the same estimate as above segmented averages. Therefore, no nonlinearity correction is recommended for the Range 3 cathode output.

TABLE 10.1
Non-linearity Correction Functions

Range	**X**	**C_0**	**C_1**	**C_2**	**C_3**
1	Net_counts	0.0	0.0	0.0	0.0
2	Net_counts	5.8712E-03	–5.5563E-06	–3.2157E-10	6.7372E-15
3A	Log_{10}[Net_counts]	–3.8387E+00	3.5141E+00	–1.1234E+00	1.2619E-01
3C	Log_{10}[Net_counts]	0.0	0.0	0.0	0.0

$$NL = C_0 + C_1*X + C_2*X^2 + C_3*X^3$$

$$\text{Non-linearity correction} = 1.0 / (1.0+(NL/100))$$

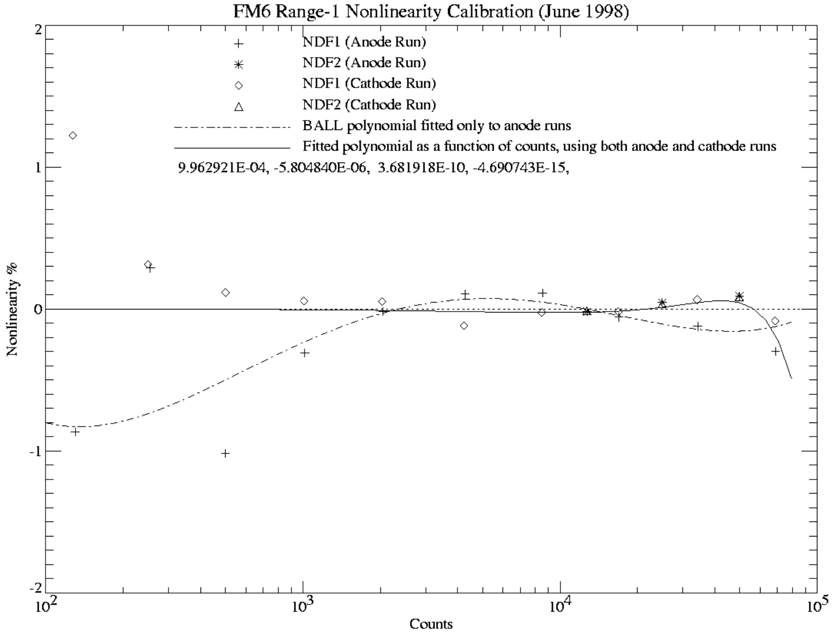

Figure 10.1: Prelaunch Range 1 non-linearity test data.

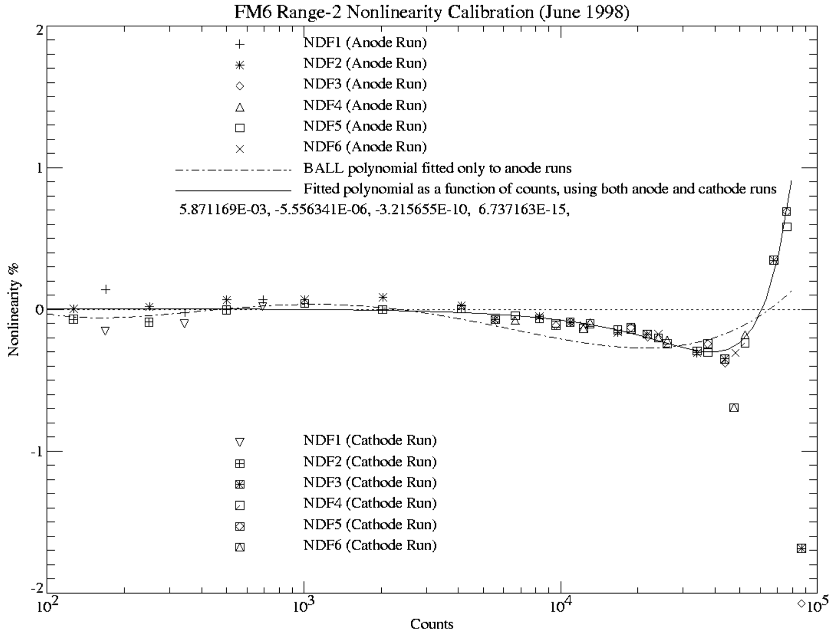

Figure 10.2: Prelaunch Range 2 non-linearity test data.

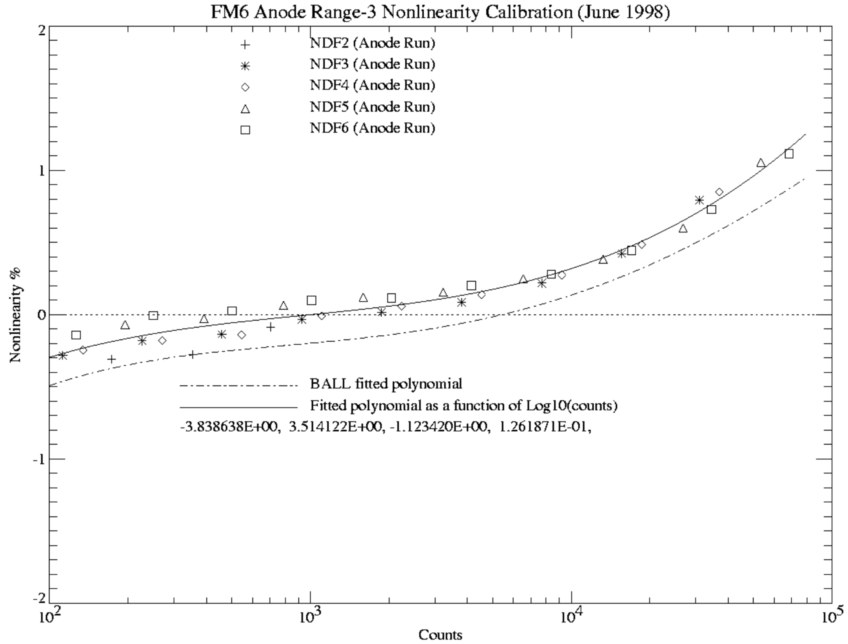

Figure 10.3: Prelaunch Range 3 anode non-linearity test data.

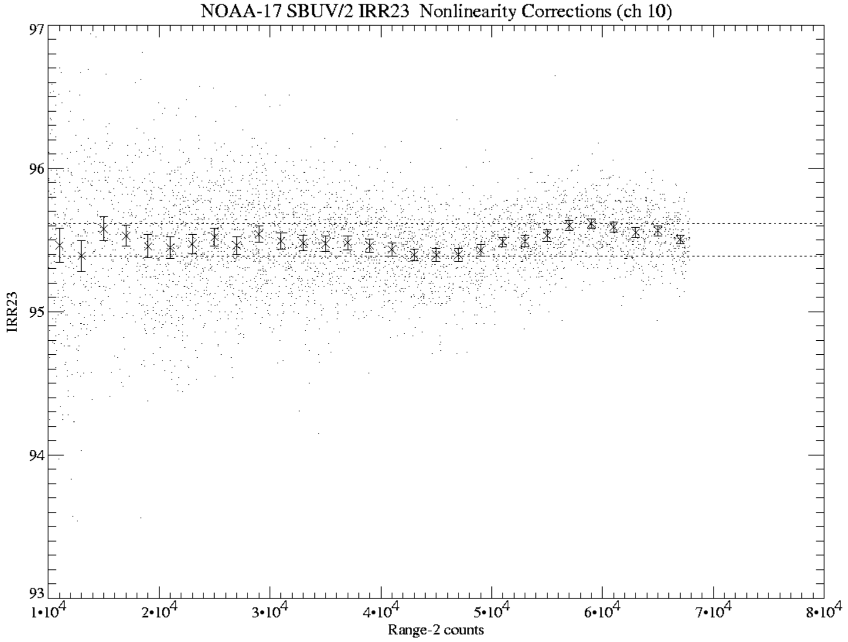

Figure 10.4: $IRR_{23}A$ dependence on Range 2 counts.

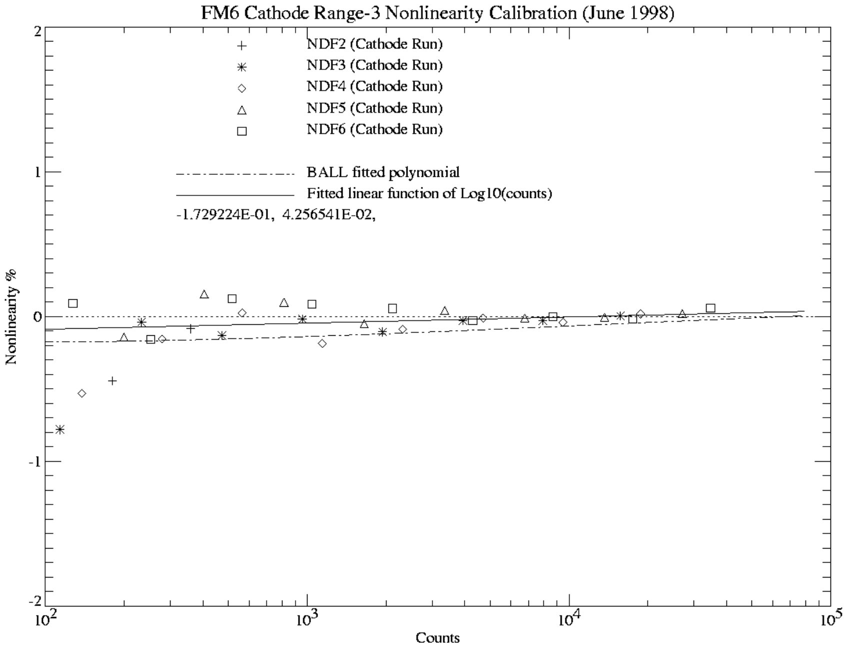

Figure 10.5: Prelaunch Range 3 cathode non-linearity test data.

11. Diffuser Reflectivity Characterization

11.1 Introduction

In the BUV technique, the ratio of earth radiance to solar irradiance (defined as the geometrical albedo, $\alpha = I / F$) is the fundamental quantity in ozone retrieval. Whereas backscattered radiance is directly viewed by the spectrometer, the measured solar irradiance is reflected from a diffuser plate. Most instrument changes, with the exception of the diffuser reflectivity, are common to both radiance and irradiance measurements, and thus cancel out in the albedo. Thus, properly characterizing time dependent changes in the reflectivity is the single most important part of our long-term calibration process.

All SBUV/2 instruments have an on-board calibration system to monitor diffuser relative reflectance as a function of time and wavelength. The on-board calibration system uses a Hg lamp as the spectral source. Measurements are made in two configurations, lamp view and diffuser view. Figure 11.1 illustrates the two configurations. In the lamp view, the Hg lamp is placed in front of the entrance slit of the spectrometer. In the diffuser view, the spectrometer faces the solar diffuser and light from the lamp is reflected off the diffuser into the entrance slit. The diffuser reflectivity is defined as the ratio of the signal measured in the diffuser view to that measured in the lamp view. This on-board reflectivity measurement does not provide the bidirectional reflectance distribution function (BRDF) of the diffuser, nor does it fully simulate the diffuser reflection of the solar light [*Jaross et al.*, 1998]. The angular dependence of the reflectivity (part of the BRDF) is characterized in the goniometric calibration (see Section 7), and is assumed to be time-independent. While the illumination of the diffuser plate by the mercury lamp in the calibration is not identical to that provided by the solar irradiance, we assume that the measured relative diffuser reflectivity changes are consistent with the reflectivity changes in the solar viewing geometry.

During the last two weeks in July 2002 and the first week in August 2002, we performed a total of 23 runs of the standard diffuser reflectivity calibration sequence immediately before and after the diffuser decontamination procedure and the first solar exposure. NOAA-17 SBUV/2 began regular weekly diffuser reflectivity calibrations on October 2, 2002. Discrete mode reflectivity calibrations were also performed from July 23 to August 2, 2002. The initial orbital measurements of the relative diffuser reflectivity are compared with the prelaunch calibration data to determine any changes from laboratory to orbit.

11.2. Sweep Mode Data

11.2.1 Measurement Sequence

The sweep mode diffuser reflectivity calibration is a preprogrammed measurement sequence that executes with a single command. This is the standard reflectivity monitoring procedure for all SBUV/2 instruments. Figure 11.2 shows the nominal reflectivity sequence, which consists of ten consecutive spectral scans. Six scans are taken in the diffuser view mode, and four scans in the lamp view mode. Each spectral scan takes 192 seconds, starting at 406 nm and ending at 160 nm. Nominally, each sequence should take place over the night side with the start and finish of the 32 minute sequence scheduled to avoid daylight contamination. In practice, we select scans with solar zenith angles larger than 120°.

Figure 11.3*a* shows the Hg lamp spectrum from the lamp (direct) view in sweep mode. Ten emission lines are identified in this figure. Six of the lines (185.0, 253.7, 296.8, 312.6, 365.1, 404.7 nm) have consistently high signal-to-noise ratios, and are designated as “strong” lines. Data from these lines are the primary source for the reflectivity analysis. Figure 11.3*b* shows the corresponding spectrum in the diffuser view. The increased relative continuum noise level is caused by the approximate factor of 50 decrease in signal intensity. Because of the increased noise, certain lines (265.3, 289.4, 302.1, 334.2 nm) have poor signal-to-noise ratios and are designated as “weak” lines. Data from these lines are generally not suitable for the reflectivity calibration. Figure 11.4 shows examples of typical emission line profiles at 253.7 and 404.8 nm in lamp and diffuser view. The ‘×’ symbols show data points recorded at 2 step intervals. Note that the actual grating position readout in the sweep mode occurs only at the end of every 10 samples, which are marked with long ticks on the grating position axis. This means that no direct information is available regarding the grating position values or errors at all other locations.

11.2.2 Reflectivity Calculation

Before computing the spectral line intensity, all raw measurements are corrected for the electronic offset, PMT temperature, and non-linearity. The corrected counts in Range 1 and Range 2 are then converted to equivalent values in Range 3 using the interrange ratio values IRR_{12} and IRR_{23} from Section 9. The line intensity is calculated by summing the corrected counts over either 14 or 15 points around the center of a line profile, as shown by the solid curves in Figure 11.4. The choice of the number of data points in the summation depends on how the peak location is centered in the sweep scan. The summation covers a range of data points slightly narrower than the full line profile in order to minimize background light contamination. This is also consistent with the data reduction in the prelaunch diffuser reflectivity monitoring.

Figure 11.5 shows a typical example of the spectral line intensities evolving during 10 consecutive scans in a calibration sequence in August 2002, where ‘+’ represents diffuser view data and ‘✳’ represents lamp view data. In order to plot all data in the same figure, the diffuser view line intensities are normalized to the average intensity from scans 7 and 8, and the lamp view line intensities are normalized to the average of scans 6 and 9. During a normal calibration sequence, the lamp is warming up during the first 3 (or 4) scans. We use only scans 7 and 8 for the diffuser view measurements, and use only scans 6 and 9 for the lamp view measurements. We use linear interpolation of the line intensity to minimize the impact of the lamp drift. Therefore, all reflectivity values are calculated using the following formula:

$$R = \frac{I_7 + I_8}{I_6 + I_9} \qquad [11.1]$$

where I_7 and I_8 are the line intensities at scans 7 and 8 in diffuser view, and I_6 and I_9 are the line intensities at scans 6 and 9 in lamp view. Tests were performed to include other scans for the reflectivity calculation, such as $R = [(I_4 + I_7)/(I_5 + I_6)+(I_7 + I_8)/(I_6 + I_9)]/2$. No improvement was found due to large uncertainty during scan 4. Figure 11.6 shows absolute diffuser reflectivity values at 254 nm and 406 nm calculated using Equation 11.1. The symbols '◊' and '✳' indicate different lamp polarity states. Further discussion of this effect is presented in Section 11.4.

11.2.3. Statistical Uncertainty

The statistical uncertainty for a reflectivity measurement includes the signal fluctuations, instrument noise, lamp source intensity drift (*i.e.* stability), repeatability between measurements, and grating position error effects. It is difficult to determine the measurement noise directly from the line intensity with only two scans. However, we can define a noise profile of percentage changes between two measurements of the same spectral profile in the same view, weighted by intensity,

$$N(\lambda_i) = 100 \times \left[f_2(\lambda_i) / f_1(\lambda_i) - 1 \right] \times \rho(\lambda_i) \qquad [11.2]$$

where f_1 and f_2 are the two line profile measurements, and ρ is the normalized spectral line intensity profile. If two profiles are identical at every data point, $N(\lambda_l)$ would be zero everywhere. The noise in the line intensity measurements is defined as the standard deviation of $N(\lambda_l)$ multiplied by the square-root of the number of data points for the line intensity. This definition makes the estimated noise level statistically meaningful with about 16 measurements in a line profile. The noise level in lamp view is less than 0.2%, which is negligible. The average noise level in diffuser view is less than 0.5% for the strong lines, and less than 2% for the weak lines.

The statistical uncertainty for the reflectivity is derived using the following formula,

$$\sigma = \sqrt{\sigma_L^2 + \Delta_L^2 + \sigma_D^2 + \Delta_D^2} \qquad [11.3]$$

where σ_L and σ_D represent the estimated noise in the line intensity measurements, Δ_L and Δ_D are uncertainties due to the lamp source intensity drifts, and subscripts L and D correspond to lamp view and diffuser view, respectively. Δ_L and Δ_D are equal to the standard deviations of the line intensities in scans 6 and 9 for the lamp view and scans 7 and 8 in the diffuser view, respectively. The uncertainty due to grating drive error is missing from the above equation because no grating drive errors have been recorded.

11.3 Discrete Mode Data

The discrete mode calibration sequence was originally designed to check the wavelength calibration, as well as a backup to the sweep mode calibration sequence. Six spectral lines at 185.0, 253.7, 289.5, 296.8, 334.3 and 404.8 nm were selected. Each line profile was repeatedly scanned in the SBUV/2 discrete mode in both diffuser view and lamp view. The discrete mode calibration tests were performed between July 23 and August 2, 2002. We use these data to validate the sweep mode reflectivity calibration.

11.3.1. Discrete Mode Measurement Sequence

Figure 11.7 illustrates the discrete mode diffuser reflectivity calibration sequence. Only one spectral line profile is scanned in each discrete mode sequence. The complete calibration sequence has approximately 60 scans and lasts about 32 minutes. As with the standard sweep mode diffuser reflectivity monitoring operation, the discrete mode operation is performed on the night side of an orbit. The discrete mode calibration sequence is constructed so as to approximate the standard sweep mode sequence. It begins with 24 scans in diffuser view, then alternates between lamp and diffuser views three times with 12 scans each. These 4 groups of scans are approximately equal in timing and function to those in a sweep mode sequence. As indicated in Figure 11.7, some mixed view modes may occur at times during transition from the lamp view to diffuser view. These scans in the mixed modes are rejected from the reflectivity calculation.

Because of the much longer total integration time for a single line profile, the signal-to-noise ratio for discrete mode data is generally much better than for sweep mode data. Note also the difference in data sampling. The grating in the discrete mode is locked at a designated position to get each data sample, while the grating in the sweep mode is moved 2 steps for a single data point. Each grating position in the discrete mode is actually measured by the grating position decoder, while only one grating position at the end of every 20 steps in a sweep mode scan is actually read from the instrument. NOAA-17 SBUV/2 has shown no grating position errors in discrete mode to date. Differences between discrete mode and sweep mode reflectivity measurements do not affect the results, as shown for NOAA-14 SBUV/2 [*DeLand et al.*, 1998].

11.3.2. Reflectivity Calculation in Discrete Mode

In discrete mode, each scan has 12 samples. By using a sample separation of two grating steps, a single discrete scan covers a large part of the emission line profiles (about 1.8 times the FWHM). Figure 11.8 shows the measured 253.7 nm and 404.8 nm line profiles. The peak positions in discrete mode are slightly shifted in comparison with sweep mode data due to differences in data sampling and grating position readout methods as mentioned above. After applying the same corrections for the detector characteristics as were used for the sweep mode measurements, all 12 samples were summed to give the integrated line intensity.

Figures 11.9 and 11.10 illustrate the line intensity drift for two calibration sequences at 253.7 nm and 404.8 nm, respectively. Data from both diffuser view and lamp view are plotted together to show the overall lamp behavior. In the diffuser view (*crosses*), the line intensity is normalized to minimize the difference between the interpolated values in lamp view and the measured values in diffuser view. After a significant decrease during initial lamp warming up time, the line intensity at 405 nm still drifted about 1% during the scans used for the reflectivity calculation. In addition, the time dependence of the drift was not linear during the measurement sequence. Therefore, the line intensity measurements in diffuser view in the last 8 (or 10) scans of the first group and the middle 8 (or 10) scans of the third group were fitted with a cubic function (*dot-dash line*) to provide interpolated line intensity values in diffuser view that correspond to the lamp view measurements in the second group of scans. The first diffuser reflectivity value is then derived as the ratio of the interpolated line intensity in diffuser view to the measured line intensity in lamp view. In the lamp view (*asterisks*), the line intensity is normalized to the last available scan. Cubic interpolation is used in this instance to estimate the lamp view line intensities for the third group of scans (*solid line*), and the second diffuser reflectivity value is derived as the average of the measured line intensities in diffuser view to the interpolated line intensities in lamp view. The deviation between the two derived reflectivity values are less than 0.1%, which is better than the sweep mode results using linear interpolation. Finally, the two derived reflectivities are averaged to give a daily value.

11.3.3. Statistical Uncertainty in Discrete Mode

The statistical uncertainty for a discrete reflectivity measurement also includes signal fluctuations, instrument noise and lamp intensity drift. The uncertainty due to the line intensity drift was estimated using the maximum deviation of the line intensity from the average value used for the line intensity interpolation. Scan-to-scan measurement noise was estimated from the standard deviation of the measured line intensities from the fitted or interpolated values in the same view configuration, divided by the square root of the number of measurements. No uncertainty is associated with the grating position error because there has been no grating position drive error. The total statistical uncertainty in the calculated reflectivity is expressed as:

$$\sigma = \sqrt{\Delta_1^2 + \sum_{i=1}^{3} \sigma_{1i}^2 + \Delta_2^2 + \sum_{i=1}^{3} \sigma_{1i}^2} \qquad [11.4]$$

where Δ_1 and Δ_2 are respectively the line intensity drift for the first and second derived reflectivities, σ_{1i} and σ_{2i} are respectively the standard errors due to the noise and the summations are taken over three groups involved in each derived reflectivity. As shown in Figures 11.9 and 11.10, the lamp source drifts dominated the estimated uncertainties, representing ~70% of the uncertainty at 404.8 nm.

11.4. Lamp Polarity Effect

The power supply to the Hg lamp reverses polarity each time the lamp is turned on. This feature was added for FM#5 and all subsequent SBUV/2 instruments to improve long-term lamp stability by varying the position of the Hg lamp arc. Figure 11.11 shows the impact on the 254 nm line intensity for lamp view and diffuser view data. Note that the Hg lamp intensity decreases by approximately 30% through October 2002, comparable to the NOAA-16 SBUV/2 lamp changes during early operations. The two symbols in Figure 11.11 represent the different polarities, assigned arbitrarily since there is no telemetry information about the polarity state. The polarity for each lamp usage was assigned according to the Hg lamp operation history. The polarity effect shows up in the reflectivity calculation, Figure 11.6. There is no physical reason why the true diffuser reflectivity would change in conjunction with mercury lamp polarity changes. Therefore, we believe that this effect is an artifact in the reflectivity data. There is no reason to prefer one polarity state over the other, so we use an average reflectivity between the two polarities.

We fit the data with a functional form that includes a polarity term. The fitting function can be written as:

$$f_\lambda(x) = R_\lambda + a_{p\lambda} p(x) \qquad [11.5]$$

where x is the time, $p(x)$ is equal to ±1 depending on the polarity state at the measurement time, $a_{p\lambda}$ is the correction for the polarity, R_λ is the reflectivity after the polarity correction. We choose a constant reflectivity at the present time since we have not accumulated sufficient measurements to uncover the reflectivity drift from noise. Table 11.1 lists the derived polarity corrections for strong lines, based on fitting Equation 11.5 to the first 11 days of measurement. The average polarity correction is –0.27%, which is slightly larger than NOAA-16 (–0.20%) but significantly smaller than NOAA-14 (–0.50%). Figure 11.12 shows the reflectivity measurements with the polarity effect removed.

11.5. Diffuser Reflectivity Stability

11.5.1. Reflectivity Changes after Diffuser Decontamination

The diffuser decontamination procedure was performed on July 24, 2002. The diffuser reflectivity calibration was immediately performed once before the decontamination and twice after the decontamination. Then, the first series of the solar irradiance measurement followed, interleaved with more diffuser reflectivity calibrations. As shown in Figure 11.6, uncertainty in single reflectivity measurement is larger than any possible reflectivity changes in the same day. Therefore, averages of 6 measurements before the decontamination and averages of 2 measurements right after the decontamination are computed after the polarity correction. The results are plotted in Figure 11.13 and compared in Table 11.2. The comparison shows no significant changes in the reflectivity with an uncertainty less than 0.5%. Therefore, all of the 8 measurements before the solar exposure will be averaged as the diffuser initial state in the orbit.

11.5.2. Reflectivity Changes after Initial Solar Exposure

Figures 11.14 and 11.15 show the measured diffuser reflectivity data at 253.7 nm and 404.8 nm through October 2002. Symbols '×' and '✳' indicate the lamp polarities, which have been corrected in the fitting. NOAA-17 SBUV/2 began regular weekly diffuser reflectivity calibrations in October 2002. It is still too early to evaluate long-term trends. Table 11.3 lists averages of the reflectivity values before and after the initial solar exposure, using data form the first two weeks of measurements. Figure 11.16 shows that the changes are mostly statistically insignificant, with the largest change at 253.7 nm (–0.44%).

11.5.3. Comparison with Prelaunch Calibrations

Extensive prelaunch diffuser reflectivity calibrations in air were performed in June through October 2000. The prelaunch values in Table 11.4 are averages over the last 4 calibration sequences. The 185 nm data were corrected for absorption in air using results from previous vacuum calibration tests, which may have large uncertainties. Ball Aerospace processed the prelaunch reflectivity data with nominal interrange ratio values (IRR_{12} = IRR_{23} = 100) rather than the observed values (IRR_{12} = 99.31, IRR_{23} = 95.77). We estimated corrections for the gain ratio difference. A single scan over a triangular profile may use different gain ranges for the wings and the peak. Therefore, corrections in different gain ranges are respectively weighted by their total counts. The weighting, thus the correction, would drift as the mercury lamp line intensity drifted. The line intensities in the initial orbital reflectivity calibration sequence were used to estimate the correction factors for the prelaunch reflectivity data. Ball Aerospace did not correct these data for nonlinearity errors. Because of the increased sensitivity of the FM#3 instrument, numerous Hg lamp emission lines may have peak values in Range 3 during prelaunch calibration tests (prior to the large degradation shown in Figure 11.11). Table 11.4 lists the estimated correction to the original prelaunch values at each wavelength, as well as revised prelaunch values. These corrections are somewhat uncertain because the raw prelaunch data were not available. Figure 11.17 shows that the initial diffuser reflectivity values observed on-orbit are slightly higher than the revised prelaunch data at most wavelengths, with larger variations at 185.0 and 313.1 nm. No changes were made for analysis of the initial solar irradiance data.

TABLE 11.1
Hg Lamp Polarity Correction: On-Orbit Data

Wavelength [nm]	*Polarity Correction*
185.00	–0.38(±0.09)%
253.71	–0.34(±0.03)%
296.82	–0.21(±0.12)%
313.13	–0.17(±0.12)%
365.24	–0.27(±0.11)%
404.81	–0.22(±0.11)%

TABLE 11.2
Inflight Diffuser Reflectivity Changes Following Decontamination

Wavelength [nm]	*Before Decontamination*	*After Decontamination*	*Reflectivity Change*
185.00	0.012842(±0.000041)	0.012882(±0.000037)	0.32(±0.43)%
253.72	0.017322(±0.000052)	0.017280(±0.000036)	–0.24(±0.37)%
296.84	0.019081(±0.000058)	0.019082(±0.000063)	0.00(±0.45)%
313.13	0.019099(±0.000043)	0.019146(±0.000070)	0.25(±0.43)%
365.24	0.019499(±0.000053)	0.019451(±0.000076)	–0.25(±0.48)%
404.81	0.019479(±0.000044)	0.019447(±0.000059)	–0.16(±0.38)%

TABLE 11.3
Inflight Diffuser Reflectivity Changes Following Solar Exposure

Wavelength [nm]	*Before Solar Exposure*	*After Solar Exposure*	*Reflectivity Change*
185.00	0.012853(±0.000022)	0.012861(±0.000014)	0.06(±0.20)%
253.72	0.017322(±0.000015)	0.017246(±0.000005)	–0.44(±0.09)%
296.84	0.019079(±0.000041)	0.019018(±0.000029)	–0.32(±0.26)%
313.13	0.019110(±0.000036)	0.019082(±0.000032)	–0.14(±0.25)%
365.24	0.019492(±0.000036)	0.019475(±0.000029)	–0.09(±0.24)%
404.81	0.019470(±0.000033)	0.019438(±0.000029)	–0.17(±0.22)%

TABLE 11.4
Prelaunch Diffuser Reflectivity Calibration

Wavelength [nm]	***Reflectivity Before Correction***	***Correction Factor***	***Reflectivity After Correction***	***Changes after Launch***
185.00	0.01299(±0.00012)	1.02273	0.01328	–3.00(±0.95)%
253.72	0.01640(±0.00003)	1.03025	0.01689	1.71(±0.27)%
296.84	0.01892(±0.00002)	1.00694	0.01905	0.11(±0.33)%
313.13	0.01832(±0.00004)	1.00217	0.01836	4.68(±0.58)%
365.24	0.01871(±0.00003)	1.02265	0.01914	1.42(±0.47)%
404.81	0.01870(±0.00002)	1.03363	0.01933	0.40(±0.37)%

The reflectivity at 184.9 nm in air was scaled up by the reflectivity change from air to vacuum in the thermal-vacuum chamber test.

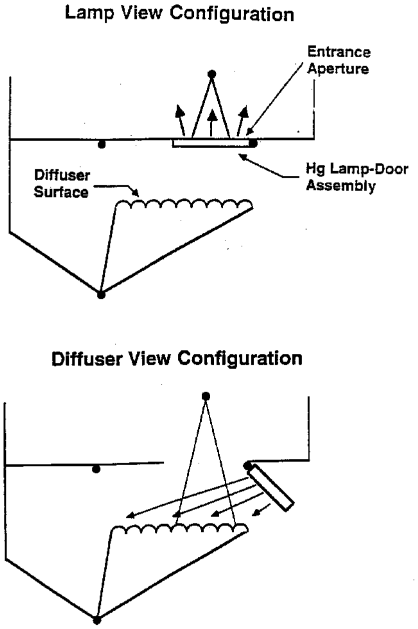

Figure 11.1: Onboard calibration system configuration: Lamp view, diffuser view.

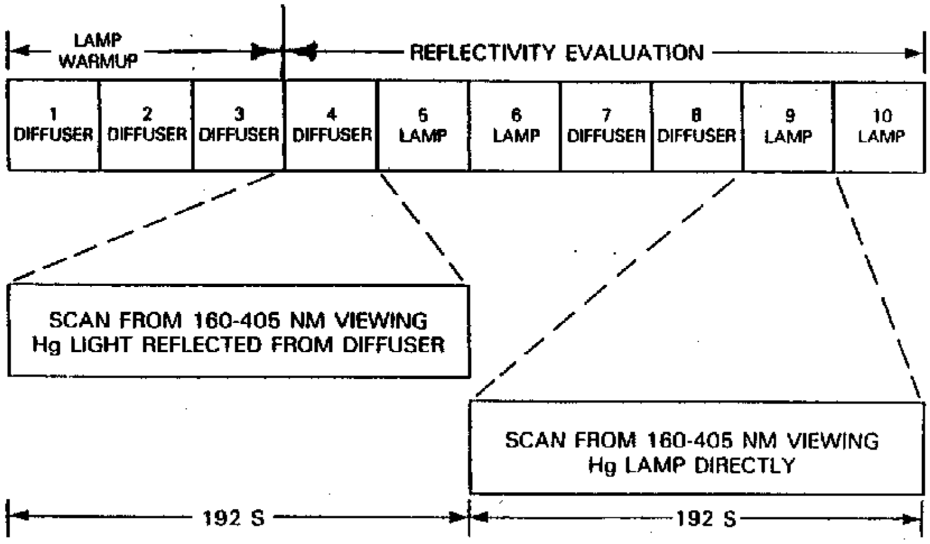

Figure 11.2: Sweep mode diffuser reflectivity measurement sequence.

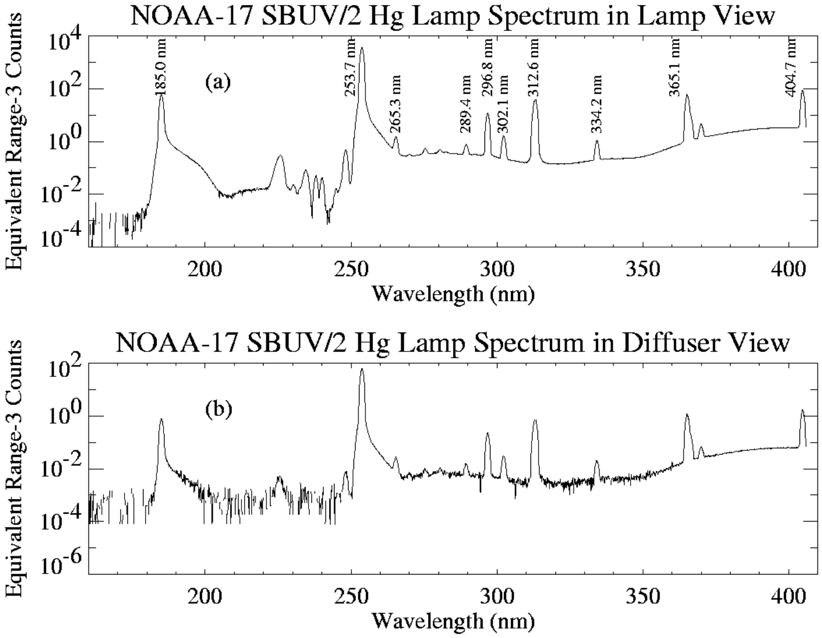

Figure 11.3: Mercury lamp spectrum: (*a*) Lamp view; (*b*) Diffuser view.

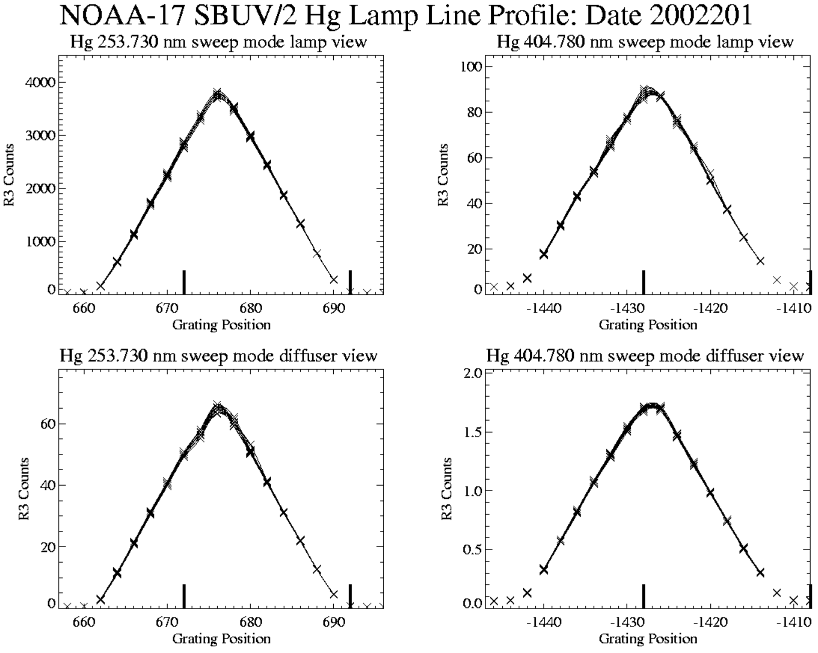

Figure 11.4: Sweep mode line profiles (lamp, diffuser): 253.7 nm, 404.8 nm.

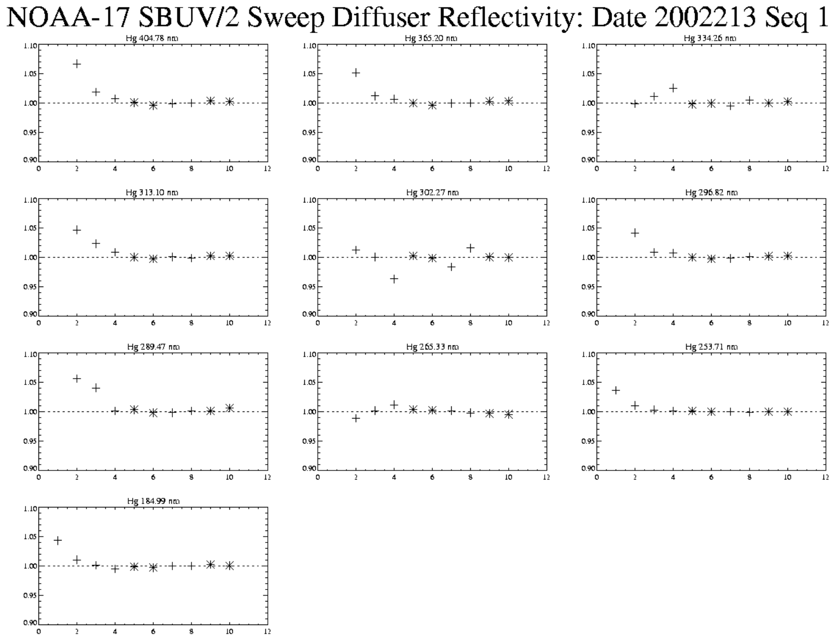

Figure 11.5: Line intensity evolution during sweep mode sequence: All lines.

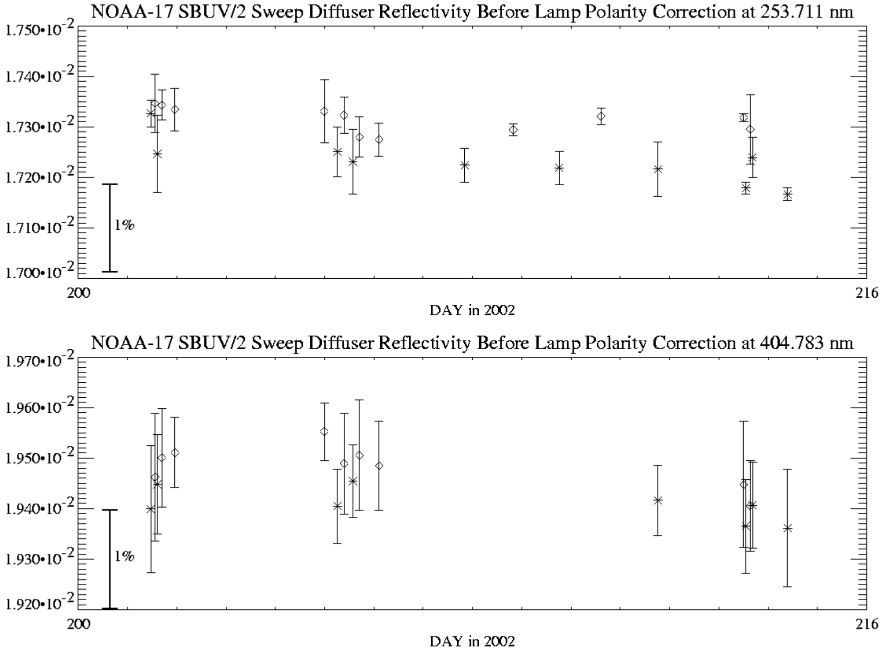

Figure 11.6: Diffuser reflectivity time series (no polarity correction): (*top*) 253.7 nm; (*bottom*) 404.8 nm.

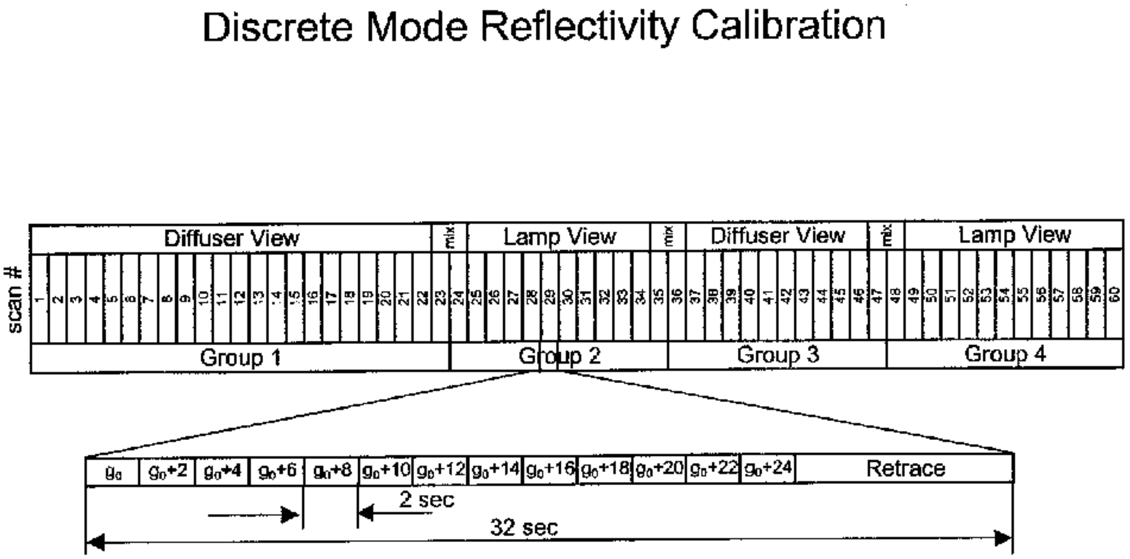

Figure 11.7: Discrete mode diffuser reflectivity measurement sequence.

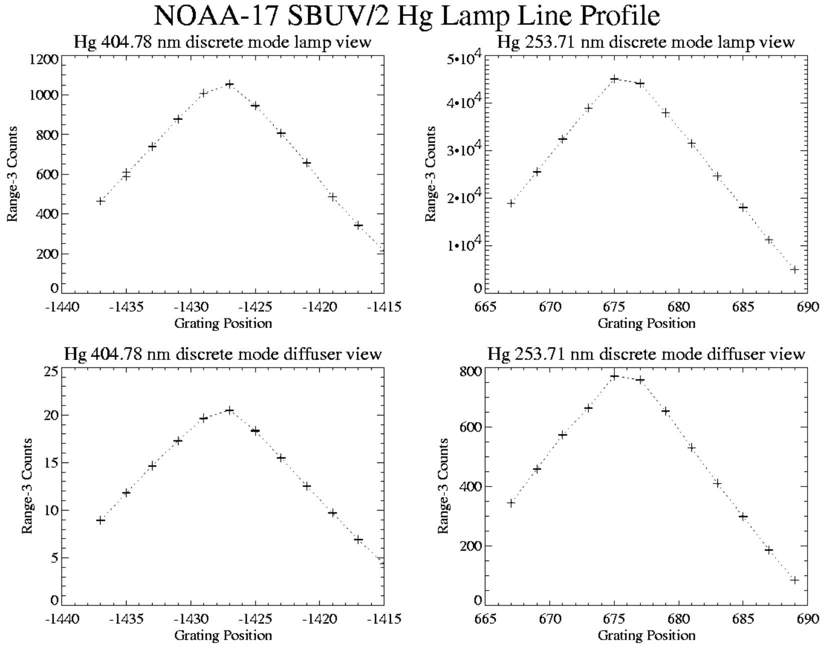

Figure 11.8: Discrete mode line profiles (lamp, diffuser): 404.8 nm, 253.7 nm.

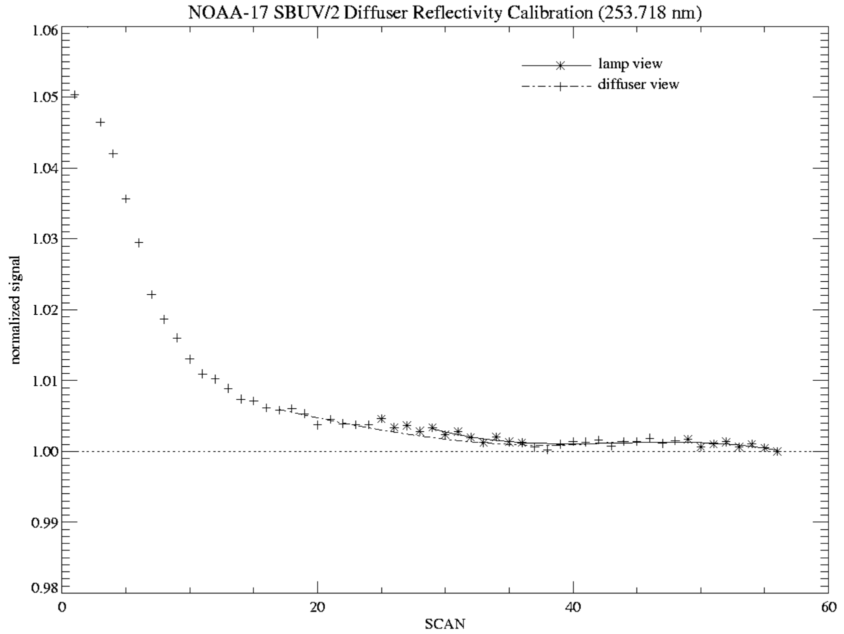

Figure 11.9: Discrete mode line intensity evolution at 253.7 nm.

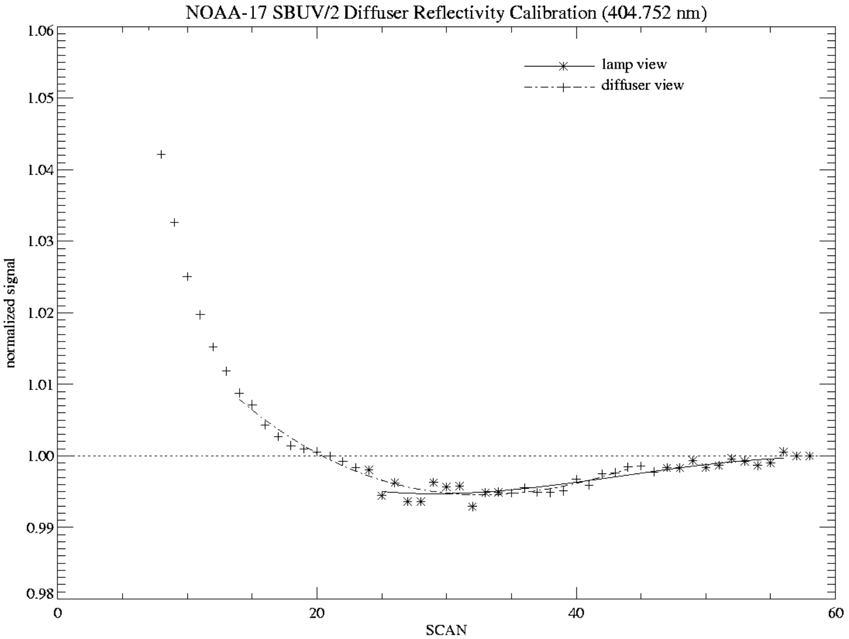

Figure 11.10: Discrete mode line intensity evolution at 404.8 nm.

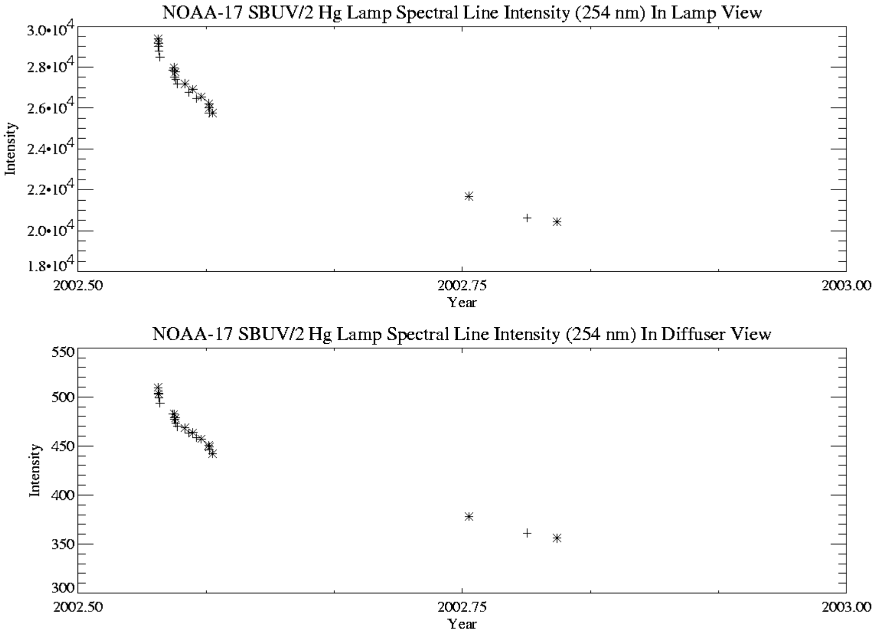
NOAA-17 SBUV/2 Hg Lamp Spectral Line Intensity (254 nm) In Lamp View

NOAA-17 SBUV/2 Hg Lamp Spectral Line Intensity (254 nm) In Diffuser View

Figure 11.11: Hg lamp intensity time series at 253.7 nm: (*top*) Lamp view; (*bottom*) Diffuser view.

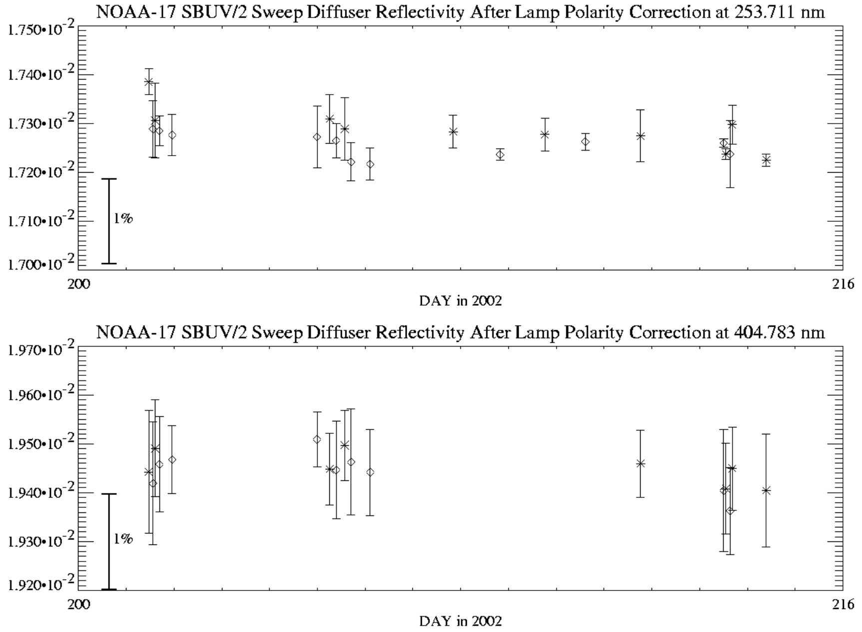
NOAA-17 SBUV/2 Sweep Diffuser Reflectivity After Lamp Polarity Correction at 253.711 nm

NOAA-17 SBUV/2 Sweep Diffuser Reflectivity After Lamp Polarity Correction at 404.783 nm

Figure 11.12: Diffuser reflectivity time series (after polarity correction): (*top*) 253.7 nm; (*bottom*) 404.8 nm.

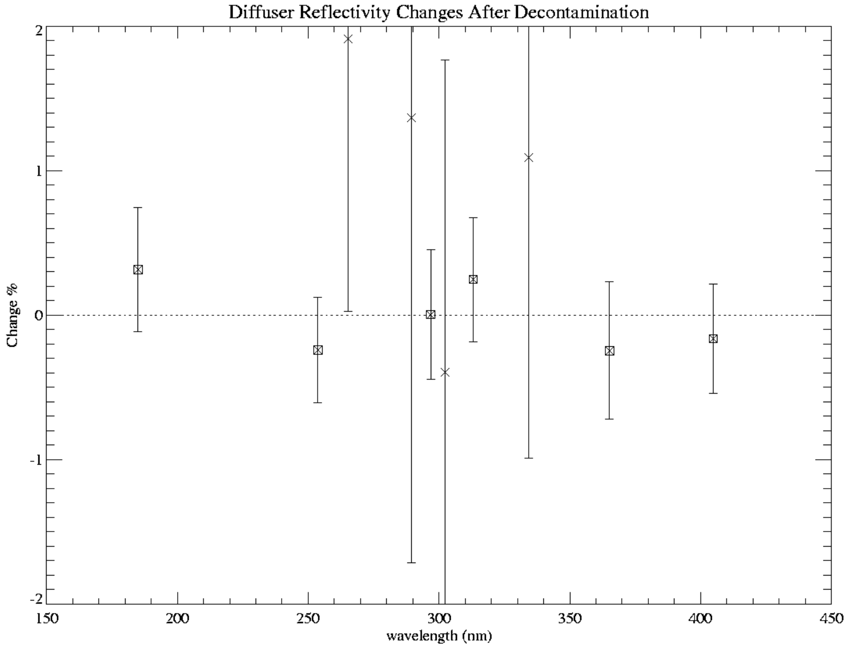

Figure 11.13: Inflight diffuser reflectivity changes after decontamination. Strong lines are indicated by squares.

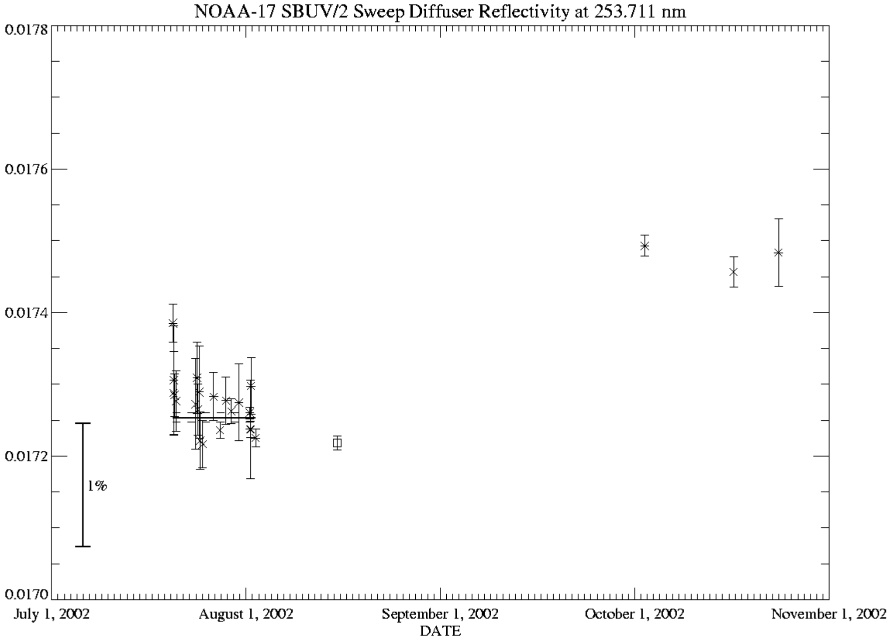

Figure 11.14: Diffuser reflectivity time series at 253.7 nm: July-October 2002.

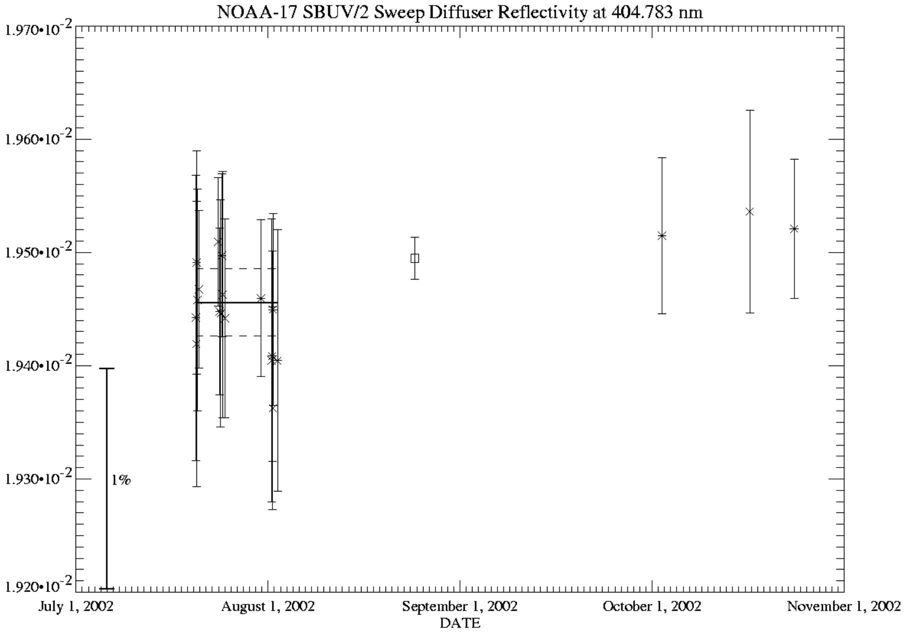

Figure 11.15: Diffuser reflectivity time series at 404.8 nm: July-October 2002.

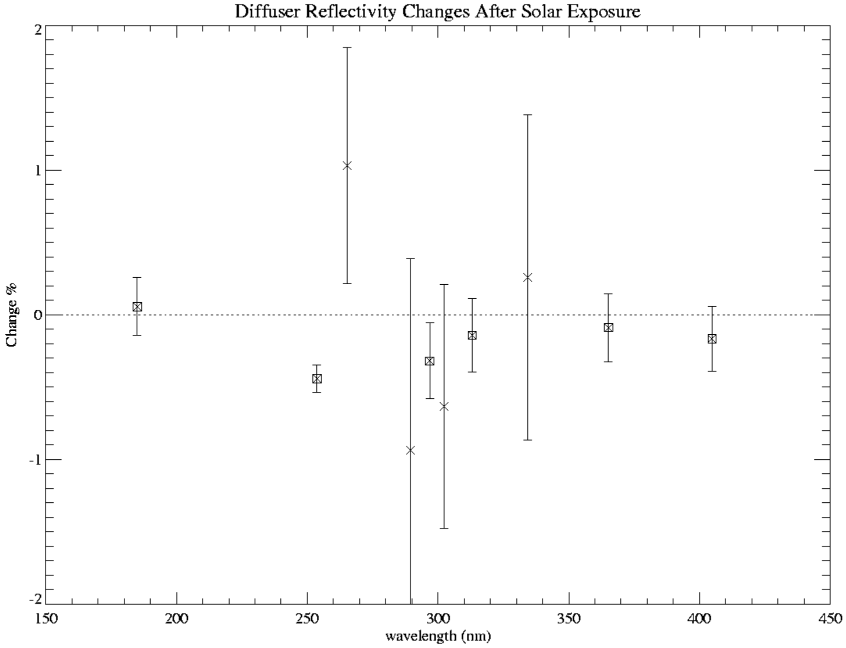

Figure 11.16: Inflight diffuser reflectivity changes after initial solar exposure. Strong lines are indicated by squares.

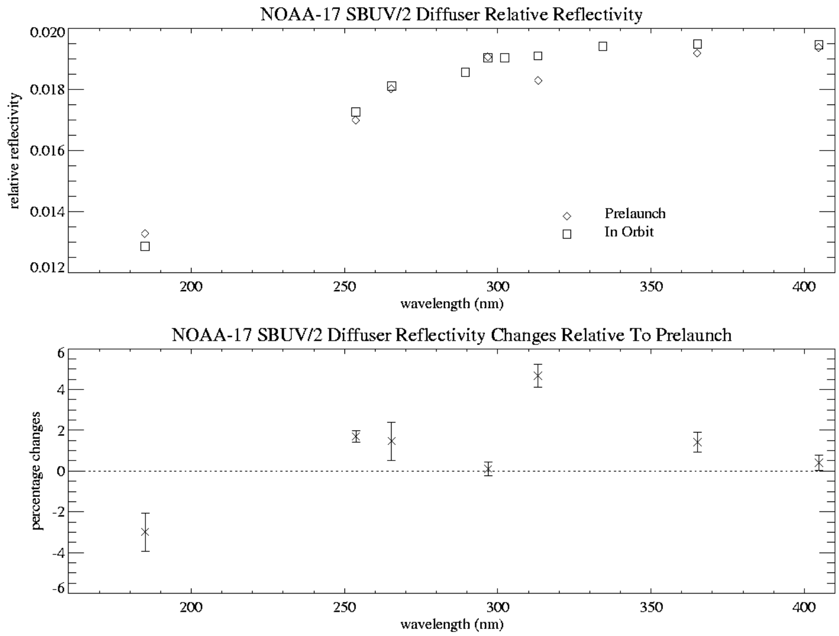

Figure 11.17: (*top*) Diffuser reflectivity spectral dependence; (*bottom*) Spectral dependence of diffuser reflectivity change: Inflight *vs.* prelaunch.

12. Radiometric Calibration

12.1. Prelaunch Characterization

The NOAA-17 SBUV/2 absolute radiometric calibration is based on measurements made in the laboratory before sensor launch and adjustments to the prelaunch constants suggested by observed on-orbit sensor behavior. The initial measurement procedures and results are described in depth in the prelaunch calibration report prepared by the sensor manufacturer, Ball Aerospace. Prelaunch procedures and results are reviewed only briefly here.

In basic principle, radiometric calibration of a sensor in the laboratory requires a known or fully characterized radiation source, a controlled method to introduce the source into the field of view of the sensor being calibrated, and observations of sensor response to the fully characterized source. To reduce uncertainties in source irradiance, Ball Aerospace used three samples of each type of source required: FEL lamps (1000 watt tungsten-halogen incandescent bulbs with quartz envelopes) for wavelengths from the visible down to approximately 250 nm and deuterium-arc lamps to provide adequate signal at shorter wavelengths (required below 250 nm). The spectral and goniometric (angular) characteristics of each source lamp were measured by NIST preceding and following each sequence of calibration measurements. Two sequences of laboratory calibration measurements were completed for the NOAA-17 sensor after extensive mechanical and electronic modifications affecting sensor calibration were implemented in the mid-1990’s. Radiometric calibration measurements in a normal ambient air environment were obtained in 1998 and again in 2000.

Side-by-side calibration measurements in air and vacuum were obtained during the initial round of NOAA-17 calibration measurements obtained soon after construction of this sensor in 1991. Figure 12.1 shows the ratio of calibration constants observed in sweep mode operation. Outside the Woods anomaly region near 232 nm, air-to-vacuum differences can be as large as 7%. The large magnitude of these differences relative to air-to-vacuum differences observed with previous SBUV/2 instruments has been considered and analyzed in several Ball Aerospace memoranda [*Fowler*, 1994, 1995].

The ratio between sweep mode and discrete mode calibration constants is nominally 12.5, based on the difference in sample integration times. Previous SBUV/2 instruments have observed slightly lower sweep/discrete ratios, although the differences are typically less than 1%. The NOAA-16 sweep/discrete calibration constant ratio is within 0.5% of the nominal value at all wavelengths for both radiance and irradiance data, as shown in Figure 12.2.

12.2. On-Orbit Validation

After the NOAA-17 SBUV/2 sensor was launched and on-orbit solar observation data became available, it was apparent that solar spectral irradiances based on the pre-launch calibration were inconsistent with expected solar irradiances (based on a long and rich history of solar irradiance measurements made by other sensors in the SBUV/2 program and other Earth and space-based solar sensors in completely independent programs). Differences between NOAA-17 discrete mode solar observations based on prelaunch calibration constants and solar irradiances obtained in the Space Shuttle Backscattered Ultraviolet (SSBUV) programs are plotted as a function of wavelength in Figure 12.3. At the shortest wavelengths, differences exceed 13% and all deviations at the SBUV/2 discrete wavelengths exceed 2%. Note that these irradiance values were processed with radiometric calibration constants measured in air for consistency with the radiance calibration used in ozone processing. NOAA-17 sweep mode measurements made on the first day of observations also show spectrally dependent errors. These results are discussed further in Section 13.

As a first step towards reconciling the inconsistent measurements, a table of calibration adjustment factors that produce agreement between NOAA-17 and SSBUV solar observations at SBUV/2 discrete wavelengths was prepared (see Table 12.1). The values in this table are essentially reciprocal values of the points plotted in Figure 12.3. A table of discrete irradiance calibration constants obtained by multiplying measured pre-launch calibration constants by the calibration adjustment factors listed in Table 12.1 is presented in Table 12.2. A corresponding table of corrected radiance calibration constants is presented in Table 12.3. These tables present the discrete calibration constants currently recommended for use in NOAA operational ozone processing. Note that the CCR calibration value was not adjusted.

TABLE 12.1
Calibration Adjustment Factors

Channel	***Grating Position***	***Wavelength*** [nm]	***Adjustment Factor***
1	700	251.911	1.1557
2	410	273.509	1.1365
3	281	283.049	1.1148
4	219	287.619	1.1054
5	157	292.178	1.0764
6	84	297.534	1.0650
7	24	301.925	1.0628
8	–29	305.795	1.0701
9	–121	312.494	1.0721
10	–190	317.503	1.0719
11	–380	331.222	1.0416
12	–500	339.830	1.0303

TABLE 12.2
Revised Irradiance Calibration Constants [*mW/m^2/nm/count*]

Channel	***Grating Position***	***Wavelength*** [nm]	***Range 1***	***Range 2***	***Range 3*** *[anode]*
1	700	251.911	7.7452E-06	7.6918E-04	7.3664E-02
2	410	273.509	8.0688E-06	8.0131E-04	7.6742E-02
3	281	283.049	9.3467E-06	9.2822E-04	8.8895E-02
4	219	287.619	9.7670E-06	9.6996E-04	9.2892E-02
5	157	292.178	9.5503E-06	9.4844E-04	9.0832E-02
6	84	297.534	8.9078E-06	8.8463E-04	8.4721E-02
7	24	301.925	8.2343E-06	8.1774E-04	7.8315E-02
8	–29	305.795	7.7518E-06	7.6983E-04	7.3727E-02
9	–121	312.494	7.0958E-06	7.0468E-04	6.7488E-02
10	–190	317.503	6.7401E-06	6.6936E-04	6.4105E-02
11	–380	331.222	6.1491E-06	6.1067E-04	5.8484E-02
12	–500	339.830	5.2976E-06	5.2610E-04	5.0385E-02
CCR	—	378.62	—	—	9.3381E-02

TABLE 12.3
Revised Radiance Calibration Constants [*mW/m^2/nm/count/ster*]

Channel	***Grating Position***	***Wavelength*** [nm]	***Range 1***	***Range 2***	***Range 3*** *[anode]*
1	700	251.911	1.4712E-06	1.4610E-04	1.3992E-02
2	410	273.509	1.5683E-06	1.5575E-04	1.4915E-02
3	281	283.049	1.8298E-06	1.8172E-04	1.7404E-02
4	219	287.619	1.9141E-06	1.9008E-04	1.8205E-02
5	157	292.178	1.8783E-06	1.8654E-04	1.7865E-02
6	84	297.534	1.7596E-06	1.7475E-04	1.6735E-02
7	24	301.925	1.6310E-06	1.6197E-04	1.5512E-02
8	–29	305.795	1.5381E-06	1.5275E-04	1.4628E-02
9	–121	312.494	1.4112E-06	1.4014E-04	1.3422E-02
10	–190	317.503	1.3444E-06	1.3351E-04	1.2786E-02
11	–380	331.222	1.2373E-06	1.2288E-04	1.1768E-02
12	–500	339.830	1.0722E-06	1.0648E-04	1.0198E-02
CCR	—	378.62	—	—	1.8679E-02

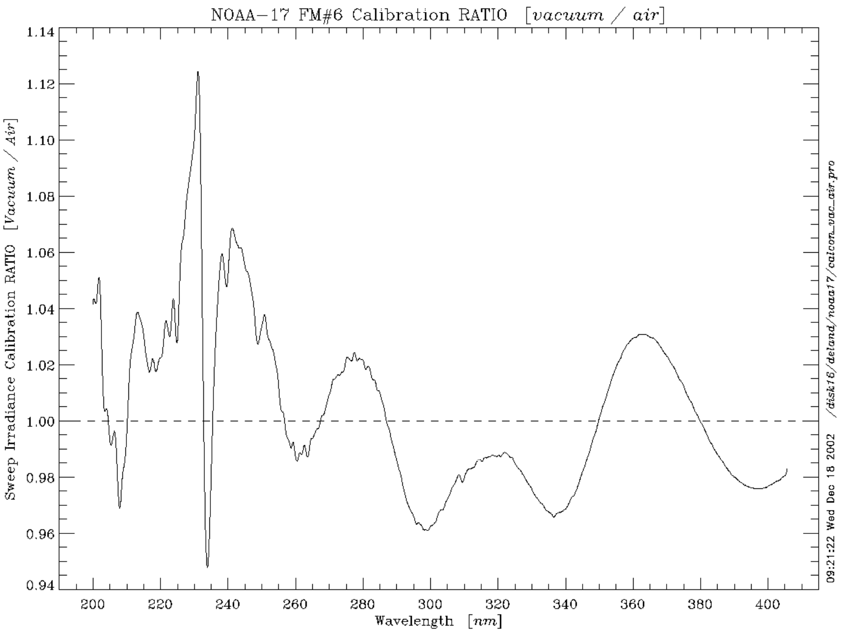

Figure 12.1: FM#6 sweep mode vacuum/air calibration ratio.

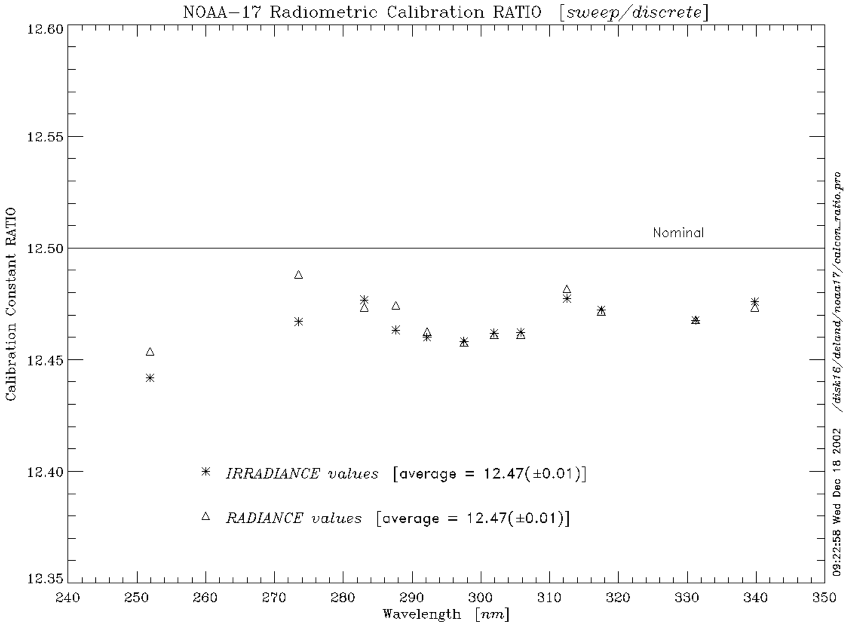

Figure 12.2: FM#6 sweep/discrete calibration ratio.

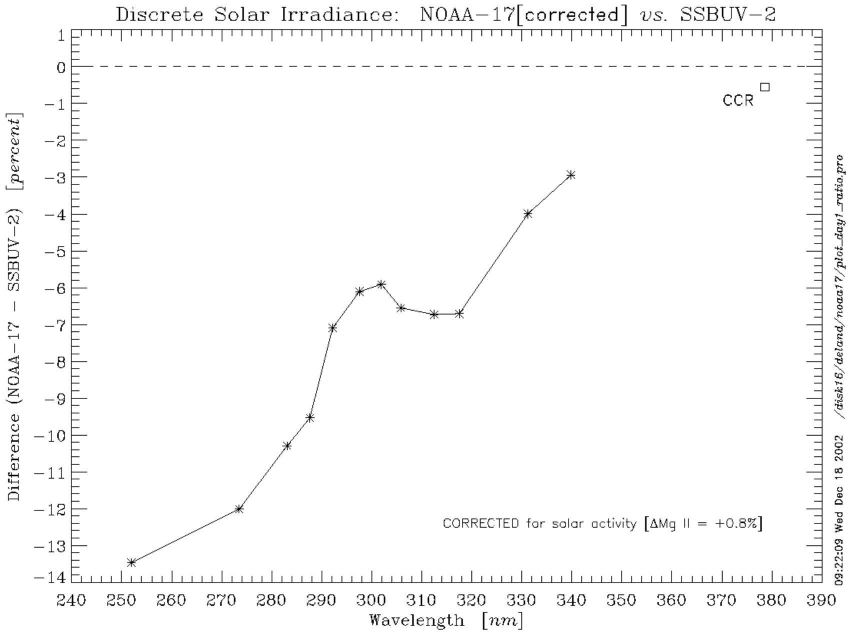

Figure 12.3: Discrete mode solar irradiance comparison: NOAA-17 SBUV/2 (24 July 2002) *vs.* SSBUV-2 (7-9 October 1990).

13. Solar Irradiance

13.1. Discrete Mode

Initial solar irradiance measurements from the NOAA-17 FM#6 instrument were made on July 24, 2002 (day 205). Two discrete mode sequences at ozone wavelengths and three sweep mode sequences were taken on this date. All measurements on “day 1” were taken at proper elevation angles but due to rounding errors in wavelength processing code, monochromator grid positions were one count below the optimum value for some wavelength settings. Post-processing routines were used to reference the observed solar irradiance at these wavelengths to the intended wavelengths. As explained in Section 12, discrete mode solar irradiance values obtained from “day 1” observations were inconsistent with expected values based on space-based solar observations in other programs (see Figure 12.3). The “Day 1” discrete mode solar irradiances obtained after application of the calibration adjustment factors discussed in Section 12 are shown in Table 13.1.

Solar irradiance measurements at discrete ozone wavelengths are nominally obtained once every week and Mg II index measurements required to characterize short-term variations in solar irradiance at the shorter wavelengths are nominally obtained every day. As of the base time for the preparation of this report (November 2, 2002), solar data at ozone observation wavelengths has been successfully collected on eight days: 2002 days 205, 211, 241, 280, 294, 301, 315, and 322. Eighteen scans were completed on the first day (day 205), eight successful scans were completed on day 315, and nine scans were completed on all of the other days listed. Sixty-one Mg II index observation sets were successfully completed; each of these sets consists of nine scans. Mg II index data begins on day 274 (October 1, 2002). Figure 13.1 shows the NOAA-17 Mg II index results from the first two months of regular operations.

13.2. Sweep Mode

NOAA-17 sweep solar measurements are processed using a vacuum calibration to provide coverage down to 160 nm. The “Day 1” irradiance spectrum was constructed by averaging three scans together. Figure 13.2 shows the difference between this spectrum and the UARS ATLAS-1 reference spectrum taken on March 29, 1992. The NOAA-17 data have been corrected for differences in solar activity level between the dates of the measurements. A significant spectrally dependent difference is also seen, with a minimum value of –2% at 360 nm and a maximum value of –18% at 180 nm. The triangles show irradiance differences for NOAA-17 position mode data over the range 170-405 nm, which lie within ~1% of the sweep mode results. The asterisks show the discrete mode differences from Figure 12.3, multiplied by the appropriate air-vacuum calibration differences from Figure 12.1. A correction function was derived for the sweep mode irradiance calibration by fitting the UARS difference data in Figure 13.2 with a CLOESS smoothing spline function (*heavy line*). The correction was fixed for $\lambda < 165$ nm because the SBUV/2 data quality is low in that region.

When regular NOAA-17 solar measurements began in October 2002, it quickly became clear that significant calibration changes continued to occur on-orbit. Figure 13.3 shows the ratio of the daily average sweep spectrum on 2002/275 (October 2) to the initial sweep spectrum measured on July 24. No correction has been made for solar variation, which was –1.2% in the NOAA-16 Mg II index. The regular spectral structure between 250-406 nm is consistent with the vacuum/air calibration ratio shown in Figure 12.1.

Most optical surfaces in the SBUV/2 instrument are coated with magnesium fluoride (MgF_2) to enhance UV reflectivity at short wavelengths. Laboratory tests with SBUV/2 instruments consistently show larger vacuum/air calibration differences than can be explained by changes in the index of refraction. Ball Aerospace personnel have studied this behavior, and speculate that the MgF_2 overcoating absorbs water vapor in the laboratory, and that outgassing effects in vacuum cause the observed spectral dependence [*Fowler*, 1994, 1997]. The potential effects are exacerbated for later SBUV/2 instruments (FM#6, FM#7, FM#8), where the change from an optically contacted 4-segment depolarizer to an air spaced depolarizer adds six coated surfaces to the optical path. Recent data suggest that the rate of sensitivity change may be slowing. Figure 13.4 shows that the magnitude of changes during October-November 2002 is considerably reduced compared with the previous period (Figure 13.3), and that the spectral variations are less severe. Nevertheless, characterization of the FM#6 long-term sensitivity changes will be challenging.

TABLE 13.1
"Day 1" Solar Irradiances

Channel	***Grating Position***	***Wavelength*** [nm]	***Irradiance*** [mW/m^2/nm]
1	700	251.911	**43.69**
2	410	273.509	**206.77**
3	281	283.049	**333.99**
4	219	287.619	**348.78**
5	157	292.178	**561.26**
6	84	297.534	**537.11**
7	24	301.925	**460.92**
8	–29	305.795	**604.32**
9	–121	312.494	**698.54**
10	–190	317.503	**813.67**
11	–380	331.222	**1001.70**
12	–500	339.830	**1050.21**
CCR	—	378.62	**1303.02**

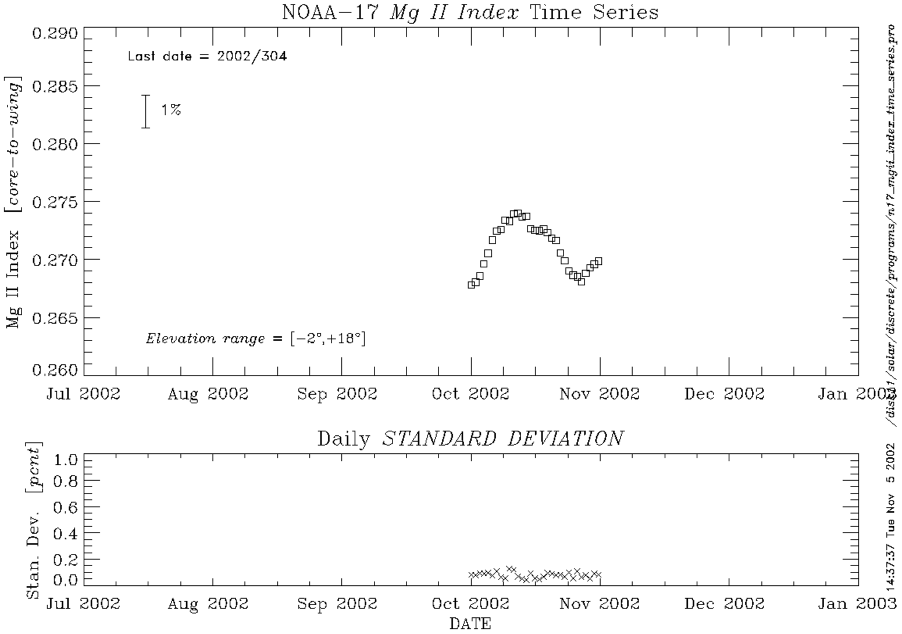

Figure 13.1: NOAA-17 discrete mode Mg II index during October 2002.

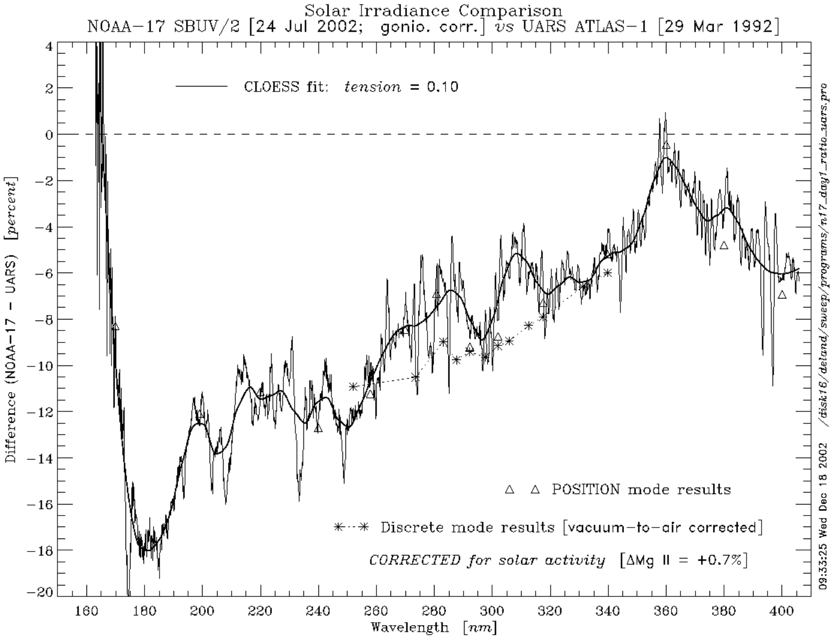

Figure 13.2: Sweep mode solar irradiance comparison: NOAA-17 SBUV/2 (24 July 2002) *vs.* UARS ATLAS-1 (29 March 1992).

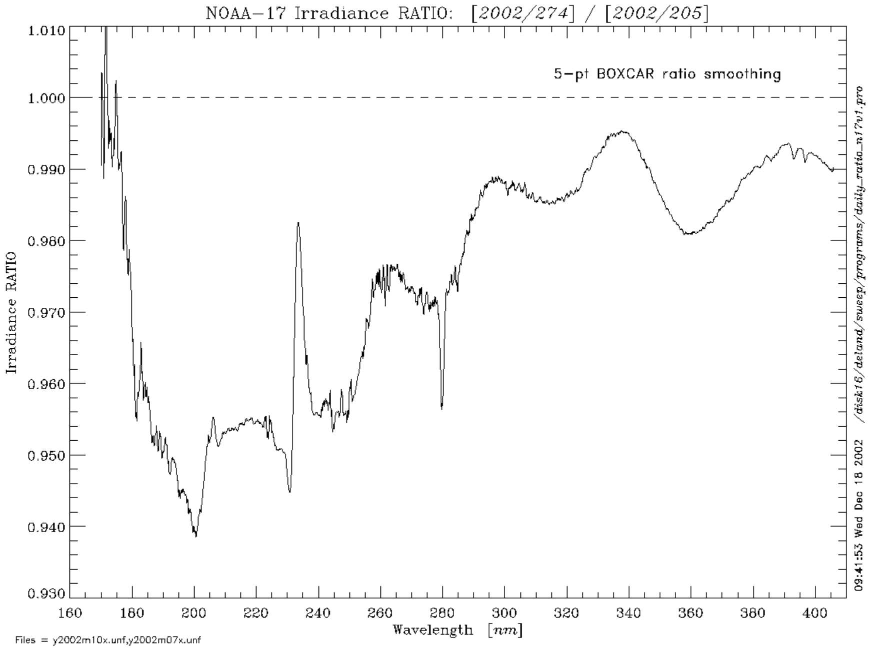

Figure 13.3: Sweep mode irradiance ratio: 2002 day 274 *vs.* 2002 day 205.

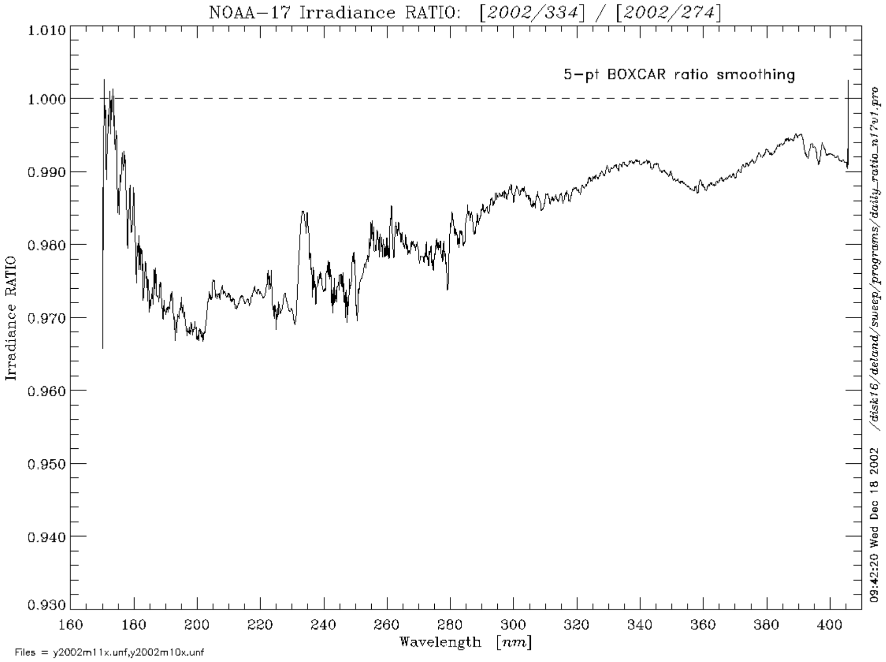

Figure 13.4: Sweep mode irradiance ratio: 2002 day 334 *vs.* 2002 day 274.

14. Ozone Validation

An initial processing of NOAA-17 ozone data was performed using prelaunch calibration data and solar irradiance values. These data showed large differences (~25 DU) between B-pair and D-pair total ozone at the Equator. SSAI reprocessed all NOAA-17 ozone data from June 2002 through August 2002 using the revised calibration constants and “Day 1” irradiances presented in Tables 12.3 and 13.1 respectively to determine initial total ozone pair adjustment factors for operational V6 processing. The B-pair *vs.* D-pair equatorial difference decreased to 3-4 DU. Figure 14.1 shows the variation in this difference during the first four months of NOAA-17 operation. The sharp jump at the beginning of the record may indicate a significant calibration change prior to the first solar measurement. We calculated A-pair/B-pair, B-pair/C-pair, and A-pair/D-pair ratios to develop pair adjustment factors. The recommended pair adjustments for V6 processing are listed in Table 14.1, and represent averages of all available data. Note that the A-C adjustment is the product of the A-B and B-C adjustments discussed here.

Figure 14.2 shows a comparison of average profile ozone data at low latitudes (±25°) on October 22, 2002, using the operational products from both NOAA-16 and NOAA-17 SBUV/2. The NOAA-17 data include the absolute calibration adjustment discussed in Section 12. There is a significant altitude dependence to the profile difference, with NOAA-17 data 5-10% higher in the lower layers, but 10-15% lower at layers 6 and above. The NOAA-16 data do not include corrections for diffuser reflectivity degradation, which may change profile ozone values by up to 5% in the upper layers. NOAA-17 data have not been corrected for the time-dependent calibration changes shown in Section 13. Thus, we expect that accurate time-dependent characterizations for both instruments will be required to effectively compare profile ozone measurements.

TABLE 14.1
Total Ozone Pair Adjustment Factors Relative to A-pair

Ozone Pair	***Adjustment Factor***	***Data Range***
B	0.974	χ = 50-60°
C	1.066	χ = 70-80°
D	0.997	χ = 25-35°, latitude = ±15°

adjustment: $\Omega_A = \Omega_{pair}$ `*Factor`

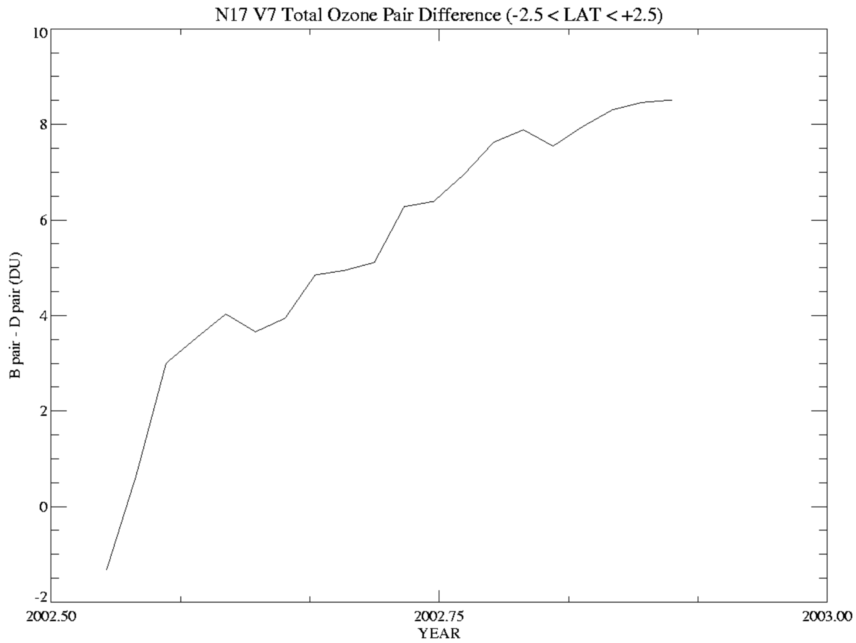

Figure 14.1: NOAA-17 total ozone: Difference between B-pair and D-pair at Equator (adjusted for “Day 1” calibration change.

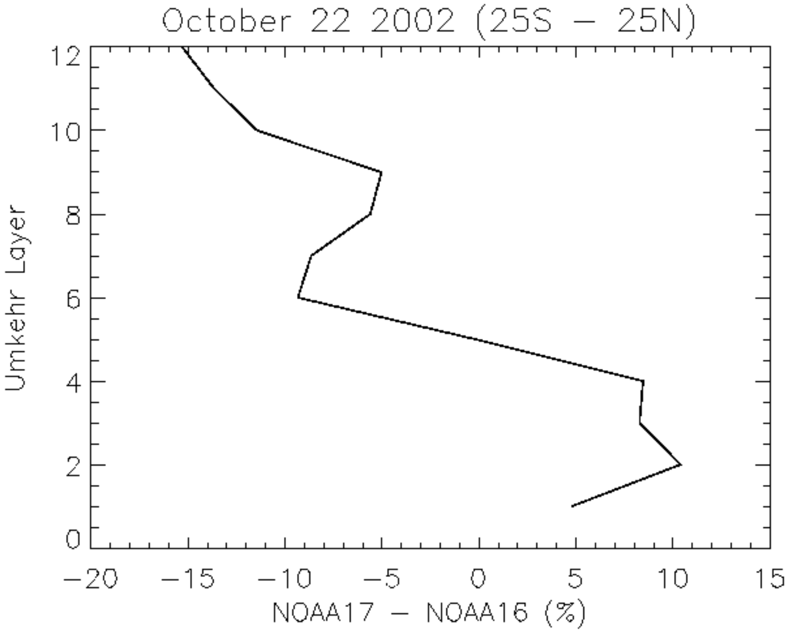

Figure 14.2: Low latitude profile ozone comparison on 22 October 2002: NOAA-17 *vs.* NOAA-16.

15. Conclusion

The NOAA-17 SBUV/2 instrument has successfully completed on-orbit activation and evaluation phase testing. The use of Range 3 anode data provides a significant improvement in data quality for total ozone products. The instrument characterization is generally consistent with prelaunch calibration data. Comparison of “Day 1” solar measurements with reference solar spectra show a significant change in absolute calibration from the final prelaunch measurements. Radiometric sensitivity changes have continued during initial operations, but appear to be slowing. Careful analysis will be required to derive appropriate time-dependent and wavelength-dependent instrument characterization, particularly during first 6 months of operation. Table 15.1 provides the location in this document of calibration data needed for SBUV/2 ozone processing.

TABLE 15.1
Ozone Processing Calibration Data for NOAA-17 SBUV/2

Quantity	***Location***
Wavelength Calibration Ebert Coefficients	Table 6.1, p. 29
Standard Ozone Wavelengths	Table 6.8, p. 32
Radiance Calibration Constants	Table 12.3, p. 86
Irradiance Calibration Constants	Table 12.2, p. 86
Electronic Offsets	Table 5.1, p. 17
Non-linearity Corrections	Table 10.1, p. 62
PMT Temperature Correction	Table 8.1, p. 47
Interrange Ratio IRR_{12}	p. 53
Interrange Ratio IRR_{23}A (anode mode)	p. 53
Interrange Ratio IRR_{23}C (cathode mode)	Tables 9.1-9.2, p. 53-54
Goniometric Correction	Tables 7.1-7.3, p. 40-41
“Day 1” Solar Irradiances	Table 13.1, p. 91
Total Ozone Pair Adjustment Factors	Table 14.1, p. 94

References

Ball Aerospace Engineering Division, Specification Compliance and Calibration Data Book for SBUV/2 Flight Unit #6, Mod. 8, **IN021-A-035, Rev. B**, April 2001.

DeLand, M. T., L. K. Huang, R. P. Cebula, S. L. Taylor, and C. G. Wellemeyer, *NOAA-14 SBUV/2 V6.1 Calibration Report,* **RSTX-3050-BJ8-MD-98-003**, 223 p., 2 October 1998.

DeLand, M. T., and L. K. Huang, *NOAA-16 SBUV/2(FM#3) Activation and Evaluation Phase (A&E) Report,* **SSAI-2015-180-MD-2001-01**, 161 p., 29 June 2001.

DeLand, M. T., L. K. Huang, and C. A. McKay, SBUV/2 FM#6 prelaunch instrument characterization for NOAA-M, **SSAI-2015-180-MD-2002-01**, 24 May 2002.

Fowler, W. K., Spectral sensitivity characteristic of the SBUV/2 instrument – differences in air and vacuum, Ball SER **SBUV-WF-94-749**, 6 September 1994.

Fowler, W. K., The differences in sensitivity of SBUV/2, FM#3, in air and vacuum, Ball SER **SBUV-WF-95-766**, 14 February 1995.

Fowler, W. K., Depolarizer test recommendation, Ball SER **SBUV-WF-97-882**, 11 July 1997.

Jaross, G., R. P. Cebula, M. DeLand, C. G. Wellemeyer, S. L. Taylor, R. D. McPeters, A. J. Krueger, P. K. Bhartia, E. Hilsenrath, and J. R. Herman, BUV instrument solar diffuser degradation, *Proc. SPIE Int. Soc. Opt. Eng.*, **3427**, 432-444, 1998.

Pitz, E., Nonlinearity measurements on photometric devices, *Appl. Optics*, **18**, 1979.

SASC Technologies, Inc., Solar Backscattered Ultraviolet Radiometer, version 2 (SBUV/2) User's Guide, **SASC-T-5-5085-028-85**, ver. 2, 198 p., 19 December 1986.